

REFERENCE COPY

SANDIA REPORT

SAND91-0672 • UC-212

Unlimited Release

Printed April 1991



SAND91-0672
0002
UNCLASSIFIED

04/91
UP STAC

Exploratory Battery Technology Development Report for FY90

Nicholas J. Magnani, Paul C. Butler, Abbas A. Akhil,
Jeffrey W. Braithwaite, James M. Freese, Stephen E. Lott

Prepared by
Sandia National Laboratories
Albuquerque, New Mexico 87185 and Livermore, California 94550
for the United States Department of Energy
under Contract DE-AC04-76DP00789

Issued by Sandia National Laboratories, operated for the United States Department of Energy by Sandia Corporation.

NOTICE: This report was prepared as an account of work sponsored by an agency of the United States Government. Neither the United States Government nor any agency thereof, nor any of their employees, nor any of their contractors, subcontractors, or their employees, makes any warranty, express or implied, or assumes any legal liability or responsibility for the accuracy, completeness, or usefulness of any information, apparatus, product, or process disclosed, or represents that its use would not infringe privately owned rights. Reference herein to any specific commercial product, process, or service by trade name, trademark, manufacturer, or otherwise, does not necessarily constitute or imply its endorsement, recommendation, or favoring by the United States Government, any agency thereof or any of their contractors or subcontractors. The views and opinions expressed herein do not necessarily state or reflect those of the United States Government, any agency thereof or any of their contractors.

Printed in the United States of America. This report has been reproduced directly from the best available copy.

Available to DOE and DOE contractors from
Office of Scientific and Technical Information
PO Box 62
Oak Ridge, TN 37831

Prices available from (615) 576-8401, FTS 626-8401

Available to the public from
National Technical Information Service
US Department of Commerce
5285 Port Royal Rd
Springfield, VA 22161

NTIS price codes
Printed copy: A04
Microfiche copy: A01

SAND91-0672
Unlimited Release
Printed April 1991

Distribution
Category UC-212

Exploratory Battery Technology Development Report for FY90

Nicholas J. Magnani,
Power Sources Department
Paul C. Butler, Abbas A. Akhil,
Jeffrey W. Braithwaite, James M. Freese,
and Stephen E. Lott
Storage Batteries Division

Sandia National Laboratories
Albuquerque, New Mexico 87185

Abstract

Sandia National Laboratories, Albuquerque, manages the Utility Battery Exploratory Technology Development Program, which is sponsored by the U.S. Department of Energy's Office of Energy Management. In this capacity, Sandia is responsible for the engineering analyses and development of advanced rechargeable batteries for stationary energy storage applications. This report details the technical achievements realized during fiscal year 1990.

Contents

Acronyms and Abbreviations	ix
1. Executive Summary	1-1
Introduction	1-1
Sodium/Sulfur Project	1-2
Technology Development	1-2
Technology Evaluation	1-3
Applied Research	1-3
Zinc/Bromine Project	1-3
Technology Development	1-3
Technology Evaluation	1-4
Applied Research	1-4
Nickel/Hydrogen Project	1-4
Technology Development	1-4
Technology Evaluation	1-4
Aluminum/Air Project	1-4
Technology Development	1-4
Technology Evaluation	1-5
Advanced Lead-Acid	1-5
Utility-Specific Systems Studies	1-5
Improvement of VRLA Technology	1-6
Battery Evaluation	1-6
2. Sodium/Sulfur Project	2-1
Technology Development - CSPL	2-1
Background	2-1
Task 1 - Core Technology Research and Development	2-2
Subtask 1.1 - Electrolyte Research and Development	2-2
Subtask 1.2 - Component Development and Qualification	2-4
Subtask 1.3 - Cell Development	2-9
Subtask 1.4 - Cell Test and Posttest Analysis	2-17
Subtask 1.5 - Module Testing	2-17
Task 2 - Battery Engineering and Testing	2-19
Subtask 2.1 - Battery Design	2-19
Background	2-19
Subtask 2.2 - Battery Build and Test	2-32
Technology Evaluation	2-35
SNL	2-38

CSPL Technology	2-38
Powerplex Technology	2-41
Ceramatec Technology	2-41
ANL	2-42
Capacity Verification and Baseline Performance	2-43
Capacity and Energy vs Discharge Rate	2-44
Driving Profile Discharges	2-44
Peak Power vs DOD	2-45
Partial DOD Operation	2-46
Charge Rate/Method Evaluation	2-46
Hill-Climbing Capability	2-46
Self-Discharge Loss	2-46
Performance vs Cycle Life	2-47
Applied Research at SNL	2-48
Improved Chromium Plating of Sodium/Sulfur Cell Containers	2-48
3. Zinc/Bromine Project	3-1
Technology Development - ERC	3-1
System Engineering and Evaluation	3-1
Hardware Development	3-1
Hardware Testing	3-4
Technology Development - JCI	3-4
Battery Testing	3-4
V1-38	3-9
V1-40	3-9
Materials	3-9
Technology Evaluation at SNL	3-10
Evaluation Procedures	3-10
Battery 494	3-10
Battery 497	3-12
Battery 459	3-14
Battery 481	3-14
Applied Research at SNL	3-14
ERC Materials	3-14
JCI Battery	3-15
Toyota Battery	3-17
4. Nickel/Hydrogen Project	4-1
Technology Development - JCI	4-1
Component Improvement, Cost Reduction, and Evaluation	4-1

Hydrogen Storage	4-1
Deliverable Design	4-3
Deliverable Fabrication	4-3
Deliverable Testing	4-6
Related Efforts	4-6
Conclusions	4-6
Technology Evaluation at SNL	4-6
Cycle Tests	4-7
5. Aluminum/Air Project	5-1
Technology Development	5-1
Background	5-1
Status of the Project	5-3
Cell Design	5-3
Materials and Energy Balances (System Analyses)	5-3
Development of Aluminum Alloys	5-10
Acoustically Aided Separation of Aluminum Hydroxide Solids	5-12
Disposal of Hydrogen Gas	5-12
Mathematical Modeling Studies Experimental Support	5-14
Technology Evaluation at SNL	5-17
Appendix: Presentations and Publications	A-1
Presentations	A-1
Publications	A-2

Figures

1-1	FY90 ETD Organization	1-2
2-1	Powder Processing Equipment for Beta Alumina	2-3
2-2	Automatic Electrophoretic Deposition Equipment	2-4
2-3	Capacity and Resistance of TD Zirconia Cell #5987	2-5
2-4	CSPL Long-Lived TD Cell - Resistance to 8000 Cycles	2-6
2-5	The Effective Resistance of the Cell Compared with the Interrupt Value, as a Function of Depth of Discharge	2-8
2-6	The Ohmic Component of Impedance as a Function of Depth of Discharge, Measured at Five Discharge Rates	2-8
2-7	Part of Largest XPB Build to Date	2-11
2-8	Graph of XPB Cell Output	2-11
2-9	Close-Packed PB Module (left); Close-Packed XPB Module B189 (right)	2-18

2-10	Resistance of Bank B189	2-18
2-11	Capacity of Bank B189	2-19
2-12	Rc/Rd Plots of Strings from XPB Bank B189	2-20
2-13	Artist's Concept of the 100-MWh Self-Contained TMS Sodium/Sulfur Load-Leveling Battery	2-21
2-14	Artist's Concept of a Self-Contained TMS Four-Module Cluster	2-21
2-15	Typical Horizontal Flow Through Self-Contained TMS Module Cross Section (left) and Over Plan View of Cell Tray (right)	2-22
2-16	Artist's Concept of an 800-lb Monobloc Battery Module	2-22
2-17	Section View of Monobloc Battery Module (Vertical)	2-23
2-18	Section View of Monobloc Battery Module (Plan)	2-23
2-19	Artist's Concept of Dense-Pack Sodium/Sulfur Load-Leveling Battery Facility	2-25
2-20	Plan View of Thermally Isolated 144-MB Module Series String	2-25
2-21	Plan Area Layout for the Close-Packed Module LL Battery Plant and Power Conditioning Equipment	2-26
2-22	144-Module Series String Thermal Shutter Closed (side view)	2-26
2-23	144-Module Series String Thermal Shutters Closed	2-27
2-24	144-Series String Thermal Shutters Open (side view)	2-27
2-25	144-Module Series String Thermal Shutters Open	2-28
2-26	Cell-to-Cell & Cell-to-Wall Radiation Heat Transfer Coupling	2-29
2-27	Heat Transfer at Corrugated Steel Module Wall	2-30
2-28	Cell-to-Cell Temperature Differences for Selected Surface Emissivities at 100% Depth of Discharge	2-30
2-29	Schematic of MB Load-Leveling Module Finite Element Model	2-31
2-30	Legend Relating MB Module Physical Entities to Their Element Representations	2-32
2-31	Nodal Temperature Profile LL Module FEM with 50°C Inlet, 25 cfm, No Insulation	2-33
2-32	Nodal Temperature Profile LL Module FEM with 50°C Inlet, 25 cfm, Tapered Insulation	2-34
2-33	1500-Ah 200-XPB-Cell Battery	2-36
2-34	Typical Output from XPB Battery Logging System	2-38
2-35	Capacity of Cell #471	2-40
2-36	Peak Power Tests	2-40
2-37	Constant Power Tests	2-41
2-38	Percent Capacity of Ceramatec Cell #454	2-42
2-39	Capacity History of CSPL 120-Cell Module for 3-hr Rate Discharges	2-43
2-40	Discharge Time vs Module Constant-Current Discharge Rate	2-44
2-41	Module Specific Energy vs Discharge Specific Power	2-44
2-42	Module Resistance vs DOD During a J227aD/IETV-1 Discharge	2-45
2-43	Module IR-Free Voltage vs DOD During J227aD/IETV-1 Discharge	2-46
2-44	Module Peak Power vs DOD During J227aD/IETV-1 Discharge	2-46
2-45	Module Sustained Hill-Climbing Capacity vs DOD	2-47
2-46	Effect of Cycle Life on Resistance vs DOD (J227aD/IETV-1 Discharge)	2-47

2-47	Effect of Cycle Life on IR-Free Voltage vs DOD (J227aD/IETV-1 Discharge)	2-47
2-48	Effect of Cycle Life on Peak Power vs DOD (J227aD/IETV-1 Discharge)	2-48
3-1	Cycle Performance for 5-Cell Stack SNL-5-4	3-2
3-2	Battery Voltage During Cycle 247, Stack SNL-5-4	3-3
3-3	Cycle Performance for 30-Cell Stack SNL-30-2	3-5
3-4	Cycle Performance for 52-Cell Stack 1500-52-1	3-6
3-5	Battery Performance During Cycle 55, Stack 1500-52-1	3-7
3-6	V1-39 Battery Voltage and SCP System Currents	3-8
3-7	Cycle Efficiency for 8-Cell Stack V1-38	3-9
3-8	Cycle Efficiency for 8-Cell Stack V1-40	3-10
3-9	Effect of Charge Current on Battery Efficiencies	3-11
3-10	Effect of Discharge Current on Battery Efficiencies	3-12
3-11	Effect of Zinc Loading on Battery Efficiencies	3-13
3-12	Efficiency Plots for Zinc/Bromine Battery 494	3-13
3-13	Surface Composition of ERC Current Collector	3-16
4-1	Cell Module with Back-to-Back Positive Design	4-4
4-2	Nominal 160-Ah Cell in Polypropylene Case	4-4
4-3	10-Cell, Nominal 12-V Battery Stack in Compression Fixture	4-5
4-4	2-kWh Battery in Fiber-Wound Vessel	4-5
4-5a	Capacity vs Cycle Number (Cell #144)	4-8
4-5b	Pressure vs Cycle Number (Cell #144)	4-8
4-6	Capacity vs Cycle Number, Cell #POO3 Parametric Tests	4-9
5-1	Aluminum/Air Process Schematic	5-2
5-2	Exploded Diagram of AT400 Cell	5-4
5-3	10-Cell Module Based on AT400 Cell	5-5
5-4	SFUDS for AT400 Single Cell	5-6
5-5	Aluminum/Air Battery System for SFUDS Base Case	5-8
5-6	Vehicle Range vs Battery System Weight Development of Aluminum Alloys	5-11
5-7	Alloy Processing Combinations	5-13
5-8	Alloy Processing Steps	5-14
5-9	Design of Multiple Chamber Acoustically Augmented Aluminate Separation Cell	5-17
5-10	Predicted Hydrogen Produced as a Function of Battery Current Density for Advanced Alloy in Full-Sized Battery	5-18
5-11	Cell Polarization Data	5-20
5-12	Corrosion Rate and Faradaic Efficiency of the Advanced Alloy	5-20
5-13	Faradaic Efficiency Comparison of Advanced Alloy and 99.995% Aluminum Anode	5-21

Tables

2-1	Weibull Statistics for Zirconia Beta Alumina TD Cells	2-5
2-2	Status of Experimental Glass Formulations	2-7
2-3	Weibull Statistics for 17-Cell MkIII SF Forerunner Group	2-9
2-4	XPB Build Record, Jan 1988 - Mar 1990	2-10
2-5	Status of Pre-Nov 1989 XPB Cells	2-12
2-6	Status of Nov 1989 XPB Cells (20 Cells, 2 Failures)	2-12
2-7	Status of Jan 1990 XPB Cells (22 Cells, 0 Failures)	2-13
2-8	Status of Feb 1990 XPB Cells (25 Cells, 0 Failures)	2-14
2-9	Status of XPB Cells Built Since Mar 1990	2-15
2-10	XPB Cell Reliability	2-16
2-11	Safety Tests on B136 XPB Cells	2-17
2-12	Monobloc Module Specifications	2-24
2-13	Sodium/Sulfur Battery Plant Specifications	2-28
2-14	Comparison of Facility Characteristics	2-35
2-15	Recommendations for Follow-On Studies	2-35
2-16	200-Cell XPB Battery	2-36
2-17	CSPL Cell Test Summary at SNL	2-39
2-18	Projected Vehicle Ranges Under Simulated Driving Profiles	2-45
3-1	Cycle Test Data for ERC Battery 1500-5-4	3-3
3-2	Cycle Test Data for ERC Battery 1500-52-2	3-7
3-3	JCI Battery Efficiency With and Without SCP	3-8
3-4	ERC Battery #494, Parametric Test Plan	3-11
3-5	Modulus Profiling of a Virgin PVC-1 Flow Frame	3-14
3-6	Fracture Toughness of ERC Flow Frame Material	3-15
3-7	Surface Modulus of JCI Flow Frame	3-17
3-8	Postmortem Characterization of Toyota Separators	3-17
4-1	Status of Laboratory Test Cells	4-2
4-2	Configuration and Test Conditions	4-7
4-3	Summary of Test Results	4-10
5-1	Polarization Behavior in the AT400 Cell	5-7
5-2	Comparison of Aluminum/Air Cells	5-7
5-3	Summary of Operating Options Used in Systems Analysis	5-9
5-4	Projected Battery System and Performance Specifications	5-10
5-5	Chemical Composition of Base Aluminum and Alloys (ppm)	5-12
5-6	Electrochemical Behavior of Alloy #3	5-15
5-7	Electrochemical Behavior of Aluminum Alloys	5-16
5-8	Performance of Alloy Plates in the AT400	5-16

5-9 Acoustic Separation Continuous Filtration Experiments 5-17
5-10 The Effect of Aluminate Ions Upon the Dissolution of Aluminum 5-18
5-11 Test Results of Pure Aluminum and Alloy Anodes 5-19

Acronyms and Abbreviations

ANL	Argonne National Laboratory
ASME	American Society of Mechanical Engineers
ASTM	American Society of Testing Methods
BEST	Battery Energy Storage Test Facility
BPA	Bonneville Power Administration
COMSAT	Communications Satellite Corporation
CPV	Common Pressure Vessel
CSPL	Chloride Silent Power, Ltd.
DCOV	discharge cut-off voltage
DOD	depth-of-discharge
DOE	Department of Energy
DSEP	Dual Shaft Electric Propulsion Program
EOC	end of charge
EOD	end of discharge
EPD	electrophoretic deposition
EPRI	Electric Power Research Institute
ERC	Energy Research Corporation
ETD	Exploratory Battery Technology Development Program
EV	electric vehicle
FEM	Finite Element Model
FETA	Finite Element Thermal Analysis
FTIR	Fourier transform infrared analysis
IDSEP	improved DSEP
INEL	Idaho National Engineering Laboratory
IPV	individual pressure vessel
JCI	Johnson Controls, Inc.
LBL	Lawrence Berkeley Laboratory
LEO	low earth orbit
M	molar
MAWP	Maximum Allowable Working Pressure
MSOE	Milwaukee School of Engineering

OCV	open-circuit voltage
OEM	DOE Office of Energy Management
OPS	DOE Office of Propulsion Systems
PPL	Princeton Plasma Physics Laboratory
PTA	posttest analysis
PV	photovoltaic
PVC	polyvinyl chloride
SAIC	Science Applications International Corporation
SCP	shunt current protection
SES	stationary energy storage
SFUDS	Simplified Federal Urban Driving Schedule
SNL	Sandia National Laboratories
SOC	state-of-charge
TBR	Tech Base Research Program
TMS	thermal management system
VLT	variable linear transformer
VRLA	valve-regulated lead-acid

1. Executive Summary

Introduction

This report documents the activities of the Utility Battery Exploratory Technology Development Program (ETD) for fiscal year 1990, ETD's tenth program year. (See SAND90-1195, *Exploratory Battery Technology Development and Testing Report for 1989*, for a description of the previous year's activities.) ETD, directed by Sandia National Laboratories (SNL), is supported by the U.S. Department of Energy, Office of Energy Management (DOE/OEM). This program is part of the effort being made by the DOE/OEM to reduce the country's reliance on imported oil, improve reliability and generating efficiency, and reduce environmentally damaging emissions. ETD coordinates its activities with the Technology Base Research Program (TBR), under the direction of Lawrence Berkeley Laboratory. The objective of ETD is to characterize the benefits of storage and advance rechargeable battery technologies to a level suitable for commercial use in large-scale utility and stationary applications that include electric utility/industrial energy storage and remote solar systems.

Specifically, ETD is responsible for the engineering development of electrochemical couples systems for which feasibility has been demonstrated by TBR. Battery development is accomplished through cost-sharing contracts with industrial partners. SNL also undertakes analytical battery and system cost-and-performance studies. ETD is responsible for the technical direction of contracts as well as project management. Additionally, SNL conducts various applied-research activities that directly support the development efforts. Evaluation and analysis of the performance of prototype components and batteries are performed either at SNL or Argonne National Laboratory (ANL).

Oversight for ETD is provided by Dr. Nicholas J. Magnani, Manager of SNL's Power Sources Department. Daily operations are guided by Paul C. Butler, Supervisor of SNL's Storage Batteries Division (see Figure 1-1).

ETD was organized into five projects in FY90:

- Sodium/Sulfur
- Zinc/Bromine
- Nickel/Hydrogen

- Aluminum/Air
- Advanced Lead-Acid

The battery development projects encompass contracted technology development and, at SNL, program management, technology evaluation, and applied research activities. Technology development utilizes a phased approach from fundamental electrochemical R&D, to component development, and through several steps of battery engineering (conceptual, prototype, and product). A battery technology suitable for commercial marketing is the desired final product. At SNL, program management involves placing the industrial development contracts with industry, monitoring and guiding progress, solving programmatic issues, and coordinating reporting. Under technology evaluation, contract deliverables are tested primarily at SNL to determine performance, lifetime, and failure mechanisms. These data are reported to the developers for use in optimizing designs and resolving problems. Applied research is performed in certain projects where SNL has specific technical expertise to address critical problems facing a technology. This applied work is closely integrated with the prime development contractor.

A new project was initiated in FY90 to develop improved valve-regulated lead acid (VRLA) batteries. In conjunction with this work, a closely related activity was begun to quantify the benefits of storage to utility power systems. Many new modes of operation for batteries have recently been identified which have greatly improved the technical and economic viability of storage; analytical work is needed to characterize the benefits of these modes individually and in combination. During FY90, many contacts were made with potential battery developers and interested utilities, and plans were made to initiate contracts early in FY91 in these important areas.

A separate testing project enhances and maintains the SNL battery evaluation facilities. Specialized hardware and software are developed to support unique test capabilities and needs. In addition, this project directs field test work for nickel/hydrogen batteries no longer being developed by SNL, and ensures that appropriate technology transfer is completed.

A summary of the highlights of ETD, organized by technology, follows. More detailed information on

SNL UTILITY BATTERY EXPLORATORY TECHNOLOGY DEVELOPMENT PROGRAM

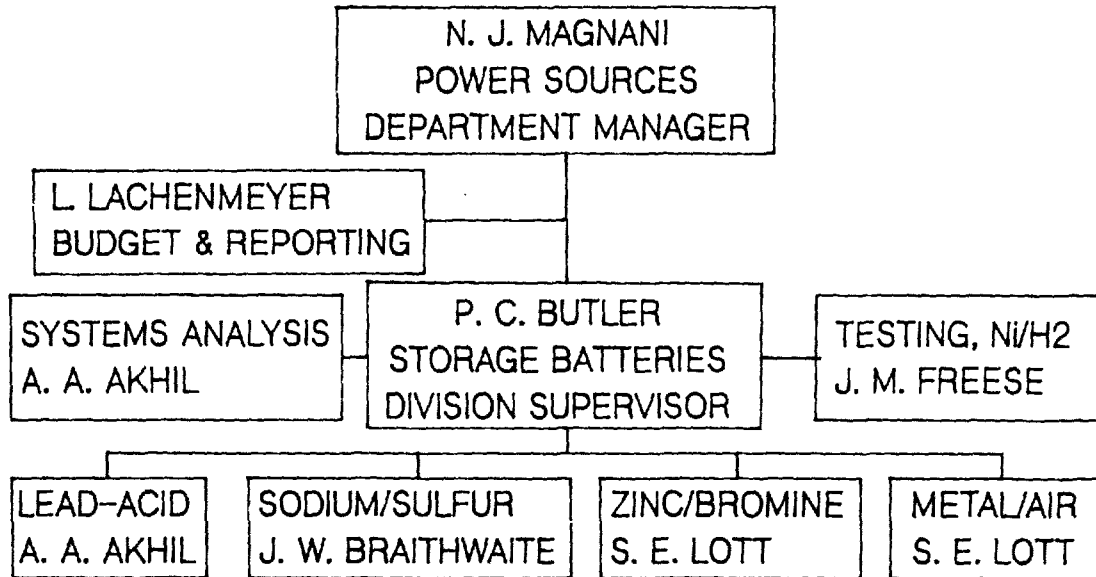


Figure 1-1. FY90 ETD Organization

sodium/sulfur, zinc/bromine, nickel/hydrogen, and aluminum/air is contained in Chapters 2 through 5 of this report.

Sodium/Sulfur Project

Technology Development

FY90 marked the conclusion of the fifth and final year of a contract with Chloride Silent Power Limited (CSPL) to further the development of the generic sodium/sulfur technology and to perform initial battery engineering for stationary-energy-storage (SES) applications. The significant accomplishments made by CSPL during the year included the following:

- A new PB cell (MkIV) was designed and put into limited production that is more suitable for fabrication using automated facilities.
- The PB cell technology was successfully transferred to the larger "XPB" cell design. The subsequent development and qualification of this cell, which is potentially more suitable for use in SES applications, was effectively com-

pleted. Testing results for a 40-cell module have been very good for over 250 cycles. Development goals for this cell include a Weibull characteristic life >1000 cycles, a Weibull shape parameter >2, a freeze/thaw durability >25 cycles, capacity of 80+% for 1000 cycles, stable resistance of <11 mohm, and a zero breach rate for all relevant safety test conditions.

- A first-generation 200-XPB cell SES module was designed and fabricated. The capacity of this 200-cell module is 8.5 kWh at 8 V, its resistance is slightly greater than 1 mohm, and it contains provisions for both active and passive thermal management. On-site evaluation (currently at 100+ cycles) will allow the intrinsic feasibility of the sodium/sulfur technology relative to SES to be demonstrated.
- In-cell evaluations demonstrated that improved durability is being attained. A new glass glazing composition allowed a 120-cell bank to achieve 500+ cycles with 5 extended freeze/thaw cycles. MkIIISF PB cells reached 2000 cycles. An XPB module completed over 500 cycles with the first failure occurring at 300

cycles. The longest lived CSPL cells now have over 8000 cycles.

- An analysis was completed that showed a significant improvement in sodium/sulfur cell lifetime appears to be associated with the use of zirconia-toughened beta"-alumina electrolyte. A group of cells containing this electrolyte formulation commenced test in 1984 to 1986. The Weibull characteristic life for this population is 7200 cycles with a modulus of 3.5 (compared with data from similar cells without toughening: life - 3500, modulus - 0.8). Each of the remaining cells on test has accumulated at least 4000 deep-discharge cycles.
- A significant revision was made to the conceptual design of a load-leveling battery that was described in the 1989 ETD Annual Report. This revision was motivated by an investigation of alternate thermal management system (TMS) approaches. The objective of the revised design was to reduce the capital cost and operating expense associated with this component of SES battery systems. What emerged from this study was an entirely new TMS concept that not only promises to achieve the desired lower cost but also significantly reduces the overall facility footprint.

Technology Evaluation

During this fiscal year, SNL evaluated two groups of individual cells and 4-cell series strings from CSPL. Also evaluated were two 40-Ah cells from Powerplex and two 40-Ah cells from Ceramatec. Tests included performance characterization and life cycle.

Results of the characterization tests on the 4-cell strings indicated that the maximum specific energy of the string was 170 Wh/kg. The maximum specific peak power was 195 W/kg with the string being discharged to 2/3 of the open-circuit voltage. These tests were performed at a temperature of 350°C and an unencumbered string weight of 520 grams was used.

One cell from each of the three technologies completed over 2000 baseline cycles. A gradual decline in capacity was observed on both the CSPL and Powerplex cells while the Ceramatec cell maintained a high capacity for most of its life.

An 8-V, 300-Ah CSPL module is undergoing performance and life characterization tests at ANL. There are 120 cells in this module that are configured into 30 parallel-connected strings of 4 series-connected cells.

The hardware assembly used with this module is of the same design and configuration as that of the 24 series-connected modules in the full-sized battery system for the ETX-II vehicle. Performance testing has been completed, and the module is undergoing life evaluation. A specific energy of 79 Wh/kg and a peak power capability of 94 W/kg at 50% DOD were achieved at an operating temperature of 330°C. A maximum 3-hr rate capacity of 304 Ah (2310 Wh) was obtained at 350°C. Results of driving profile discharges indicate that the Eaton DSEP van would have a range of 148 miles on the SFUDS. At the end of FY90, the module had successfully completed 141 cycles and still retained ~100% of its initial 292-Ah capacity (3-hr rate).

Applied Research

One of the promising materials that could be used to impart significant corrosion protection to a sodium/sulfur cell container is chromium. The objective of this task was to improve chromium electroplating techniques when applied to the fabrication of sodium/sulfur cells. Specifically, this year's activity was concerned with determining if inexpensive techniques could be used to effectively plate chromium onto aluminum-based cell containers. The latter phase of this effort focused on plating from trivalent chromium electrolytes, a process that also has minimal environmental impact.

The results from accelerated testing were poor. The predicted lifetime for the best plating formulation is less than 6 months in an actual cell environment. These negative results leave the "conventional" methods identified earlier in this task as the only chromium plating options. Unfortunately, cost and the environmental aspects of using the required hexavalent chromium electrolyte are probably not acceptable. The DOE/SNL sodium/sulfur program must therefore continue to seek better containment alternatives.

Zinc/Bromine Project

Technology Development

The development program at Energy Research Corporation (ERC), which began in September 1985, concluded in January 1990 with the delivery of a 52-cell, 18-kWh module. The objective of this program was to improve the core technology and perform the engineering and evaluation of a 50-kWh zinc/bromine proof-of-concept battery for stationary applications. During FY90, efforts at ERC were focused on battery testing in

order to verify whether progress on core development issues had resulted in increased battery performance. The final program deliverable was scaled down to a 52-cell, 18-kWh battery. Performance of the final deliverable was disappointing. The final program report was issued in May 1990.

The objective of a new program at Johnson Controls, Inc. (JCI), initiated in August 1990, is to extend the JCI technology from an electric vehicle application to a load-leveling application and to design, fabricate, and evaluate a 100-kWh load-leveling system. The JCI contract is organized into two 18-month development periods in which progress during the first period towards battery stack integrity and performance must be demonstrated prior to initiating the second development period in February 1992.

Technology Evaluation

During FY90, SNL evaluated two zinc/bromine batteries from ERC. A set of parametric tests was conducted on a 5-cell battery along with numerous baseline capacity tests. A total of 127 charge/discharge cycles was placed on this battery before it was removed from test due to a decrease in performance. A posttest analysis of the battery revealed a wetted titanium end plate which lowered the voltaic efficiency.

A 52-cell battery completed 61 charge/discharge cycles before it was removed from test due to poor performance. A posttest analysis of this battery provided no evidence which could explain the poor performance of the battery.

Posttest analyses were conducted on two other ERC batteries which were evaluated during the previous fiscal year. The results indicated cracks in the flow frames and wetting of the current collectors which lowered the voltaic efficiency.

Applied Research

SNL has characterized several separator materials used in zinc/bromine batteries manufactured by ERC, JCI, and Toyota. The purpose of this exercise is: 1) to obtain baseline data for subsequent battery tear-downs, and 2) to detect property variations which may be attributable to nonuniform processing. Materials from two Toyota batteries underwent postmortem analysis. A conclusion from that study indicated that significant chemical degradation had occurred during battery operation.

Nickel/Hydrogen Project

Technology Development

During FY90, a metal-lined fiber-wound pressure vessel which provides a safe and practical means of hydrogen retention was developed and qualified at JCI. Hydrostatic burst-testing defined a pressure capability exceeding the 5:1 safety factor required by ASME code, and demonstrated the predicted noncatastrophic failure mode. A total of 30,000 pressure cycles, at room temperature, without failure, was also demonstrated.

Four 2-kWh batteries, enclosed in fiber-wound vessels, were fabricated and delivered to sites in Florida and New Mexico where they have been coupled to photovoltaic arrays for application testing.

Technology Evaluation

Contracts for the development of nickel/hydrogen batteries at JCI provide for periodic delivery of cells and batteries to SNL for evaluation purposes. Typically, these cells consist of several modules and represent state-of-the-art technology or contain experimental components modified to reduce cost or improve performance. Four nickel/hydrogen cells were on test during this fiscal year.

Two of the four cells on test have exceeded 1700 cycles while the other two cells are in their early cycle life testing. One problem common to all the cells was the gradual increase in pressure at the end-of-charge. This problem is being examined at JCI.

Aluminum/Air Project

Technology Development

In August 1987, SNL contracted with Eltech to develop the aluminum/air battery technology for electric vehicle applications. Case Western Reserve University, Helipump Corporation, and Kaiser Aluminum were subcontracted for some of the program tasks. The technical effort of this 3-yr development program was completed in September 1990. The objective of this program was to improve the technology and to engineer and evaluate an advanced aluminum/air battery. The program addressed two areas: 1) design of the aluminum/air cell, and 2) design of the auxiliary systems, i.e., the heat exchanger, solids separation, control of carbon dioxide and disposal of hydrogen gas. A

systems study projected that vehicle range under steady-state operation would be 380 miles, while range under batch operation would be 180 miles. Separation of aluminum trihydroxide particles from aqueous solutions of potassium hydroxide was demonstrated in an acoustic cell in which a standing wave was used to coagulate the aluminum trihydroxide. Although scale-up and power requirements may be a concern, the acoustic separation is a novel technique that may have other applications. At the final review in June 1990, the panel of reviewers stated that while Eltech had made a "good" effort towards the program technical goals, aluminum/air is not an economically viable technology for electric vehicle applications.

Technology Evaluation

An Eltech aluminum/air cell was installed at SNL in June. The unit consisted of a single cell based on a new compact design. The weight and volume were reduced by approximately 86% and 65%, respectively. Tests were run with pure aluminum anodes and with an advanced aluminum alloy. The tests indicated that the corrosion rate of the advanced alloy was much lower than the corrosion rate of the pure aluminum anode and that the advanced aluminum alloy development program had succeeded.

Advanced Lead-Acid

During FY90, SNL initiated an advanced lead-acid program with the objective to commercialize a lead-acid battery technology suitable for use in the utility industry by the mid- to late-1990s. This initiative is different from other SNL advanced battery development programs in that the commercialization objectives for this program are nearer term and driven by a window of opportunity that exists for introducing this technology in the utility industry in a short time frame.

Early in 1990, SNL supported the planning of and participated in a meeting sponsored jointly by the DOE and EPRI to identify key issues that need to be resolved for the commercialization objective to be achieved. The 37 attendees, including representatives of electric utilities and several major lead-acid battery manufacturers, identified the need for storage benefits quantification, additional battery improvement R&D, optimized system design, and test and demonstrations.

Later in the year, SNL visited six lead-acid battery manufacturer sites to assess their manufacturing capabilities and gauge their research interest in the further improvement of lead-acid battery technology.

The information obtained at the meeting and the site visits was important in the further definition of the lead-acid battery initiative as a comprehensive program plan. The program plan that evolved was designed to address three key issues:

- Analysis and quantification of benefits for battery storage in a wide range of utility applications, including, but not limited, to load-leveling.
- Improvement of the existing Valve-Regulated Lead-Acid (VRLA) battery technology, with emphasis on improving battery life and performance in the full range of electric utility applications.
- Continued testing of VRLA batteries at the BEST Facility and at other test sites and seeking of opportunities for demonstration of VRLA batteries at utility test sites.

Various activities were initiated to develop contacts with the utility and battery manufacturing industry to inform them of SNL program goals and solicit programmatic input to keep the program aligned with earlier recommendations and user requirements. Specific lead-acid activities performed in FY90 are detailed below.

Utility-Specific Systems Studies

Traditionally, load-leveling has been the application that has dominated as the most economic and technically feasible application for electric utility battery energy storage. However, recent studies suggest that there are other applications that may have higher economic value to a utility system. These applications have the potential of enhancing system stability and reliability, while potentially reducing the size of the battery. The size reduction is an important consideration, because the longer and deeper discharges of a load-leveling battery substantially increase its cost, while the deep-discharge requirement reduces battery life.

While there are several non-load-leveling applications, the ones that most likely have near-term application potential are:

- Spinning reserve
- Frequency regulation
- Transmission line deferral
- Transmission line stability
- Area regulation

- **Generation benefits.**

The load profile that the battery would experience in these applications might impose less stringent performance requirements than load-leveling applications. But the economic value to the utility for these applications is difficult to assess in general terms. It can only be determined by evaluating each utility on a case-by-case basis, using planning scenarios and economic parameters of that specific utility system.

This necessitates a system-specific approach to quantify the benefits of battery storage to the utility system. Thus, the systems study concept was implemented in the program to attempt to quantify the benefits for several utility systems during FY90. Utilities were screened as potential candidates to select four or five with a high potential for battery storage applications and a high degree of interest in supporting the effort. A cost-sharing requirement by the utility was included as a token of utility commitment and support of the effort. By the end of FY90, negotiations were under way with the Bonneville Power Administration (BPA) to perform a systems study for the Puget Sound area supplied by the BPA system. A preliminary scope of a systems study was also being discussed with San Diego Gas and Electric for their systems study. Discussions were also held with Southern California Edison to share the results on their ongoing internally funded study.

Other utilities were also informed of the SNL systems study plan, and it is expected that firm commitments with them will be made in early FY91.

Improvement of VRLA Technology

An RFP for technology improvement was released on August 14, 1990, requesting proposals from battery

manufacturers to improve the existing VRLA technology in a two-phase, 2- to 3-yr effort. The battery manufacturers were asked to form project teams with "host utilities" that would provide requirements for two applications of battery storage on their system. In parallel with the cell and battery level research, contractors would perform conceptual designs of the battery for the selected utility applications and perform parametric economic studies to guide the technology improvement aspects of the effort.

Six "host utilities" volunteered to be included in the RFP, as a potential candidate host utility. But the responders could select any other utility of their choice, provided the utility identified the two applications and participated in the project at the required level of effort.

Responses to the RFP were due on November 19, 1990.

Battery Evaluation

GNB and JCI fabricated two test batteries for evaluation by the BEST Facility for the Princeton Plasma Physics Laboratory (PPL), Princeton, NJ, project with funding for testing from EPRI. However, due to budgetary constraints, EPRI could no longer support the testing and requested DOE/OEM funding support to continue the test effort. SNL assumed this responsibility, and final negotiations are under way with the BEST Facility to finalize a one-year contract to support the tests. BEST Facility has proposed that these batteries be tested under a simulated area regulation cycle to obtain life-cycle performance data to support the PPL project.

2. Sodium/Sulfur Project

The sodium/sulfur technology is one of the leading candidates for large-scale mobile and stationary-energy-storage (SES) applications because of its potential for low cost, excellent performance (e.g., energy and power density, electrical efficiency), long life, and reliable operation. During FY90, advancement of this technology continued under ETD support. The primary development effort was performed under a contract with Chloride Silent Power Limited (CSPL), Runcorn, England. Additionally, the performance of their technology was evaluated at SNL and ANL and one activity was active at SNL that directly supported the improvement of the CSPL technology. Accomplishments during FY90 in each of these areas are reported separately in the following three sections.

Technology Development - CSPL

A five-year contract with CSPL concluded in December 1990. The objective of the CSPL program was to advance the development state of the sodium/sulfur technology with respect to components, cells, and small batteries for both stationary and mobile applications. Overall, CSPL cost-shared ~35% of this \$11.0M effort. The final deliverables from the program included qualified cells suitable for use in both mobile and stationary applications and a subscale battery module (200 cells) that is being evaluated in a SES mode.

The DOE-funded program at CSPL was intended to complement a parallel effort sponsored by the Electric Power Research Institute (EPRI). The objective of the EPRI contract was to design and construct a 500-kWh sodium/sulfur battery for evaluation in the BEST facility. The EPRI contract was effective in December 1985, but was substantially reduced in content during February 1986. At that time, plans to construct the 500-kWh battery were deferred.

Because of the EPRI action, the original 3-year DOE/ETD program at CSPL was extended by one year to reduce the annual program costs and to allow the statement of work and the contract deliverables to be appropriately adjusted. Subsequently, a \$1.5M, 1-yr extension to this contract became effective during the first quarter of FY90. During this final year, the design, development, and qualification of the "XPB-cell" technology and the refinement of the conceptual design of a

SES battery was completed. This final effort has provided the needed solid foundation for initiating the first major SES battery engineering development program.

The activity at CSPL was divided into the following two tasks:

Task 1 - Core Technology Research and Development

Task 2 - Battery Engineering and Testing

Task 1 was devoted to research and development in the areas that were generic to both stationary and electric vehicle (EV) applications. Major emphases of the program were improving cell performance, reliability, safety, and cost. The following subtasks were part of Task 1:

Subtask 1.1. - Electrolyte Research and Development

Subtask 1.2. - Materials Development and Qualification

Subtask 1.3. - Cell Development

Subtask 1.4. - Cell Testing and Posttest Analysis

Subtask 1.5. - Module Development and Testing

The Task 2 effort was directed toward the design and fabrication of batteries for SES applications.

Background

The CSPL sodium/sulfur cell design strategy is based on a family of cells designated as "PB" cells. Two specific sizes are currently being developed: a 45-mm-diameter by 45-mm-high cell called the "PB" cell and a 45-mm-diameter by 110-mm-high cell, called the "extended PB or XPB" cell. The cells are both central sodium designs and are based on identical components as far as possible, particularly in the seals.

The XPB has been proposed for stationary applications and the PB for EV applications, although it was the intention to develop generic technology. This generic technology will enable the commercialization of optimized cell designs that are close in size to those for which a performance database has been established. Selection of optimum cell size is a complex issue that involves interactions with battery voltage, capacity, cell reliability, physical dimensions of the battery, and cost.

CSPL has a long-term technology database from their evaluation of two earlier, central sulfur cells: 150-Ah NaS7 and 30-Ah TD cells. These designs have now been tested for up to 8000 deep-discharge cycles. The longest lived operating cell has completed more than 68,000 hours on test (7.8 yr). The longest lived PB cell has completed 2590 cycles and the longest lived XPB cell has completed 1400 cycles. Several networks of PB cells have exceeded 500 charge/discharge cycles.

During 1987, the production capability of PB cells was increased to 350/wk. A substantial proportion of the output was used in the construction of a battery for a Bedford CF delivery van. This vehicle was powered for more than 100 miles on the second battery discharge and added considerably to CSPL's experience in terms of road trials, cell production, and design. During the evaluation, deficiencies in the cell and battery were observed and modifications were made and qualified during 1988. These improvements were embodied in a sub-battery designed and fabricated under a complementary DOE/OPS program with CSPL (EV Battery Engineering). This sub-battery was tested at ANL for 241 electrical cycles. Following this test, another battery was built and delivered (Nov. 89) under a separate, non-DOE contract, to Electrotek Concepts Inc. for testing on their track at Chattanooga, TN. This battery completed more than 5200 equivalent miles on board a GM Griffon van during a 6-mo test run. In 1990, the final deliverable of the DOE/OPS battery program, a 50-kWh battery for the Ford ETX-II, was delivered and is currently undergoing evaluation at INEL. This battery contains cells that were designed and qualified under this contract.

A significant milestone for CSPL was reached in 1988 when approval was given for the construction of an automated pilot production plant at Chloride Industrial Batteries' Clifton Plant. This facility has been specified for the production of 5000 cells/wk of either the PB or XPB design. The output will be used in the construction of batteries for extensive field trials. In March of 1990, a German electric utility, RWE, signed an agreement with Chloride Group, CSPL's holding company. A new joint venture company, CRWE, was established and will purchase the Clifton Sodium/Sulfur Production Plant and the associated Electrolyte Plant at Runcorn. At the time of writing, construction of the production module was well advanced with all of the equipment undergoing commissioning trials.

A significant effort to transfer the CSPL technology to the US commenced during 1989. This is being accomplished by means of a phased schedule in which parts of the manufacturing processes are introduced to the Beta Power Inc. facility at Salt Lake City, Utah.

Eventually Beta Power will have the ability to manufacture cells using the CSPL technology. In order to increase the technical support directly available to the US-based efforts, P. Bindin was transferred to Beta Power in 1990.

For reference when reading the remainder of this section, some background on the various modifications of the PB cell that have existed will be useful. The PB cell has undergone a variety of design changes since the idea of using small cells was conceived in June 1981. The metal-to-ceramic seal component is of critical importance to the satisfactory life and performance of any sodium/sulfur cell. Many of the variations have been designated according to the seal type employed. Two basic seal concepts have been studied at CSPL: a direct metal-to-ceramic bonded seal (designated MkII) and one employing an aluminum interstrate between a chromized steel component and the alumina header (MkI). In 1986, a hybrid of the two seal concepts was selected for further development and designated the MkIII. This design, which was being progressed under this program, then became the mainstream design of all CSPL's efforts.

A major advance in the PB cell technology involved the incorporation of a closed end tube in the sodium electrode (a component added to improve the safety performance of the cell). This variation came to be known as the MkIII SF. The suffix "SF" was added in order to differentiate it from the MkIII cell without this feature, the latter referred to as the MkIII NSF. The MkIII SF became the production standard in 1988 and the majority of cells have since been made to this design. The ETX-II battery contains MkIII SF cells.

While the production of batteries that used the MkIII SF cell was ongoing, further analysis was being conducted by the CSPL engineering teams to assess the manufacture of PB cells at high production rates. As a result of this analysis, the MkIV cell concept was developed. This design represents the status of the CSPL program at mid-1989 and is intended for the initial output of the Clifton Production Facility.

Task 1 - Core Technology Research and Development

Subtask 1.1 - Electrolyte Research and Development

The emphasis of the electrolyte subtask changed in 1989 with the completion of the core technology development. Activity was then essentially transferred to the work required for larger scale manufacture in the

pilot production plant. The scale-up effort utilized the core technology developments but was funded internally by CSPL.

Figure 2-1 shows some of the equipment in the electrolyte area and gives an indication of the scale of the investment.

XPB Ceramic Manufacture

In order to address the requirements of this program and also to take account of CSPL's desire to effect cost savings via a larger cell, the scale-up of the capabilities of XPB ceramic production continued during 1990. The 4-chamber EPD rig was modified to include automatic deposit weight control. Automatic green shape extraction was also implemented using technology developed on CSPL's Production Engineering program. The full-time use of the XPB ceramic production line was consolidated during the reporting period. After a relatively difficult start in November 1989, the yield of XPB ceramics was doubled each month through February 1990. The line has run at 48 shapes per day for the majority of the reporting period, but it has occasionally been operated at 96 tubes per day by using a fast-drying process after deposition. At the end of 1990, the number of shapes deposited was 2772 compared with 3992 for the whole of 1989. However, there were also improve-

ments in the overall yield that increased the number of ceramics of cell build quality being produced. Prior to the recent process refinements, the record batch yield was 41%. This value was exceeded in 13 batches during 1990 and a new high of 62.5% was achieved early in the year. For cell builds in 1990, 783 XPB ceramics were issued, 91% of which were of "zero defect quality." These improvements were achieved against a background of difficulties caused by the extensive building modifications being undertaken to scale up electrolyte production to 5000/wk cell output levels.

New deposition procedures were tested on the XPB line and subsequently transferred to the PB 12-chamber rig. The new procedures provide better conditions in the vicinity of the deposition chamber, leading to fewer rejects due to blow holes and higher predictability of deposition times. Utilization of the powder slurry has been significantly increased as an additional benefit.

To increase the output still further, modifications have been made to the 12-chamber production rig so that it can produce XPB ceramics. The rig can be converted once the production of PB ceramics is moved onto the 24-chamber units intended for the pilot production plant. Commissioning of the 24-chamber rig was well advanced at the time of writing with over 1200 shapes

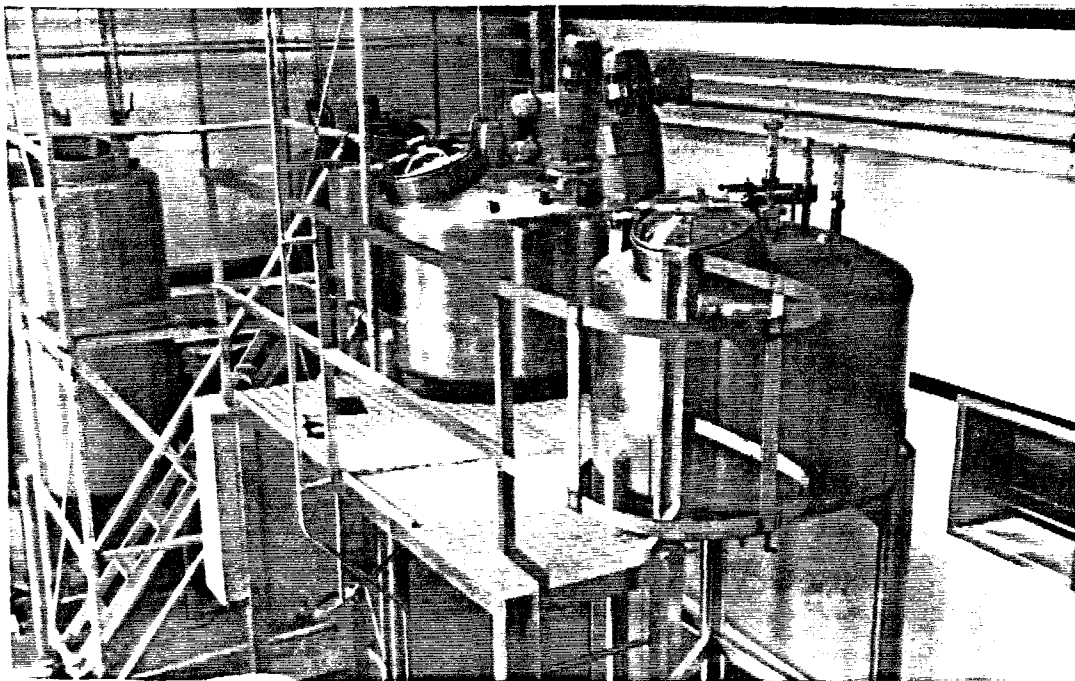


Figure 2-1. Powder Processing Equipment for Beta Alumina

per day being produced. Part of the 24-chamber automatic deposition machine is shown in Figure 2-2.

Zirconia Toughening

A group of cells containing beta alumina toughened by the addition of zirconia commenced test before the start of this program. A failure occurred in a cell containing a nonoptimized zirconia addition in 1986 at 949 cycles (1986 ETD Annual Report). Since that time the remaining cells have continued to cycle and have been supplemented by the storage experiment described in the 1987 ETD Annual Report. The total population became 20 with the additional cells that are all of the 30-Ah, central sulfur, Technology Demonstration Cell (TD) design. A cell failed in 1988 at 3383 cycles and another failed in early 1989 at 3005 cycles. A fourth cell has failed in the reporting period at 3988 cycles. Each of the cells remaining on test has accumulated at least 4000 deep discharge cycles. The six oldest cells, part of the group that commenced test prior to the start of this program, have each completed more than 5000 cycles. The accumulated cell cycles are almost 76,000. It is possible, following the fourth cell failure to compute rough estimates of the Weibull parameters. Two calculations are possible depending on the assumed status of the first cell to fail. This cell (5982), which failed at 949 cycles in 1986, only contained 3% of

zirconia, a sub-optimal level. The statistics are shown in Table 2-1 and compared with data from TD cells containing non-toughened electrolyte. A graph of both the resistance and capacity of one of the cells is shown in Figure 2-3.

In addition to the TD cells, a number of PB cells have also been constructed with zirconia ceramic. Two 4-cell strings of these cells have each completed 1750 cycles without failure.

Subtask 1.2 - Component Development and Qualification

The major objective of this subtask was to identify and qualify cost effective candidate materials for cell and system design. The subtask originally included the following activities: alpha-alumina to beta-alumina glass seals, alpha-alumina ceramic-to-metal seals, sulfur electrode and sodium electrode design, and finally, sulfur electrode containment. However, during this final year of the contract, the effort concentrated upon seals and cell terminations.

A materials database had been established before the start of the contract. This information was based on CSPL's NaS7 and TD cell designs that contain materials and materials combinations pertinent to the present PB

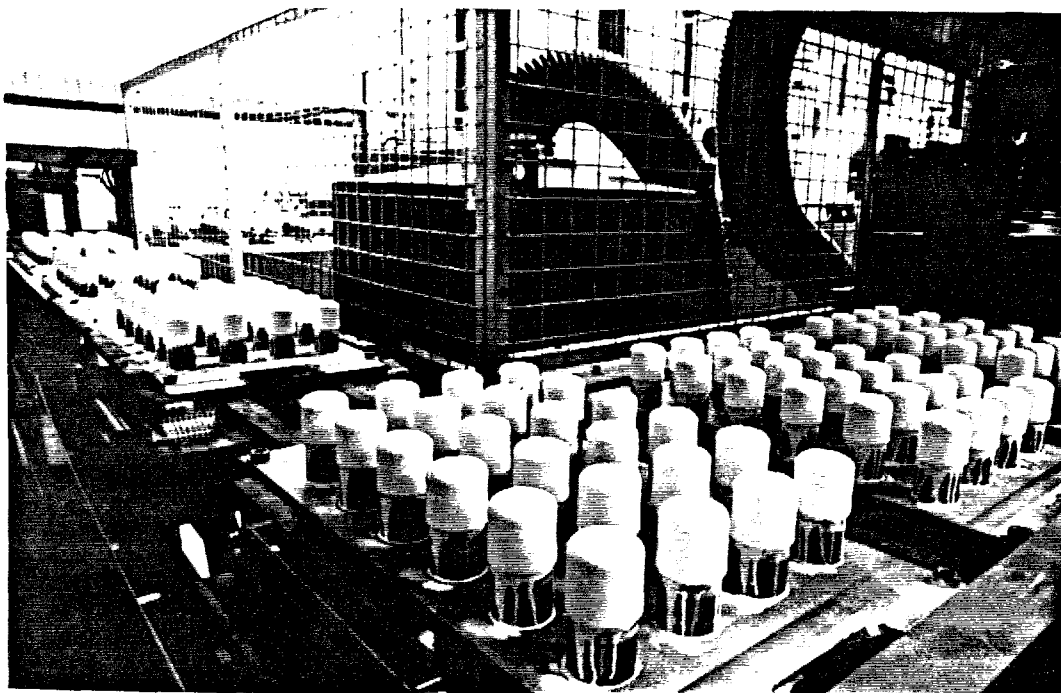


Figure 2-2. Automatic Electrophoretic Deposition Equipment

Table 2-1. Weibull Statistics for Zirconia Beta Alumina TD Cells

Population	Weibull Characteristic Life (cycles)	Weibull Modulus
With 5982	3900 9400 ^{23,000}	0.8 1.9 ^{4.5}
Excluding 5982	4200 7200 ^{12,000}	1.3 3.5 ^{9.2}
TD Reliability Group	1730 3485 ⁷⁰²⁰	0.5 0.8 ^{1.4}

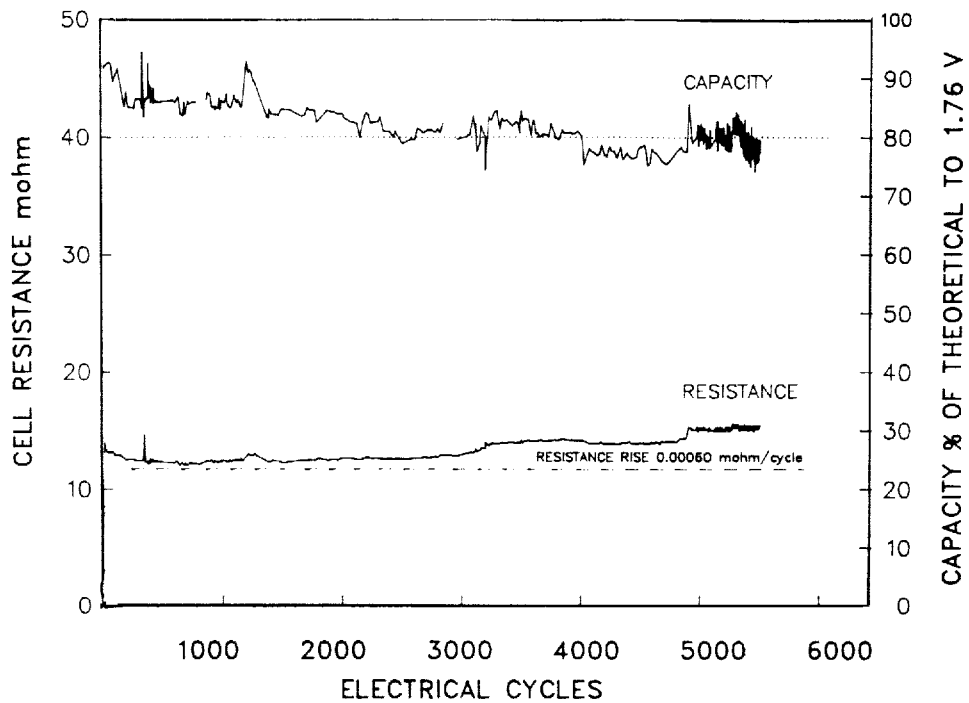


Figure 2-3. Capacity and Resistance of TD Zirconia Cell #5987

family of cells. The population has been on test for over 8000 electrical cycles during 1990, approaching 8 yr of operation.

Alpha-Alumina to Beta-Alumina Glass Seals

A glass joint is used to hermetically seal the alpha-alumina seal header to the beta alumina. CSPL's longest lived cell contains a barium aluminoborate glass modified with silica in a TD configuration. The cell contains two glass seals, one at each end of the electrolyte, and it had completed 8095 deep discharge

cycles to 1.76-V open circuit over 7 yr and 9 mo of operation. A graph of the cell resistance over the first 8000 cycles is shown in Figure 2-4.

The present composition, employed in all standard production cells, is also an aluminoborosilicate glass. This has been tested for 7,400 cycles in 62,376 hr.

During the reporting period, work on this subtask has concentrated on improving the intrinsic stability of the glass to sodium attack and on gaining further knowledge of the mechanism involved in failure. Two 120-cell banks were tested to assess the durability of

TD CELL 5601 AT 8000 ELECTRICAL CYCLES

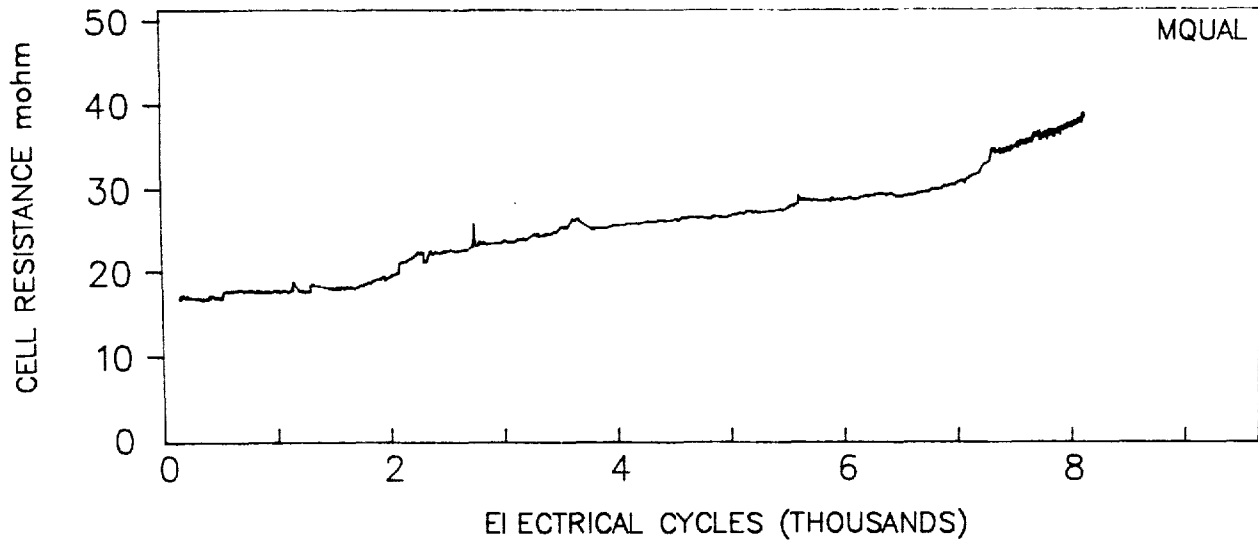


Figure 2-4. CSPL Long-Lived TD Cell - Resistance to 8000 Cycles

new glass formulations. The first bank (QB165) contains three glass variations and a set of controls and is being subjected to periodic thermal and routine electrical cycling. At the time of writing, it had completed 516 electrical cycles and 5 thermal cycles (to room temperature). The experiment has been successful in that a very promising formulation has been identified that has not failed during the test period. Cells of this group contain a new formulation of glass in combination with a variety of processing conditions and geometry. Of the 30 strings in the bank, 15 of the new formulation are still running while 14 of the less favored combinations have failed. The second bank (QB175) was removed from test after 217 cycles. Posttest analysis revealed electrolyte damage due to processing conditions unrelated to the glazing. The condition of the glass seals was good.

Posttest analysis has been conducted on individually tested cells containing new formulations of glass. Two compositions were tested in a total of 14 cells. The status of the cells is summarized in Table 2-2.

The posttest analysis of both the long-lived removals was encouraging, with evidence of enhanced glass durability. The exposed interfaces of one of the glass joints were apparently free of the preferential attack that has been observed in other glass joints.

In addition to the testing described above, finite element stress analysis is being conducted to assess the effect of seal shape upon stress levels. Microfocused radiography was also been used to examine seals in a nondestructive manner. This resulted in the highest quality X-ray images achieved to date, in which bubble size and distribution could be accurately assessed. Real-time imaging was also attempted, but with less success as the resolution was degraded too far. Further test work was conducted but led to the conclusion that the method was not capable of detecting incipient cracks. Despite this, the method has promise for examining other aspects of glass joint quality on a routine basis.

Metal-to-Alpha Alumina Seals

An experiment to test the MkIV seal concept was completed during the reporting period. A single cell of the original group of 14 remains on test at 1952 cycles. The Weibull statistics for the group of 14 cells is shown below.

Weibull Characteristic Life (cycles)	Weibull Modulus
1175 1451 ¹⁷⁹²	1.8 3.2 ^{5.9}

Table 2-2. Status of Experimental Glass Formulations

	Cycling	Removed	Failed
Composition A	1816, 1389, 1389	224, 224, 785, 1380	0
Composition B	1389, 1389	1380, 144 x 3	144

As a result of the extensive testing of the MkIV PB cells, the MkIV seal and its attendant materials and process specifications has been qualified and transferred to the XPB cell.

Sulfur Electrode and Fundamental Studies

CSPL routinely measures cell resistance by a current interruption method because of the inherent ease of data logging that this offers despite the limitations of the technique. The internal resistance of a cell is a critical parameter as it affects the energy efficiency, peak power output, and heat generation within the cell. Knowledge of how this parameter behaves under battery conditions is necessary to enable the design of thermal management systems. An ongoing study of the resistance of the CSPL cells was partly completed during the reporting period. The aim of this work is to accurately measure the true ohmic resistance of both the PB and XPB cells to provide data for thermal modeling.

The heat generated by a cell will arise from Joule's loss, the heat due to entropy changes, and Peltier heat. Polarized cells recover after the removal of load, so that entropic heating effects may not be coincident with Joule or Peltier heating. It is believed that the major contributor to heating will be Joule heating, which is dependent on the ohmic resistance of the cell.

The reactive components of impedance make no contribution to heat generation, and so in this context the term resistance is used in the true sense of the word, i.e., the real component of impedance. The simplest definition is then based on Ohm's law, and the cell resistance is the quotient of the difference between the equilibrium open circuit voltage (OCV) and the load voltage and the current flowing through the cell. The difficulty in determining the resistance in accordance with this definition is the measurement of the equilibrium open circuit voltage. The characteristic relaxation time for a CSPL sulfur electrode is of the order of 150 min, making experimental determination of cell OCV impractical. Accurate coulometry was used to

define an equation that relates the depth of discharge to the theoretical open circuit voltage.

Figure 2-5 shows the resistance of cell 11338 as a function of depth of discharge as calculated by this method. The resistance is constant over a large part of the two-phase region, and in the single-phase region it increases by some 40%. This implies that the rate of heat generation will be considerably greater in the single-phase region. However, it would be erroneous to use this resistance value in a thermal model. The so-called effective resistance, valid for power output modeling, combines ohmic resistance and polarization loss. The energy associated with polarization loss heats the cell when it is placed on open circuit. In EV applications, regenerative braking is frequently imposed on the battery immediately after the application of discharge load and the dispersion of polarization heat occurs in a complex manner. However, this might not be the case in an SES application where the battery might be removed from the load for a sufficient period for the majority of the polarization heat to be dissipated.

Also shown in Figure 2-5 is the resistance of the cell as measured by the CSPL current interruption technique for the cell undergoing a 5-hr discharge. This is a measure of the impedance of the cell measured at the fixed frequency (ignoring the harmonic distortion) of 0.05 Hz, and so also contains a reactive component that will have no effect on the internal heat generation. For the thermal analyses of cells it is necessary to evaluate the pure resistance of a cell both as a function of depth of discharge and current density while it is under load. This was conveniently achieved by making a small change in the discharge current and observing the resulting change in load voltage. This small change is effected by applying a low amplitude ac signal to the cell while it is discharging and monitoring the response using a phase-sensitive detector coupled to a lock-in amplifier. Figure 2-6 shows the impedance of the cell measured by this method for five discharge rates (which correspond to the C/1, C/1.33, C/2, C/3.33, and C/5). The reduction in resistance with increasing discharge rate is not solely attributable to temperature effects, as

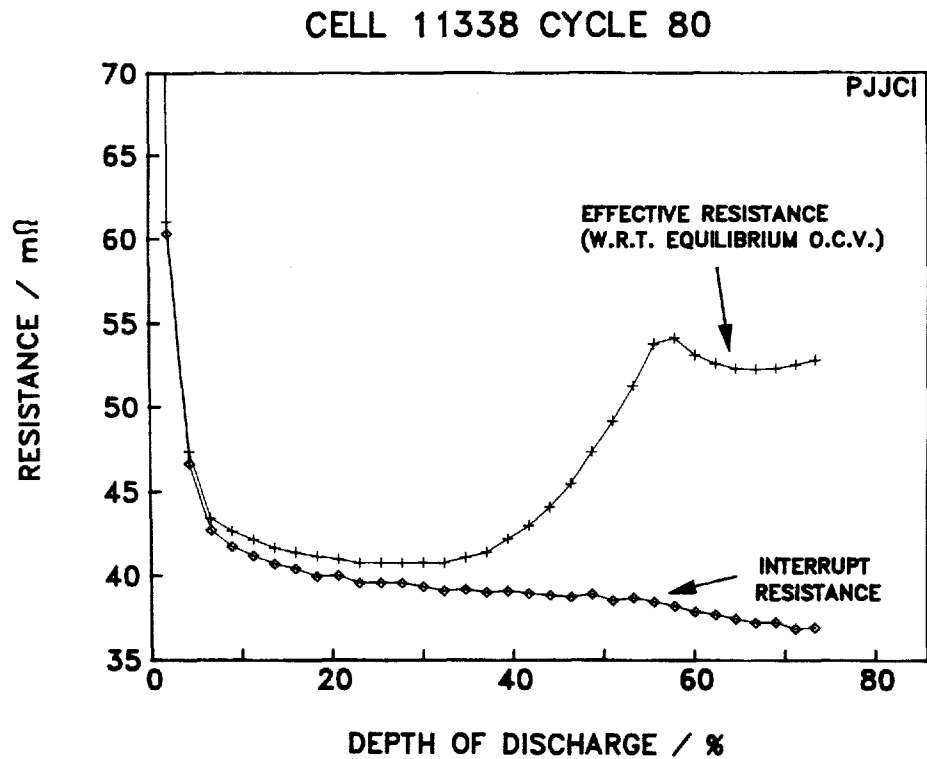


Figure 2-5. The Effective Resistance of the Cell Compared with the Interrupt Value, as a Function of Depth of Discharge

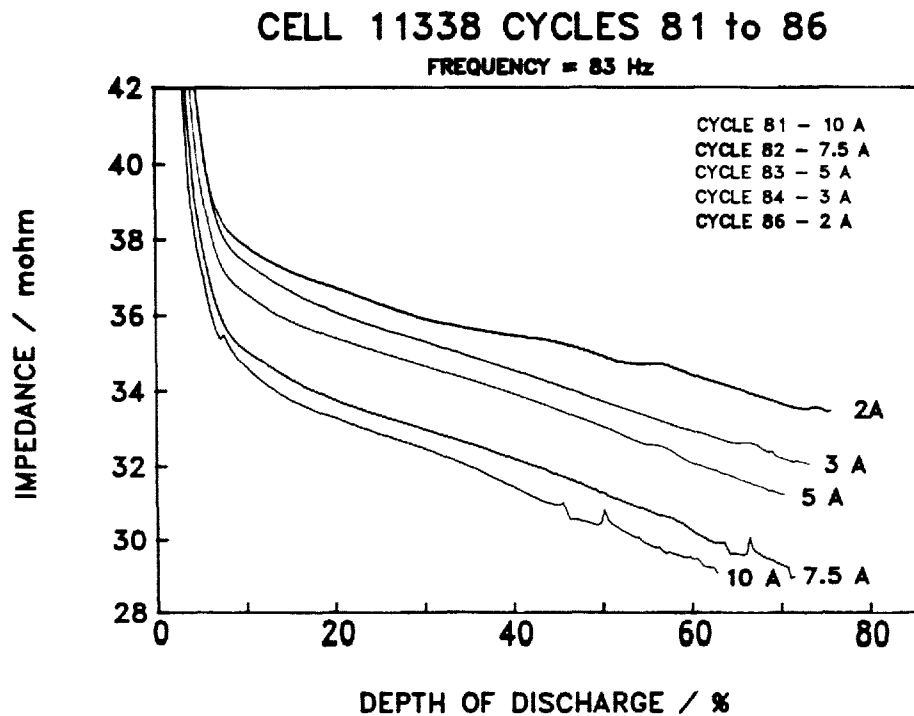


Figure 2-6. The Ohmic Component of Impedance as a Function of Depth of Discharge, Measured at Five Discharge Rates

even at the highest rate the temperature rise is less than 7°C. It has been shown that the resistance dependency on current density arises from increased polarization and the inherent conduction process within the carbon fibers of the sulfur electrode.

The heat generated during discharge will be less than would be calculated if the measured values of resistance, obtained by the interrupt method, are employed. The values reported here were obtained at a single frequency and for continuous discharge of a single cell. The work forms part of an ongoing program to map the impedance behavior of the PB cell throughout the current-density and frequency domains. XPB cells cannot be characterized in exactly the same manner because of power limitations on the equipment. However, it is proposed to characterize the sulfur electrode in the PB cell and verify the extrapolation to the XPB cell.

Subtask 1.3 - Cell Development

The objective of subtask 1.3 was to develop cell designs for both stationary and motive power applications, to establish the cell performance, reliability, safety, cost, and freeze/thaw survivability. The program changed emphasis during 1989 in that the main thrust became the XPB cell. During the reporting period, only XPB development work was conducted under the contract although the development of the PB cell is continuing under CSPL funding.

The state of the art of the PB cell developments funded by this program are best illustrated by the performance of the MkIII SF cell. A group of 17 cells was constructed as a forerunner population. These cells completed up to 2000 cycles and at the time of writing there had been 8 failures. The Weibull statistics of the cells are shown in Table 2-3 and are computed for both cycles and hours on test.

XPB Cell Development

During the reporting period, XPB cells (Figure 2-7) were produced in the CSPL manufacturing area rather than the R&D facility previously used. The output of XPB cells and their test destination is summarized in Table 2-4. The production history is illustrated in Figure 2-8.

A total of 78 single XPB cells are presently on test that include groups from builds made in 1989 (21), a build in January 1990 (19), a build in February 1990 of (21), and the remainder manufactured since March 1990 (17). A summary of their electrical characteristics is given in the Tables 2-5 to 2-9. (Note: Rc and Rd refer to cell resistance at 20% SOC for charge and discharge respectively. F or R designates a cell that has failed or been removed.)

Table 2-3. Weibull Statistics for 17-Cell MkIII SF Forerunner Group

	Cycles	Hours
Weibull Characteristic Life	1593 1924 ²³²⁴	14534 17321 ²⁰⁶⁴³
Weibull Modulus	2.18 3.88 ^{6.90}	2.34 4.21 ^{7.58}

Table 2-4. XPB Build Record, Jan 1988 - Mar 1990

Build Group	No. Cells Built	Cum Total	Test Destination
01-JAN-88	34	34	16-Cell Module
06-APR-88	4	38	Performance
10-MAY-88	20	58	Safe (10), Perf (10)
27-MAY-88	20	78	Diagnostic
09-JUN-88	20	98	Performance
21-JUN-88	20	118	Safe (10), Perf (10)
19-JUL-88	25	143	16-Cell Module
13-SEP-88	12	155	Performance
17-NOV-88	50	205	16-Cell Module, Perf (16), Safe (16)
21-MAR-89	17	222	Diagnostic
01-JUN-89	20	242	Performance
06-JUL-89	20	262	16-Cell Module
17-AUG-89	30	292	Performance
01-NOV-89	26	318	Performance
30-NOV-89	22	340	Performance
07-DEC-89	42	382	Not Tested
12-DEC-89	20	402	Performance
11-JAN-90	53	455	Not Tested
16-JAN-90	114	569	40-Cell Mod, Perf, Safe
01-MAR-90	263	832	200-Cell Battery



Figure 2-7. Part of Largest XPB Build to Date

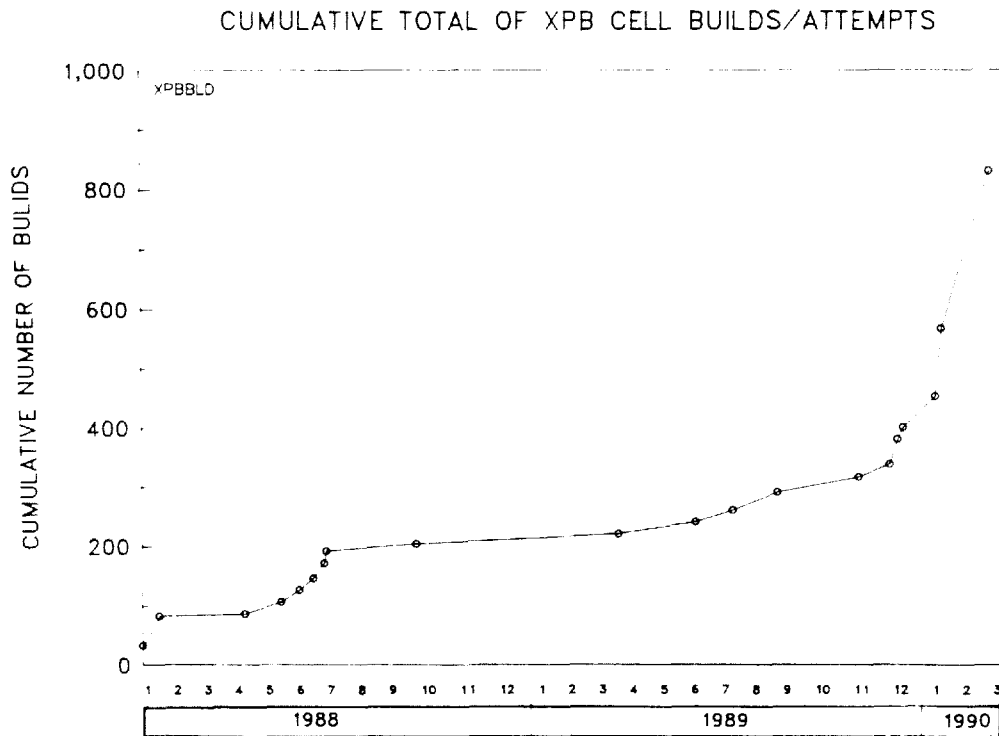


Figure 2-8. Graph of XPB Cell Output

Table 2-5. Status of Pre-Nov 1989 XPB Cells

Cell	Cyc	Temp (°C)	Rd (mΩ)	Rc (mΩ)	Cap (Ah)	Cap % Theo	Wh
10694	668	357.9	15.4	17.0	27.0	77.9	49.9
10696	668	355.1	12.7	12.9	31.0	87.3	—
10895	477	357.6	14.6	15.4	29.4	83.7	55.0

Table 2-6. Status of Nov 1989 XPB Cells (20 Cells, 2 Failures)

Cell	Cyc	Temp (°C)	Rd (mΩ)	Rc (mΩ)	Cap (Ah)	Cap % Theo	Wh
10952	303 F	355.2	11.2	11.7	32.4	93.4	61.6
10953	399	356.8	11.1	11.7	29.7	88.2	56.7
10954	399	355.9	11.5	12.1	30.2	88.5	57.4
10955	399	357.8	10.8	11.5	30.7	88.7	58.6
10956	399	356.3	11.0	11.6	30.4	89.8	57.9
10957	399	358.0	12.4	13.1	30.6	86.7	57.7
10958	290 F	356.2	11.5	12.5	33.4	94.9	63.4
10959	399	357.4	11.4	12.1	30.7	90.8	58.3
10960	399	356.4	12.3	13.0	31.1	87.3	58.9
10961	399	356.0	11.6	12.2	29.9	87.5	56.9
10962	399	355.8	12.9	13.4	31.4	90.2	59.3
10963	399	356.2	11.6	12.3	30.9	90.0	58.8
10964	399	356.7	11.6	12.2	30.7	89.6	58.2
10965	399	356.6	11.4	12.2	30.8	88.5	58.6
10966	399	357.7	11.4	12.1	30.5	89.9	58.1
10967	399	357.6	13.3	13.9	30.5	88.7	57.7
10968	399	358.4	10.4	11.0	29.4	88.2	56.2
10969	399	357.3	10.7	11.4	30.4	90.3	58.2
10970	399	358.7	13.3	13.4	30.8	86.6	58.4
10971	399	357.6	12.1	12.8	30.4	86.2	57.6
Mean Values =		357°C	11.68	12.30	30.75	89.19	58.42

Total cycles = 7775

Table 2-7. Status of Jan 1990 XPB Cells (22 Cells, 0 Failures)

Cell	Cyc	Temp (°C)	Rd (mΩ)	Rc (mΩ)	Cap (Ah)	Cap % Theo	Wh
11032	16 R	325.7	23.8	26.4	27.5	80.6	48.3
11033	305	337.5	14.5	14.9	29.0	85.1	54.1
11034	305	337.3	13.0	13.6	30.0	87.8	56.4
11035	305	338.4	15.2	16.0	30.0	87.8	55.6
11036	305	337.7	13.7	14.3	29.2	85.6	54.6
11037	305	335.8	12.3	13.2	30.5	89.5	57.6
11038	305	336.5	12.7	11.7	31.6	92.6	59.5
11039	305	337.2	12.7	13.2	29.6	86.8	55.8
11040	305	335.7	14.0	14.6	29.6	86.7	55.4
11041	300	336.6	13.1	13.7	29.5	86.4	55.5
11042	305	332.6	13.6	14.3	30.8	90.2	57.2
11043	16 R	335.6	21.2	22.9	28.7	84.1	51.3
11044	16 R	321.9	11.0	11.4	30.6	89.7	58.4
11045	305	334.4	12.5	13.2	29.5	86.5	55.7
11046	305	336.5	11.7	12.3	28.8	84.4	54.5
11047	305	336.5	12.1	12.6	29.8	87.3	56.4
11048	305	337.8	10.7	11.3	30.5	89.3	58.2
11090	269	340.2	14.8	15.7	29.4	86.6	54.5
11091	269	339.7	13.3	14.1	30.2	88.7	56.6
11092	269	340.4	13.8	14.5	29.9	87.9	55.9
11093	269	339.0	13.5	14.1	30.0	88.2	56.2
11094	269	338.8	13.5	14.2	29.0	85.4	54.5
Mean Values =		336.0	13.9	14.6	29.7	87.1	55.5
Total cycles =	5663						

Table 2-8. Status of Feb 1990 XPB Cells (25 Cells, 0 Failures)

Cell	Cyc	Temp (°C)	Rd (mΩ)	Rc (mΩ)	Cap (Ah)	Cap % Theo	Wh
11110	244	359.7	10.2	10.7	28.7	86.5	55.0
11111	115 F	358.1	10.6	11.1	30.7	92.5	58.6
11112	244	359.9	13.2	13.8	29.7	89.5	56.0
11113	244	359.3	12.3	12.8	29.4	88.7	55.6
11114	244	359.2	10.0	10.6	31.8	95.9	61.1
11115	245	358.2	11.2	11.6	30.0	90.2	57.1
11116	244	359.1	11.6	12.0	29.4	88.7	55.9
11117	244	357.5	10.4	11.2	29.4	88.4	56.2
11118	244	357.5	10.9	11.7	28.5	85.8	54.4
11119	244	358.1	13.1	13.8	28.7	86.4	54.1
11120	244	357.3	13.1	14.0	29.0	87.2	54.5
11121	243	357.0	9.9	10.4	30.7	92.5	59.0
11122	244	357.8	10.2	10.7	29.6	89.2	56.8
11123	199 F	358.4	9.7	10.2	29.7	89.5	57.1
11124	243	358.6	11.1	12.1	29.4	88.6	56.1
11125	244	358.1	11.2	12.0	29.8	89.7	56.6
11126	244	359.5	11.0	12.1	30.2	90.9	57.4
11127	78 F	356.0	12.4	13.2	29.5	88.9	55.8
11128	244	359.5	10.6	11.3	29.7	89.5	56.8
11129	244	359.9	13.9	14.6	30.6	92.1	57.4
11130	244	359.6	12.4	13.2	30.6	92.3	57.9
11131	244	357.9	10.9	11.5	31.5	94.9	60.2
11132	244	359.4	12.3	12.9	30.7	92.3	58.0
11133	225	360.22	10.9	11.5	28.9	87.0	54.8
Mean Values =		358.6	11.4	12.0	29.8	89.9	56.8
Total cycles =	5496						

Table 2-9. Status of XPB Cells Built Since Mar 1990

Cell	Cyc	Temp (°C)	Rd (mΩ)	Rc (mΩ)	Cap (Ah)	Cap % Theo	Wh
11134	113	356.8	12.8	13.6	29.5	89.0	55.7
11135	113	359.8	12.5	13.1	27.5	82.9	52.1
11136	43 F	342.1	11.4	11.8	29.9	90.2	56.8
11157	179	341.2	14.7	15.4	27.8	83.8	51.7
11158	179	335.6	13.1	13.8	28.2	84.9	52.9
11159	179	336.3	13.0	13.4	28.1	84.6	52.7
11160	179	339.8	14.9	15.7	28.7	86.4	53.0
11161	180	359.1	14.0	14.2	28.3	85.2	53.2
11162	98	339.7	15.0	14.7	29.7	89.5	55.2
11163	98	339.4	15.1	15.3	28.5	85.8	52.9
11164	98	338.8	16.1	14.9	29.8	89.9	55.1
11165	98	339.3	13.9	14.2	29.4	88.6	54.9
11166	98	339.2	15.6	15.7	29.6	89.2	54.8
11167	98	338.7	15.3	14.9	29.3	88.2	54.3
11168	98	339.2	13.0	13.4	29.5	88.8	55.2
11169	98	340.1	14.9	14.4	30.3	91.2	56.0
11170	98	338.3	15.7	15.5	29.0	87.3	53.7
11171	98	340.2	15.4	15.7	28.8	86.6	53.2
Mean Values =		342.4	14.2	14.4	29.0	87.3	54.1

Total cycles = 2145

XPB Reliability

An estimate of XPB cell reliability has been made using 4 groups of XPB cells that have been tested since October 1989; the data for the groups are indicated in Table 2-10.

Table 2-10. XPB Cell Reliability

Group	No. in Group	No. Failed	No. Removed	No. Cycling
Oct '89	19	1 @ 116	(1 @ 145) (17 @ 151)	0
Nov '89	20	1 @ 290 1 @ 303	0	18 @ 399
Jan '90	22	0	3 @ 16	14 @ 305 5 @ 269
Feb '90	25	1 @ 78 1 @ 115 1 @ 199	1 @ 1	20 @ 244 1 @ 225
Total	86	6	22	58

The Weibull reliability characteristics of the above cell groups are as follows:

XPB Single Cells (n = 86)

Characteristic Life $415 \ 1367^{4507}$ cycles
Weibull Modulus $0.8 \ 1.63^{3.33}$

Reliability analysis has also been undertaken using data from a 40-cell XPB module, in which a failure occurred at cycle 296. The analysis for the combined 122 XPB cells, (86 single + 36 battery), is given below:

XPB Single and Battery Cells (n = 122)

Characteristic Life $462 \ 1408^{4283}$ cycles
Weibull Modulus $0.9 \ 1.79^{3.5}$

The XPB reliability figures based on the above groups compares quite favorably with the current MkIV PB cell reliability, the most recent characteristics for a group of 189 cells are:

MkIV PB Single Cells (n = 189)

Characteristic Life $684 \ 1866^{5090}$ cycles
Weibull Modulus $0.97 \ 1.6^{2.65}$

It may also be significant that none of the 22 XPB cells in the January group has failed. These are operating at a nominal 330°C.

XPB Safety Testing

Safety tests were completed on 12 cells from the 16-cell XPB Module (B136), all of which failed in a benign manner with temperature excursions between 30 and 79°C. The cells had been given more than 200 electrical cycles and 8 freeze/thaw cycles prior to the safety testing, details of which are given in Table 2-11. A total of 57 XPB cells were safety tested. There were two instances of cell leakage, representing a 3.5% failure rate. In order to further reduce this percentage, several approaches are being worked on, all of which aim to reduce the volume of sodium available upon fracture of the electrolyte.

Table 2-11. Safety Tests on B136 XPB Cells

Test No.	Tmax (°C)	ΔT (°C)	Breakdown Voltage
1	373	30	50
2	404	74	55
3	391	52	55
4	424	70	55
5	403	45	55
6	399	49	43
7	402	46	50
8	437	79	55
9	370	38	43
10	359	28	30
11	378	54	45
12	379	51	46

Subtask 1.4 - Cell Test and Posttest Analysis

The objective of this subtask was to provide test support and posttest analysis for other subtasks and as such the effort is reported elsewhere in this document.

Subtask 1.5 - Module Testing

The objective of this subtask was to develop and test sub-modules of larger battery designs in order to explore the interactions of cell connection strategy and to test groups of cells against application-specific requirements. Other objectives were to study the effect of cell failure interactions and the effect that varying cell performance has in an interconnected group of cells. More than 150 modules had been constructed by the end of 1989, the majority of which were in 120-cell units.

XPB Module Testing

The initial performance of a 16-XPB cell bank, designated B136 was reported in the ETD report for 1989. This bank, which utilized an air-cooled design, completed its electrical testing after 252 cycles. At this time a decision was taken to cease electrical cycling of the module in view of its rising resistance. This rise was subsequently isolated to an electrolyte batch and the source of the problem was eliminated. In order to max-

imize the information from the module, it was placed on freeze/thaw cycling and completed 8 such cycles with no failures detected.

Thermal management studies being conducted under Task 2 led to the concept of a close-packed XPB module design and it was considered desirable to test such a unit. A 300-Ah, close-packed, 40-cell XPB module is shown in Figure 2-9 alongside a standard 120-PB-cell monobloc. Both these units are 300-Ah, 8-V nominal and can be tested in the new CSPL Bank Testing Facility. The XPB module was assigned the number B189 and had completed 500 cycles at the time of writing.

The module exhibited a cycle vs resistance pattern that was characteristic of XPB cells produced at that time. This was typified by a slight rise in resistance over the first 20 cycles followed by a gradual decline and stabilization. The effect was isolated to an impeded gettering action during the early cycles. Diagnostics confirmed the suspected cause that involved the processing of the getter during cell manufacture. The resistance and capacity are shown in Figures 2-10 and 2-11. String 8 of the bank failed to start up and the suspected cause is a failure of an electrical connection. However, as firm diagnosis could only be obtained by cooling the bank. It was decided to leave the bank run-

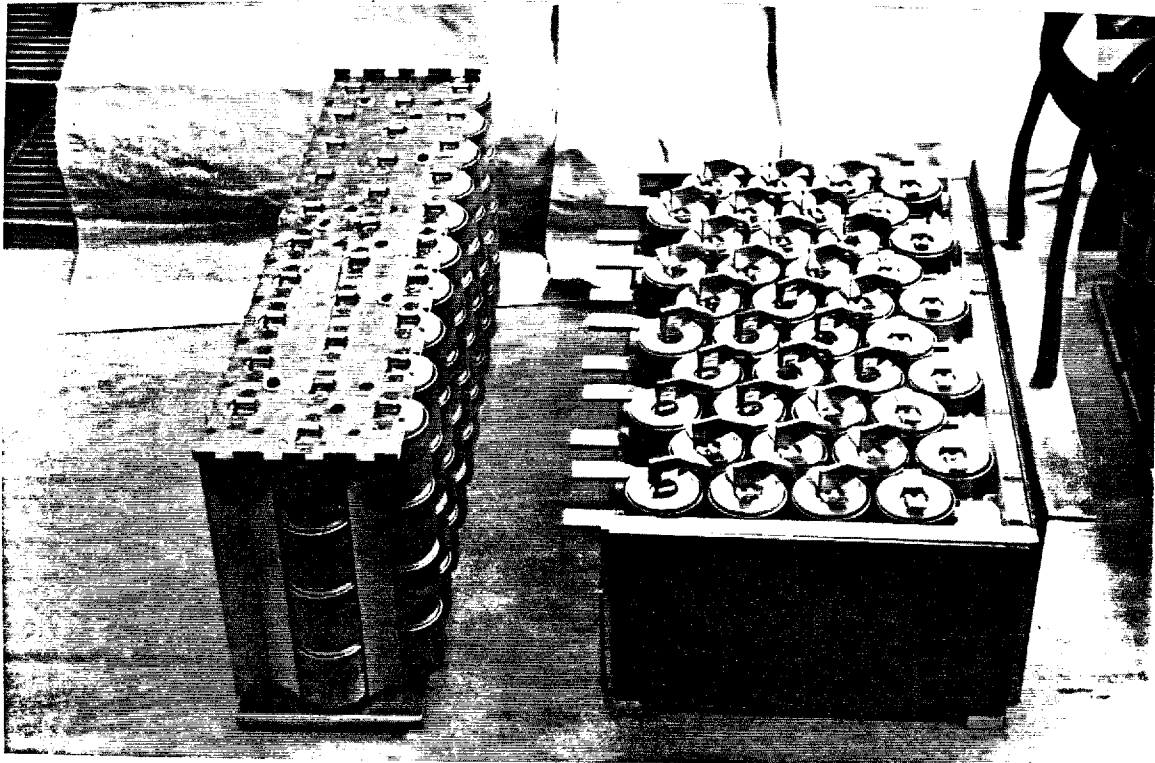


Figure 2-9. Close-Packed PB Module (left); Close-Packed XPB Module B189 (right)

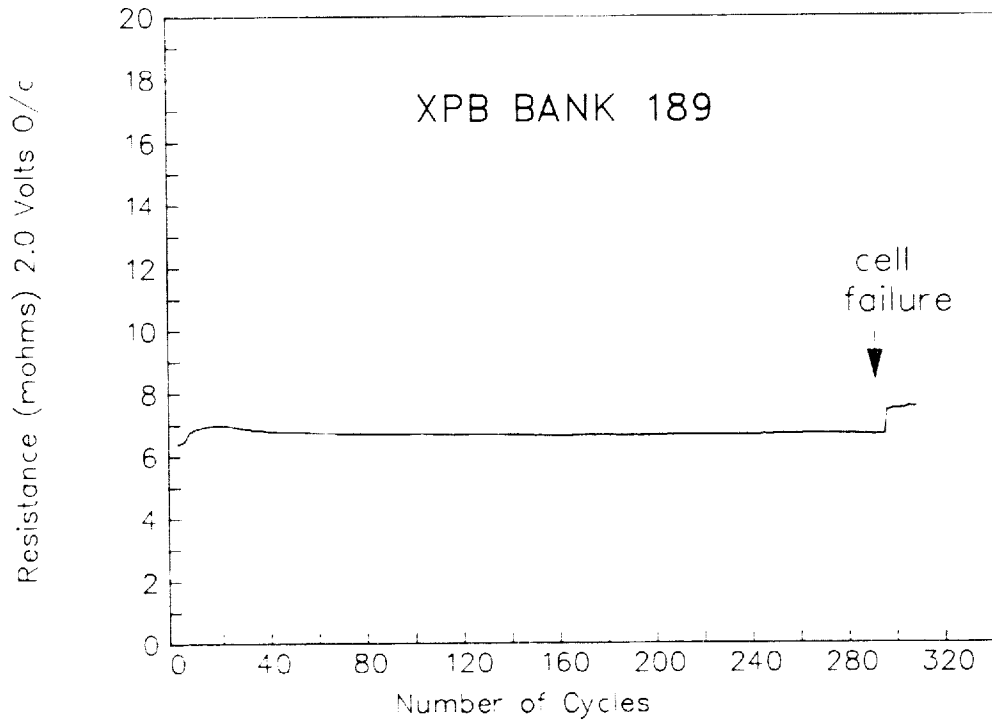


Figure 2-10. Resistance of Bank B189

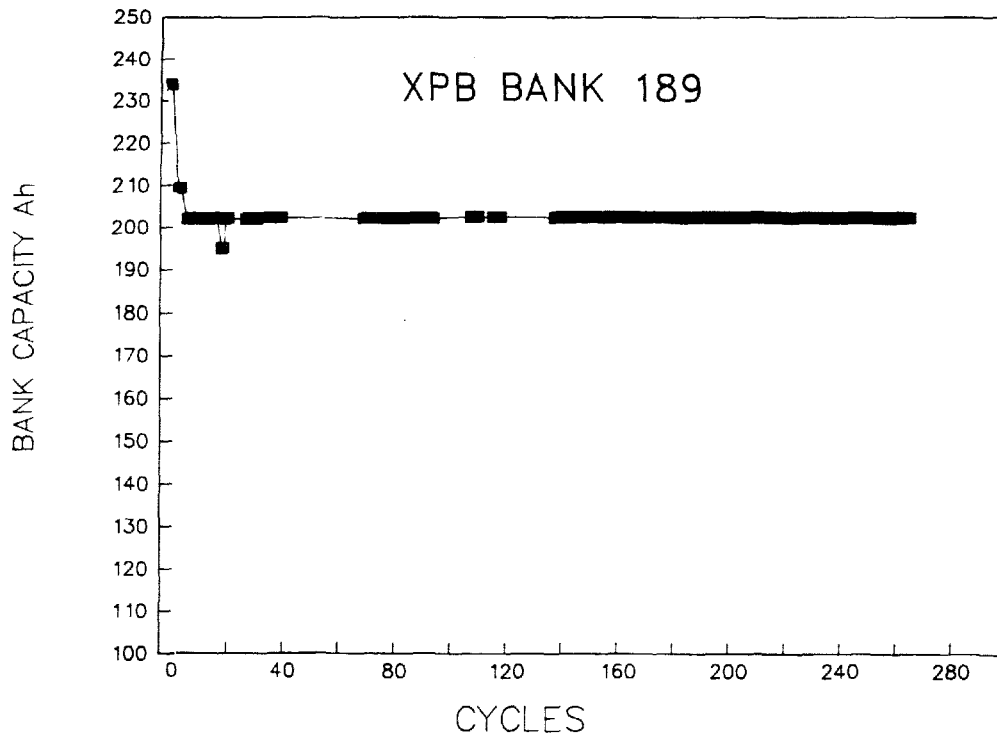


Figure 2-11. Capacity of Bank B189

ning as a 9-string unit. The capacity graph has been adjusted to account for the missing string.

In other respects the performance of the bank was satisfactory. The plots shown in Figure 2-12 indicate an almost complete lack of recharge polarization and the discharge resistance within a cycle is stable. A full thermal analysis had not been completed at the time of writing because the data logging system was not fully integrated with the computer data base. However the manual analysis of data indicated a 26°C temperature rise on discharge, compared to a rise of approximately 10°C in a typical single cell test at the same rate of discharge. The bath temperature was lowered on cycle 5 to reduce the maximum discharge temperature. This caused a slight, step rise in resistance. The increased ΔT is due to the high packing density of cells and some modifications have been made to the design of the busplate system for the subsequent modules presently under construction. By this means, it is hoped to improve the convective air circulation within the module.

Task 2 - Battery Engineering and Testing

Subtask 2.1 - Battery Design

SES Battery Design

During 1990, Beta Power completed a more detailed analysis of the conceptual design that was reported in the 1989 ETD Annual Report. The original intent of this Task 2 activity was to investigate alternate thermal management system (TMS) design approaches. The specific objective was to reduce the capital cost and operating expense associated with this component of SES battery systems. What emerged from this study was an entirely new TMS concept that not only promises to achieve the desired lower cost but also significantly reduces the overall facility footprint.

Background

The baseline battery design used in the TMS studies reported in the 1989 ETD Annual Report was developed for a load-leveling application under an EPRI-sponsored

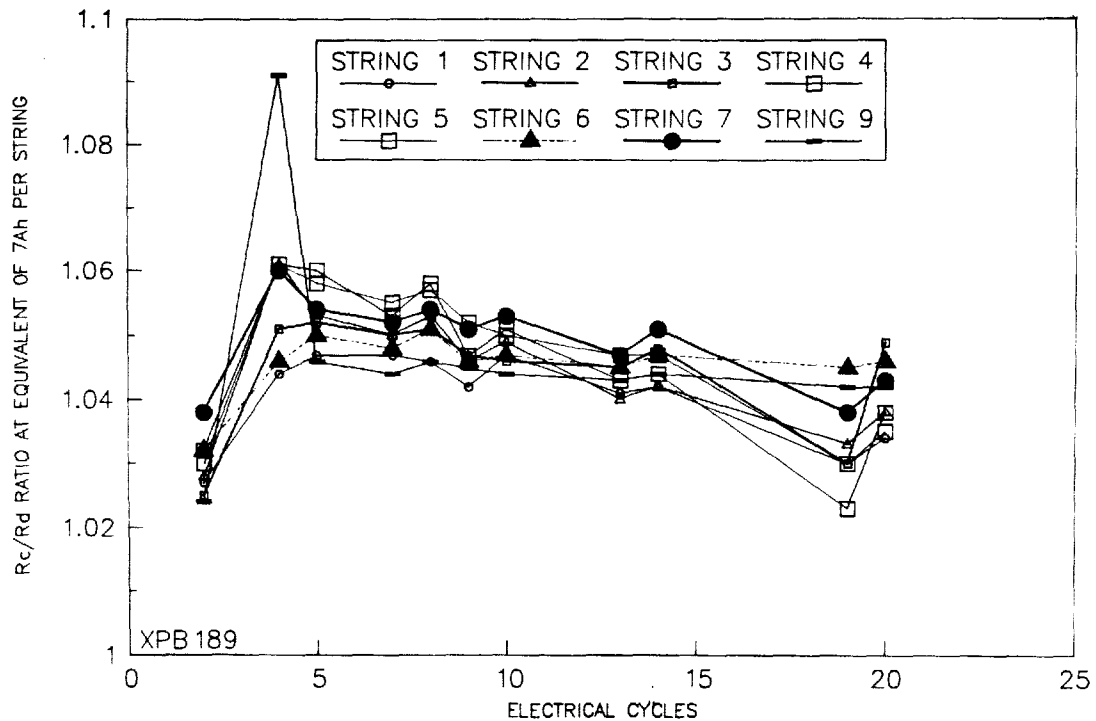


Figure 2-12. Rc/Rd Plots of Strings from XPB Bank B189

program. This design utilized a self-contained thermal management system. The self-contained TMS design called for three separately housed 2000-V, 10-MW unit batteries, each consisting of 28 5-ft-square by 10-ft-high, 10,000-lb battery modules. Modules were grouped in clusters of four, with each cluster being thermally managed by one closed-loop TMS that provided both heating and cooling. Air was directed horizontally through trays of cells, where high resistance to flow resulted in large pressure drops and accompanying high parasitic blower losses.

An artist's concept of this 100-MWh Sodium/Sulfur Load-Leveling Battery Facility is shown in Figure 2-13, a self-contained TMS four-module cluster in Figure 2-14, and arrows representing the horizontal flow of air through both a module cross section and a cell tray are shown in Figure 2-15.

Monobloc Module

A new approach suggested for thermal management of the load-leveling sodium/sulfur battery plant is based upon the premise of localized heating and shared vertical flow cooling of densely packed "monobloc" (MB) battery modules. The size of the MB module has been dictated by both handling and thermal considerations

and approximates a standard 6500-Ah submarine battery. The cells within the MB module are networked as a complete parallel array. They are mounted in eight vertically stacked series-connected trays of 72 parallel cells per tray. Each tray is independently supported and electrically isolated from the module frame and housing. Compliant tray interconnects consist of looped sheet metal strips spot-welded to a cell current collector below and a tray bottom above. For initial warm-up or after extended periods of inactivity, heating is effected at the MB level by way of cartridge or blanket heaters that are integral to each module. Cooling of MB modules is accomplished by directing air flow vertically in a single pass over the modules' outer skin, which is constructed of corrugated mild steel sheet. The use of single-pass flow eliminates the complex mixing and control necessary when utilizing blended recirculating air.

An artist's concept of the 2-ft-square by 4-ft-high, 800-lb MB battery module is shown in Figure 2-16. Internal features of the MB module are shown in Figure 2-17 by a side view in which front and rear skins have been removed, as well as in Figure 2-18 by a plan view in which the top cover has been removed. Specifications for the MB module are shown in Table 2-12.

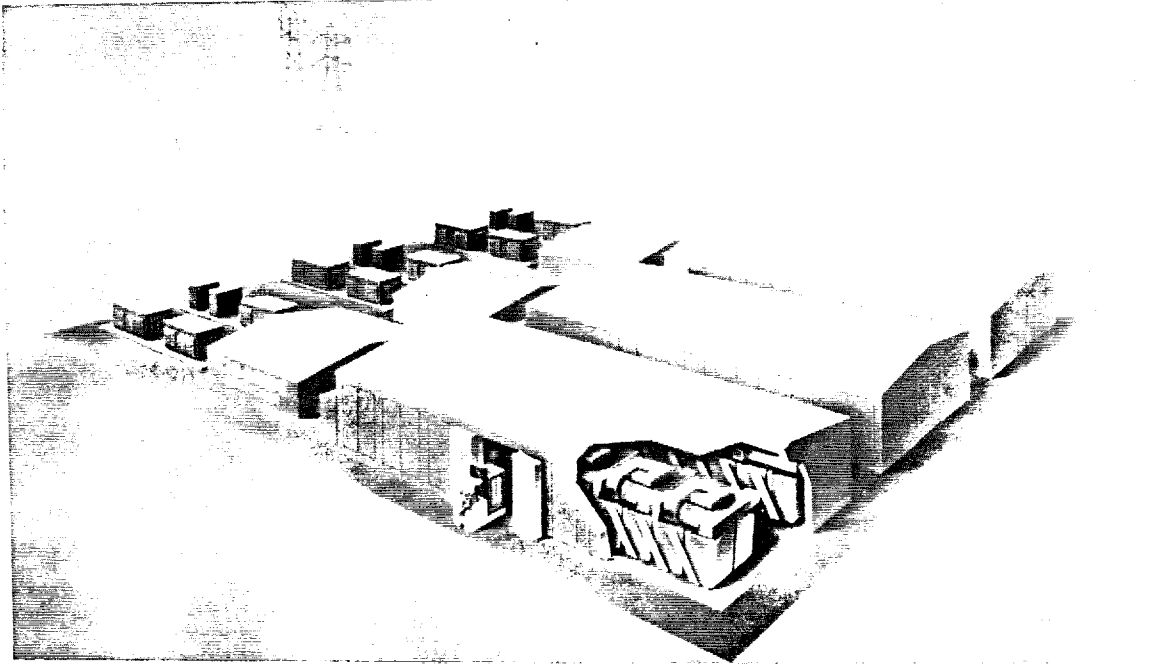


Figure 2-13. Artist's Concept of the 100-MWh Self-Contained TMS Sodium/Sulfur Load-Leveling Battery

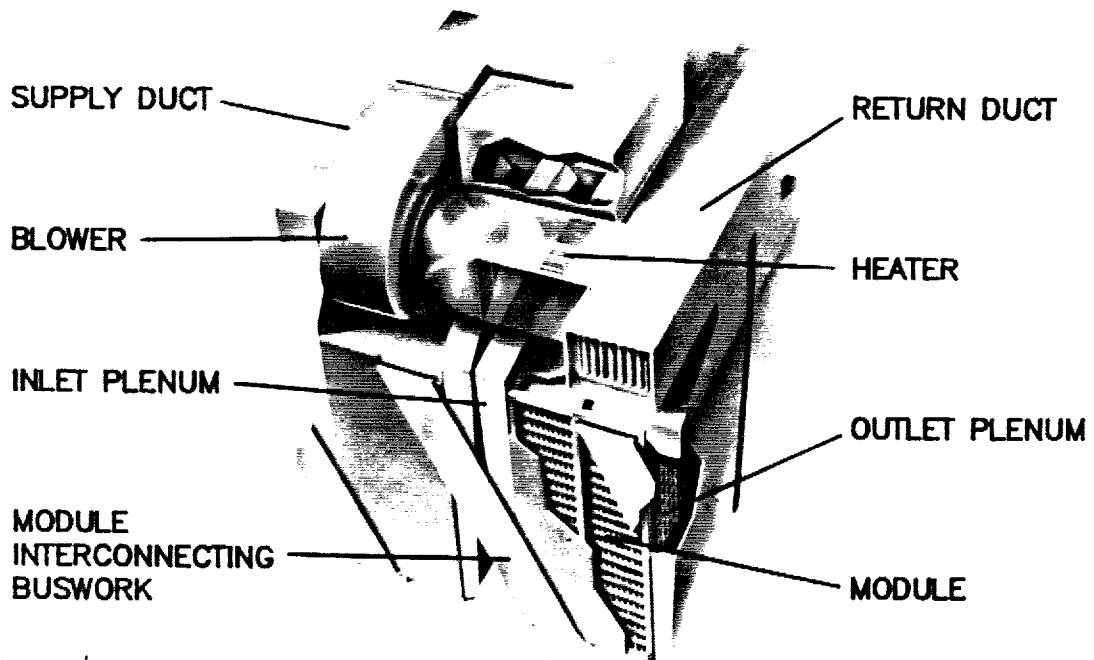


Figure 2-14. Artist's Concept of a Self-Contained TMS Four-Module Cluster

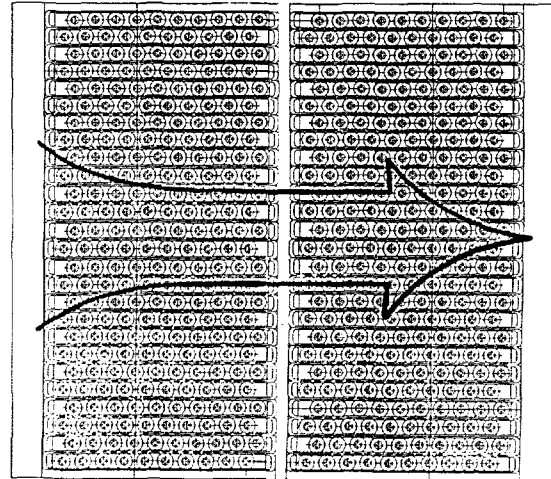
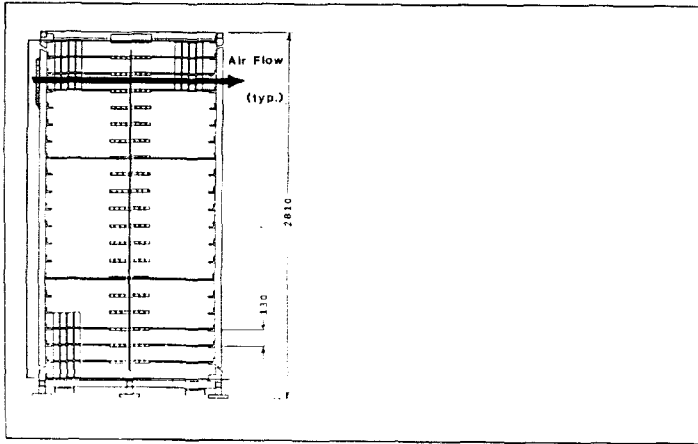


Figure 2-15. Typical Horizontal Flow Through Self-Contained TMS Module Cross Section (left) and Over Plan View of Cell Tray (right)

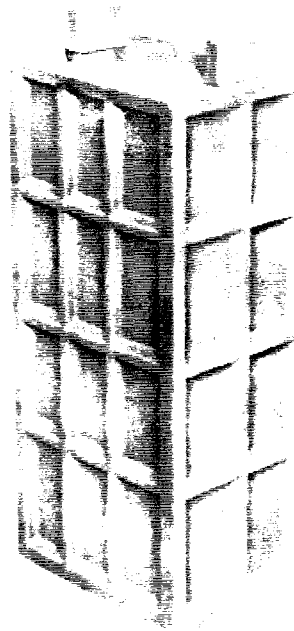


Figure 2-16. Artist's Concept of an 800-lb Monobloc Battery Module

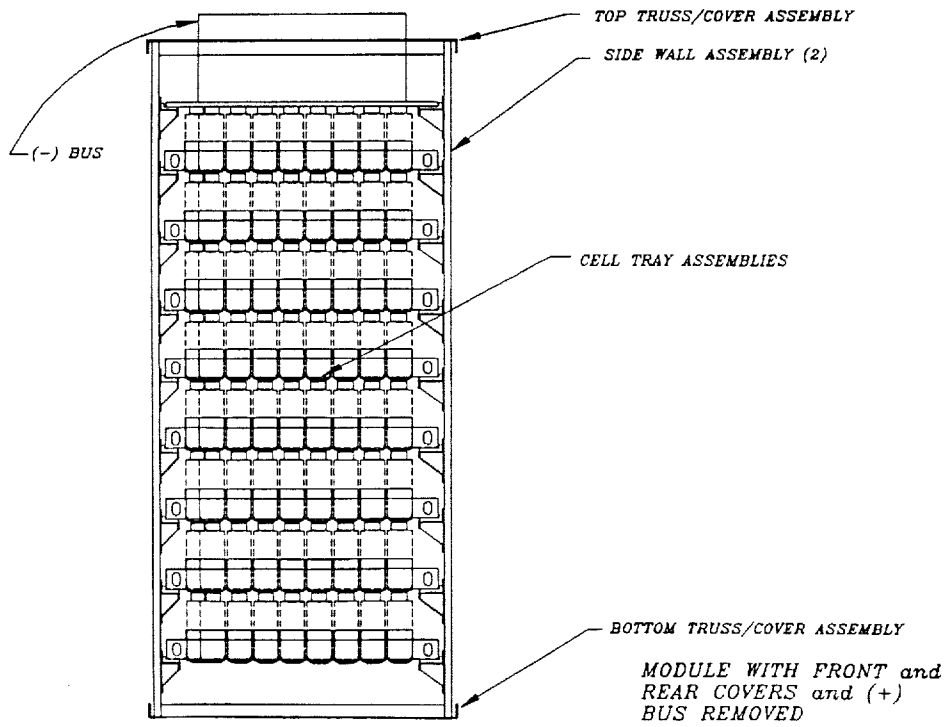


Figure 2-17. Section View of Monobloc Battery Module (Vertical)

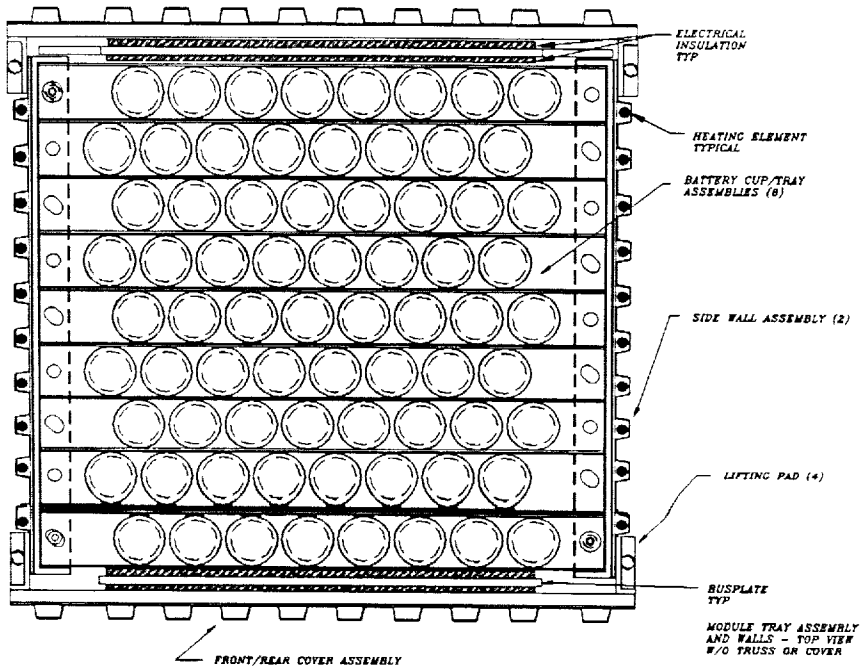


Figure 2-18. Section View of Monobloc Battery Module (Plan)

Table 2-12. Monobloc Module Specifications

Design Consideration	Specification
1. Description	Includes internal interconnects, external interconnects to unit battery, structural casing, and integral heaters.
2. Capacity - Beginning of Life (BoL)	51.1 kWh
3. Voltage - Nominal	16 V
4. Network Arrangement	8 trays of 72 parallel cells
5. Dimensions - Max. <ul style="list-style-type: none">- Height- Width- Depth	4 ft 2 ft 2 ft
6. Weight - Max.	800 lb
7. Module-to-Module	Cable Interconnect
8. Installation	Fork lift transportable. Installation from above by overhead maintenance crane.
9. Transportation	Shipped via common carrier without special permit.
10. Isolation	Electrically isolated from frame and ground.

Dense Pack Battery Design

The MB modules are densely packed within a single battery building as thermally isolated series strings with 144 modules per string. Access for MB module maintenance and replacement is from above via a track-mounted mobile crane system. Integral with the battery building slab on grade foundation are 1-ft-high cylindrical pylons upon which the MB module corners rest, thereby supporting all of the modules a sufficient distance above the floor to create a plenum into which ambient air is introduced and subsequently drawn upward to cool the modules. Approximately 1 in of free space is left open between the rows of densely packed MB modules, and it is through these openings between the rows of modules that cooling air is drawn from the plenum below. Five of the 144 module series strings form a unit battery, and each unit battery is connected to one of the facilities three Power Conditioning Systems (PCS). As air flows vertically upward past the modules, it picks up heat transferred from the module skins and exits above the modules. Five roof mounted fans extract heated air from another plenum above the modules, driving the air flow for the entire battery facility.

An artist's concept of the dense pack load-leveling battery building, its module strings, and its overhead maintenance crane is shown in Figure 2-19. A plan view of a thermally isolated 144-module series string indicating the arrangement of MB modules, location of inter-row air paths, and the isolating thermal insulation is shown in Figure 2-20. A plan area layout for the dense-pack load-leveling facility including PCS enclosures, skid-mounted transformers, and the parallel interconnection forming each of the unit batteries and connecting it to its PCS is shown in Figure 2-21.

Flow control of the air is accomplished at the module series string level by thermal shutter assemblies. There is one shutter assembly mounted above each 144-MB module series string. By varying the shutter opening, the volume of air allowed to pass upward between the modules is controlled independently for each thermally isolated module string.

Both side and perspective views of these shutters in the full closed position are shown in Figures 2-22 and 2-23, and in the full open position in Figures 2-24 and 2-25, while specifications for the 100-MWh Sodium Sulfur Utility Load Leveling Battery Plant are given in Table 2-12.

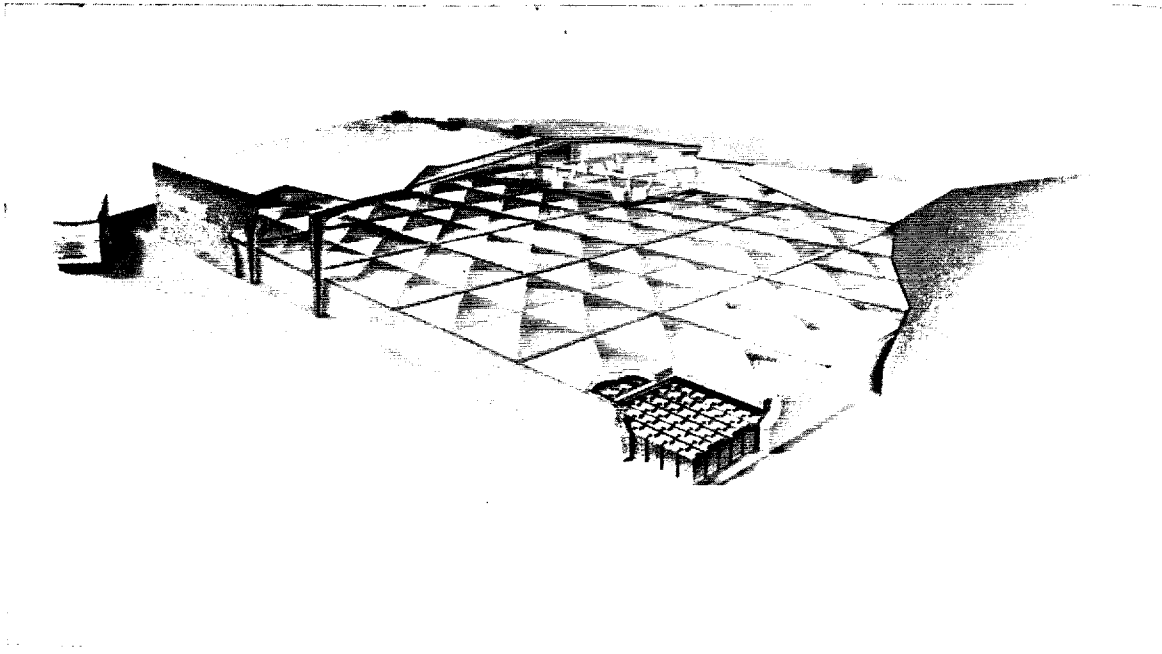


Figure 2-19. Artist's Concept of Dense-Pack Sodium/Sulfur Load-Leveling Battery Facility

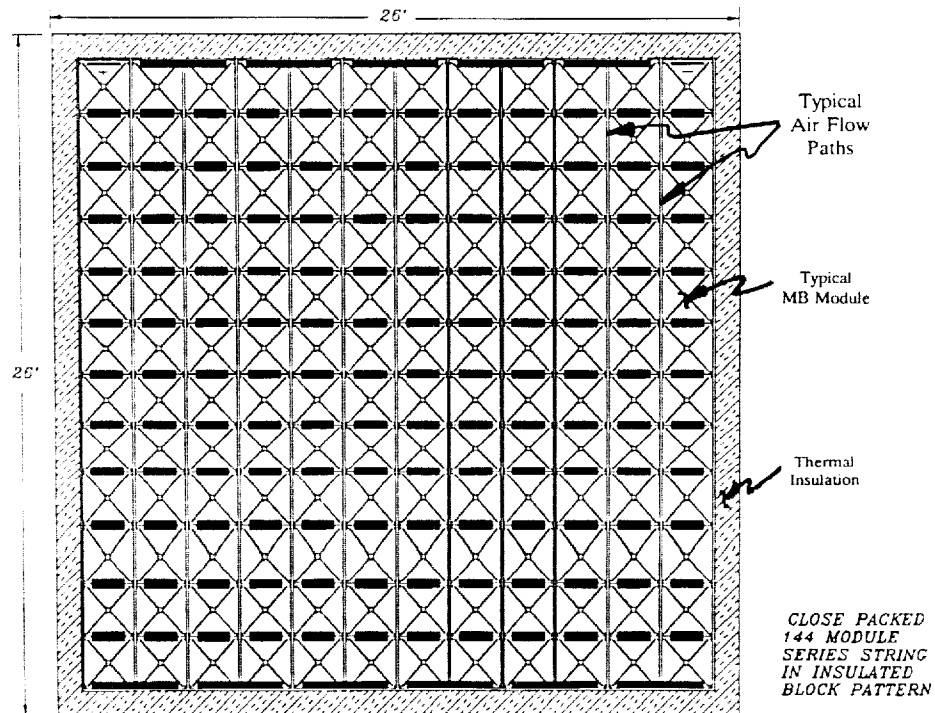


Figure 2-20. Plan View of Thermally Isolated 144-MB Module Series String

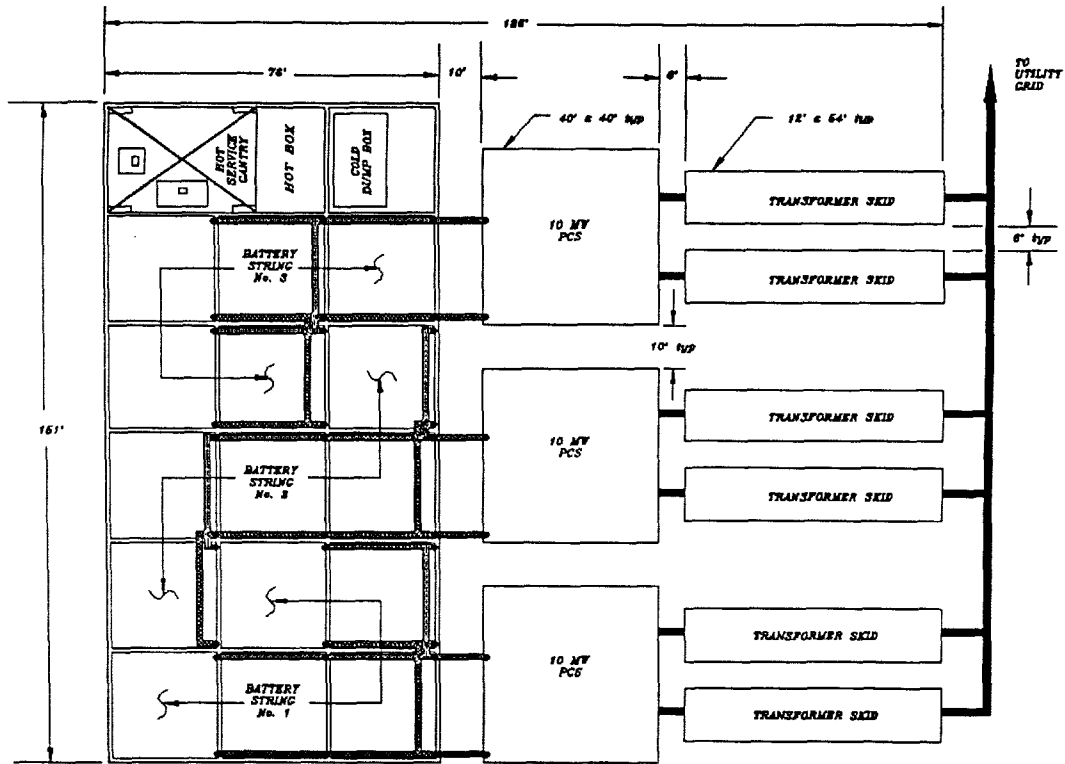


Figure 2-21. Plan Area Layout for the Close-Packed Module LL Battery Plant and Power Conditioning Equipment

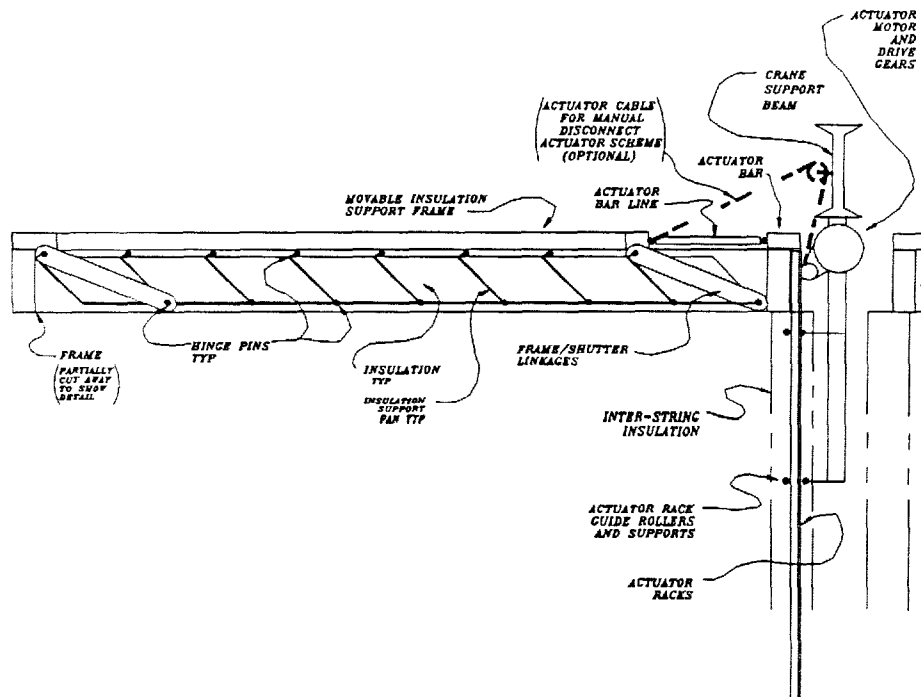


Figure 2-22. 144-Module Series String Thermal Shutter Closed (side view)

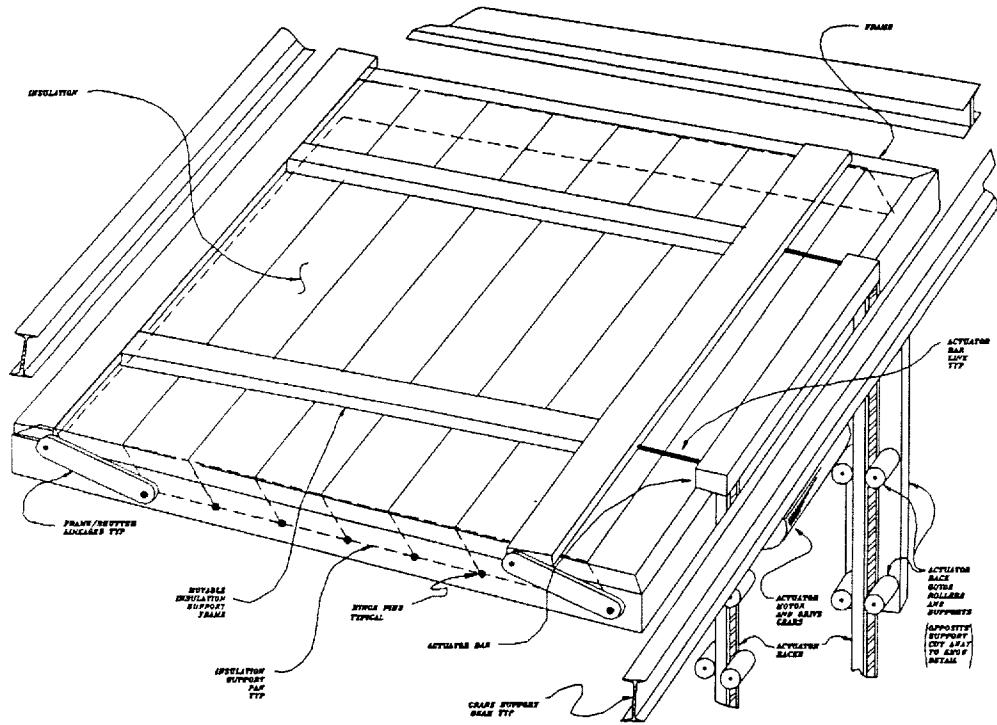


Figure 2-23. 144-Module Series String Thermal Shutters Closed

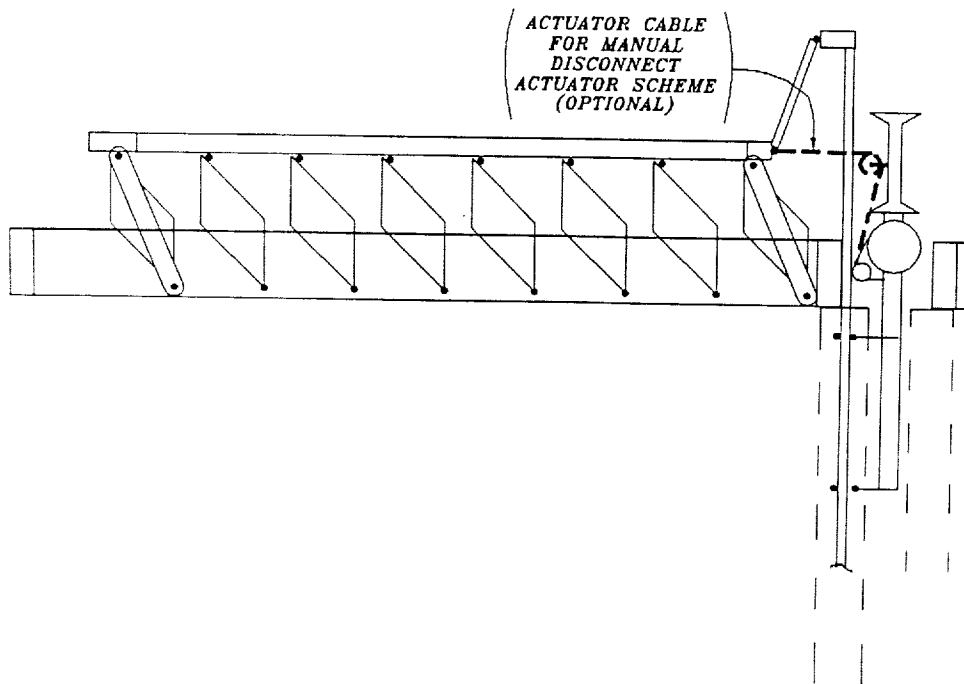


Figure 2-24. 144-Series String Thermal Shutters Open (side view)

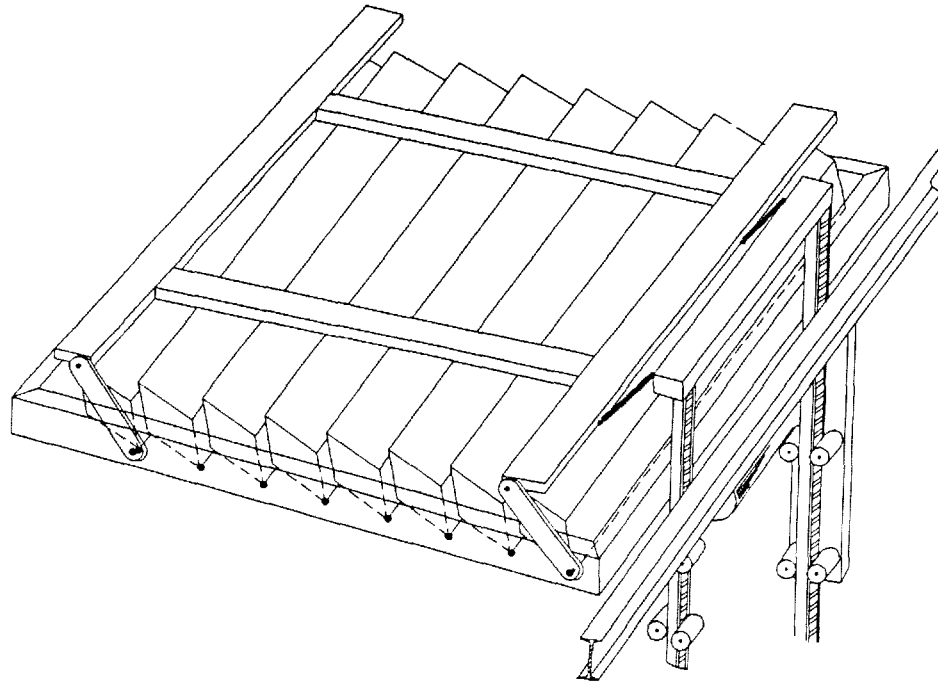


Figure 2-25. 144-Module Series String Thermal Shutters Open

Table 2-13. Sodium/Sulfur Battery Plant Specifications

Consideration	Specification
1. Capacity - Nominal	100 MWh
2. Voltage - Nominal	2000 V
3. AC Voltage Rating	13.8 kV, $\pm 5\%$
4. Configuration	3 - 10 MW Inverters
5. Duty Cycle	Constant power discharge for 3-1/3 hr; Constant power charge for 7 hr
6. Operating period	5 days/wk 50 wk/yr
7. Life	30 yr

Monobloc Module Thermal Analysis

When the preliminary design of the monobloc mechanical layout was completed, a thermal analysis was undertaken to determine if the proposed thermal management concept was viable.

Thermal control is necessary because constant power operation at 15-kW/hr for 3-1/3 hr generates 7-1/2 kWh of heating due to ohmic and entropy effects. Some of this heat must be lost in order to limit the maximum cell temperature to the prescribed 370°C. In this monobloc module/dense-pack battery design, air does not pass over or otherwise interact directly with the cells. Rather, heat transfer within the MB module is realized primarily via radiation from cell-to-cell and cell-to-wall, with excess heat removal occurring at the periphery of the module via vertical air flow. At the surface of the module, combined free and forced convection effects are present, with forced convection enhancing free convection heat transfer.

Figure 2-26 provides a schematic plan view of cells, a module wall, and the air column adjacent to the module, indicating the cell-to-cell and cell-to-wall radiation heat transfer coupling assumed in this analysis. Figure 2-27 represents heat transfer from the cells to the air flow between sections of the corrugated steel module wall and additionally shows calculation of

the hydraulic diameter used in determining heat transfer characteristics.

Due to the importance of radiation heat transfer in MB module design, a sensitivity study was performed in order to determine directly the effect that varying cell surface emissivity (ϵ) has upon cell-to-cell temperature differences and, therefore, indirectly the effect of this variation upon radiation heat transfer.

It was found that increasing the surface emissivity of the cells improved cell-to-cell radiation coupling and enhances cooling of the cells because heat generated by the cells is more readily transferred from cell-to-cell and cell-to-module wall. Results of the emissivity sensitivity study showing cell-to-cell temperature differences at selected cell surface emissivities are shown in Figure 2-28. Note the maximum 62° variation at $\epsilon = 0.3$, vs the reduction to a maximum 38° variation at $\epsilon = 0.95$ at tray number 1.

Finally, a finite element thermal analysis (FETA) was performed, assuming a cell surface emissivity of 80%. In the finite element model (FEM), cells are modeled as nodes and assigned the heat generation and capacitance values of XPB cells. Radiation was linearized and coupled with convection and conduction heat transfer coefficients to determine an equivalent conduction coefficient. This coefficient was then as-

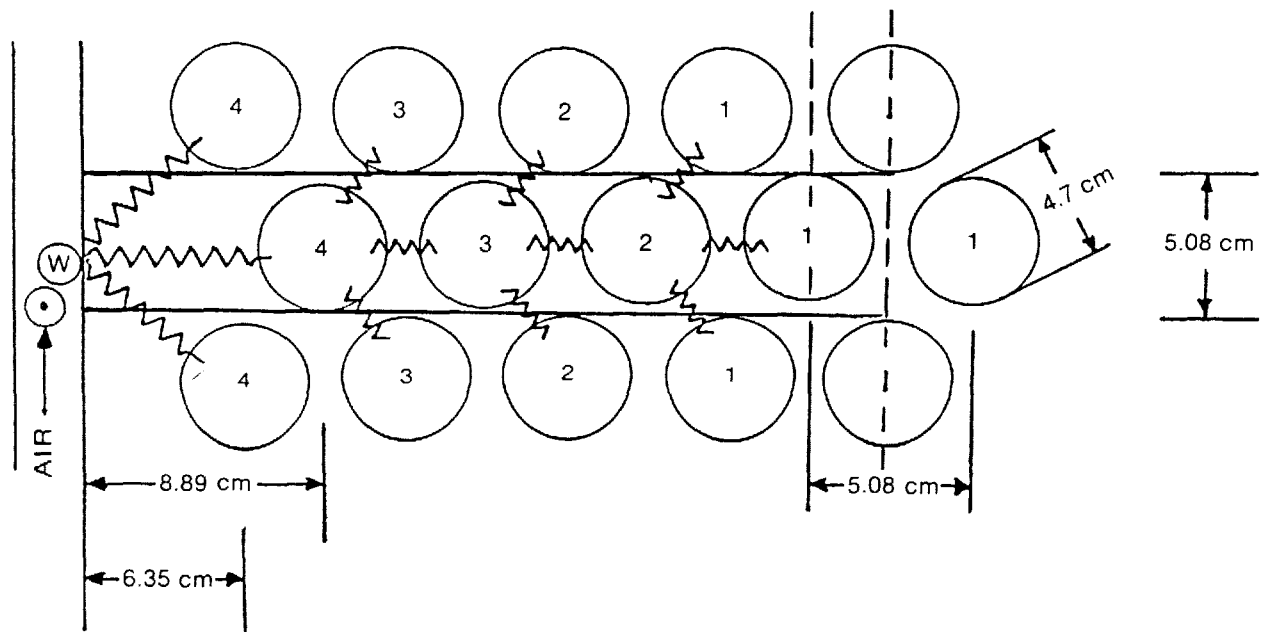


Figure 2-26. Cell-to-Cell & Cell-to-Wall Radiation Heat Transfer Coupling

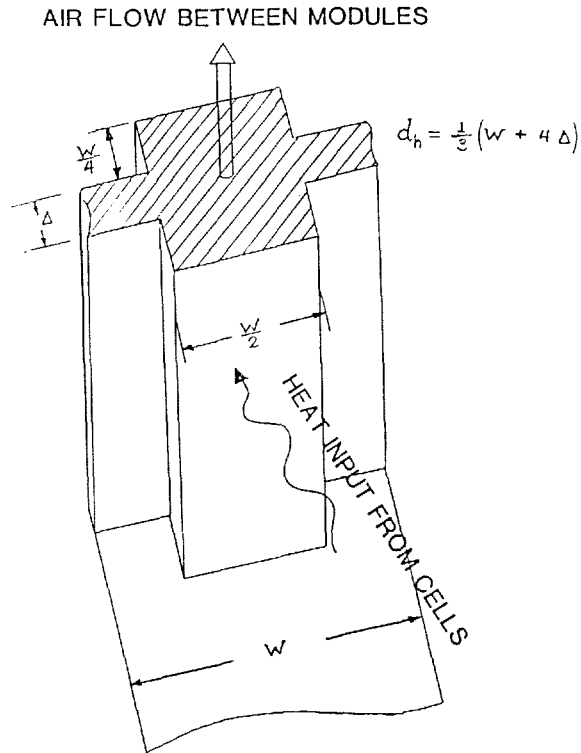


Figure 2-27. Heat Transfer at Corrugated Steel Module Wall

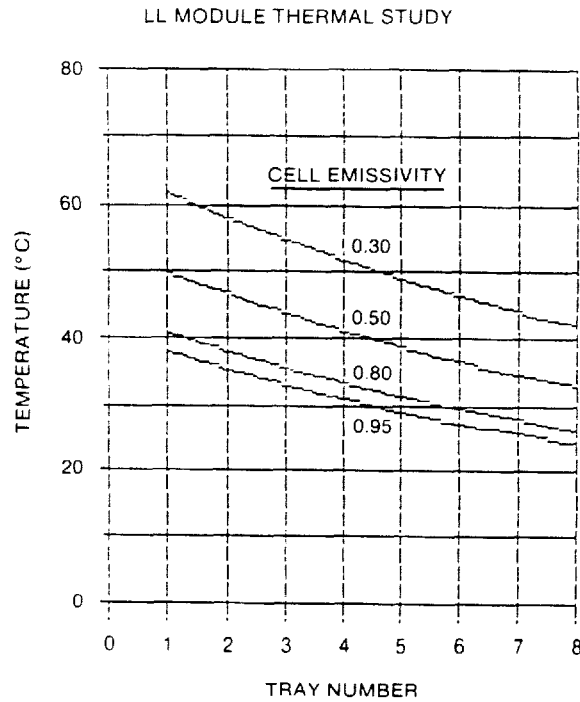


Figure 2-28. Cell-to-Cell Temperature Differences for Selected Surface Emissivities at 100% Depth of Discharge

signed to appropriate conduction elements representing module heat transfer mechanisms. A schematic of the FEM used in the FETA is shown in Figure 2-29, and a reference legend relating physical entities to their finite element representations is shown in Figure 2-30.

Results of the FETA show good control of cell-to-cell temperature differences, as well as peak cell temperatures with respect to the maximum 370°C cell temperature specification. However, some overcooling of cells adjacent to the module wall has been exhibited, particularly in the lower tray where the higher differential between cell and the inlet air temperature results in accelerated heat transfer. One method found to limit this localized cooling is installation of gradient density insulation, tapering from a maximum thickness at the bottom of the module, to a feather edge at approximately module mid-level.

Nodal temperature profiles for the bottom, middle, and top cell trays during a representative 3-1/3 hr discharge simulation FETA that assumes constant air flow and no module insulation are shown in Figure 2-31. Note particularly the profile of the outside cell in tray number 1, and its excursion below the 300°C low end of the scale.

Temperature profiles on the same scale are shown in Figure 2-32, and represent identical conditions with

the exception that certain finite element properties were modified to reflect the presence of gradient density insulation along the lower half of the module wall. A direct comparison of the profile for the outside cell in tray number 1, now completely on scale, readily demonstrates the attenuating effect of the insulation upon accelerated heat loss of the outer cells.

Another TMS consideration brought to light through review of the cell temperature profiles is the potential for enhanced thermal control through variation in the air flow rate, globally by speed control of the five roof-mounted fans, or locally through manipulation of the thermal shutters. Early in the discharge cycle, reduced flow rate would reflect the low initial heat generation of the XPB cells. As depth of discharge increases, flow rates would likewise increase in response to increased cell heat generation. Use of variable air flow, in concert with the optimization of insulation placement and configuration, is expected to bring all cell temperature extremes within the specified operating range of 330°C - 370°C.

It was concluded from the study that the application of this vertical mixed flow TMS approach to load-leveling utility battery applications would be likely to significantly reduce the capital outlay as well as the maintenance and operating expenses. Justification as to the

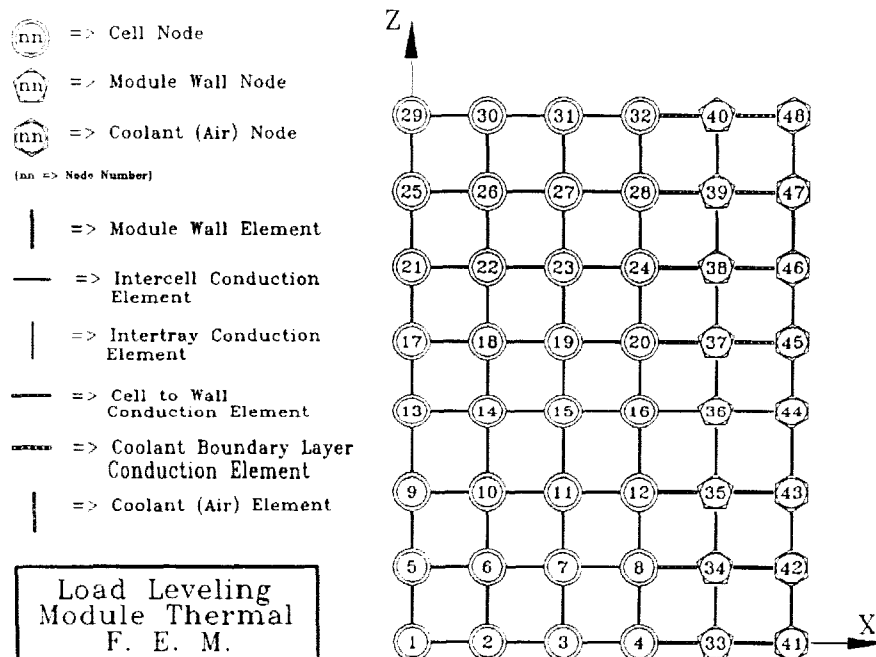


Figure 2-29. Schematic of MB Load-Leveling Module Finite Element Model

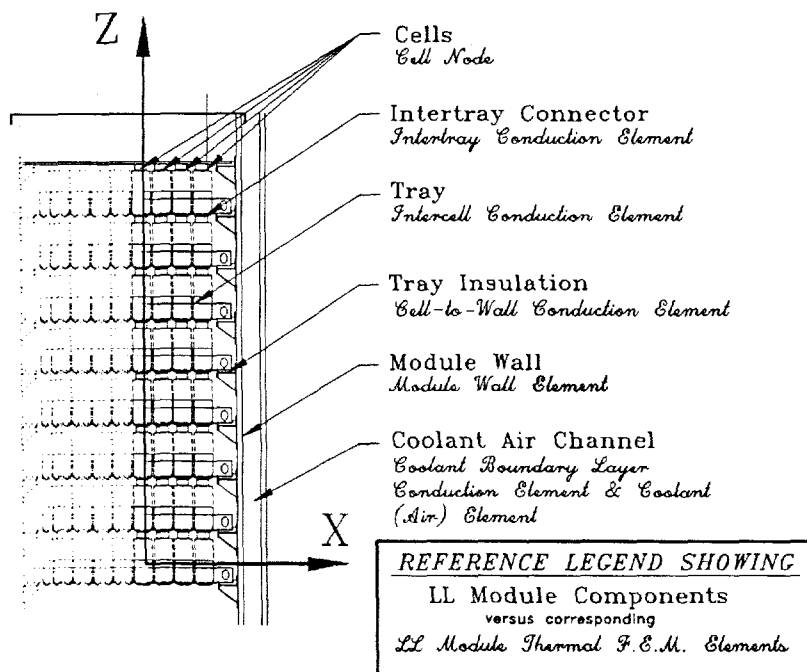


Figure 2-30. Legend Relating MB Module Physical Entities to Their Element Representations

desirability of continued investigation and refinement of this new thermal management approach is evidenced by review of the favorable comparative data that is presented in Table 2-14. Also, specific areas of study are suggested as a result of the design and analysis activity completed to date; those considered most significant are presented in Table 2-15. A continuation of effort toward refinement of an efficient TMS is necessary if the full potential of the sodium/sulfur utility/load-leveling battery concept is to be realized, and the results of this study indicate that a vertical mixed flow TMS approach holds great promise as a cost-effective solution to large-scale utility battery thermal management.

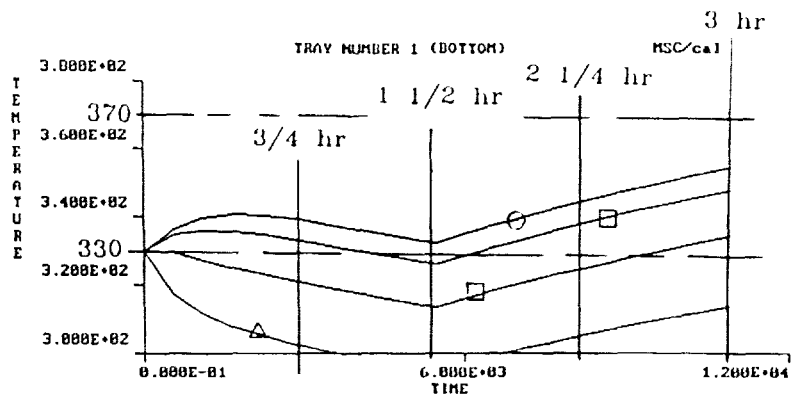
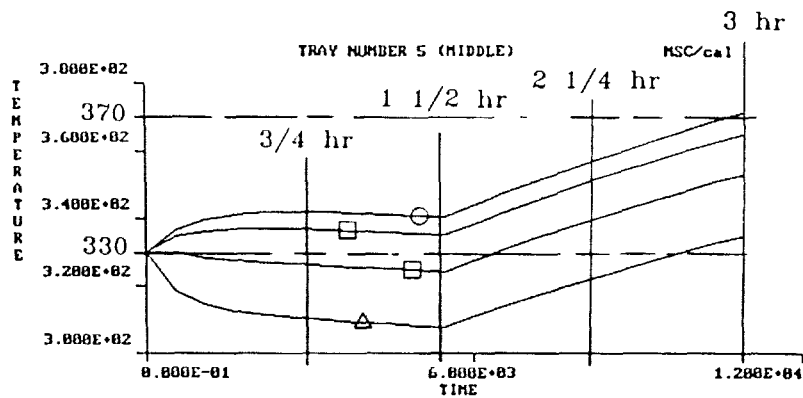
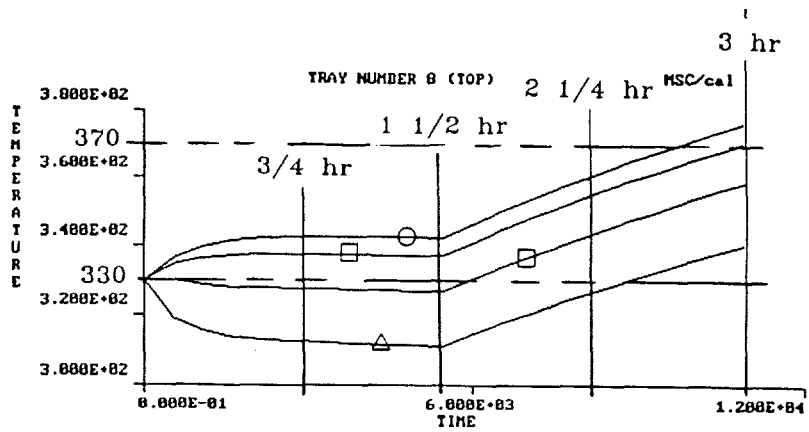
Analysis of Maintenance Approaches for Monobloc Utility Batteries

Under a subcontract to CSPL, Science Applications International Corporation (SAIC) conducted a study on maintenance approaches for the design concept proposed. Their study determined the maintenance requirements for a 100-MWh utility load-leveling battery constructed using the "monobloc" approach. Two maintenance approaches, string replacement and monobloc replacement, were studied. It was determined that 28-string replacements were necessary to

maintain the battery average capacity at 100 MWh over the 30-yr battery lifetime. For the monobloc replacement strategy, 3,999 monobloc replacements were needed. The analyses performed in this study indicate that the difference in the number of cells required for maintenance between string replacement and monobloc replacement are small (less than 1% of the number of cells required). The monobloc replacement approach has advantages: 1) it leads to less variation in the battery capacity over time and 2) allows maintenance to be performed in an ongoing fashion. The string replacement approach is attractive because it requires slightly fewer cells and involves fewer maintenance events (only 28 over the life of the battery). Additionally, the entire battery string can be cooled to ambient temperature and then replaced at once. As such, string replacement may be simpler and safer to implement than monobloc-level maintenance which would probably require replacements being made while the battery string was hot (electrically and thermally).

Subtask 2.2 - Battery Build and Test

Final design of the contract demonstration battery was completed during the reporting period. Figure 2-33 shows the battery at various stages of its construction. The size of the unit was dominated by the need to



- => Center Cell
- => Intermediate Cells
- △ => Outside Cell

Figure 2-31. Nodal Temperature Profile LL Module FEM with 50°C Inlet, 25 cfm, No Insulation

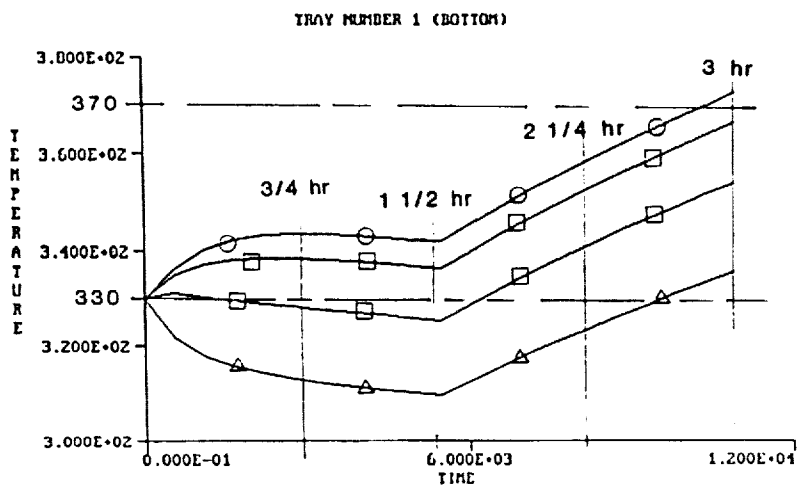
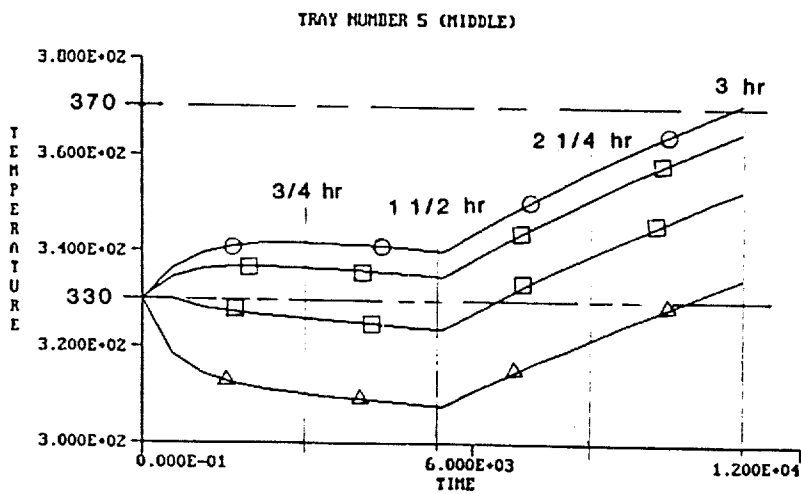
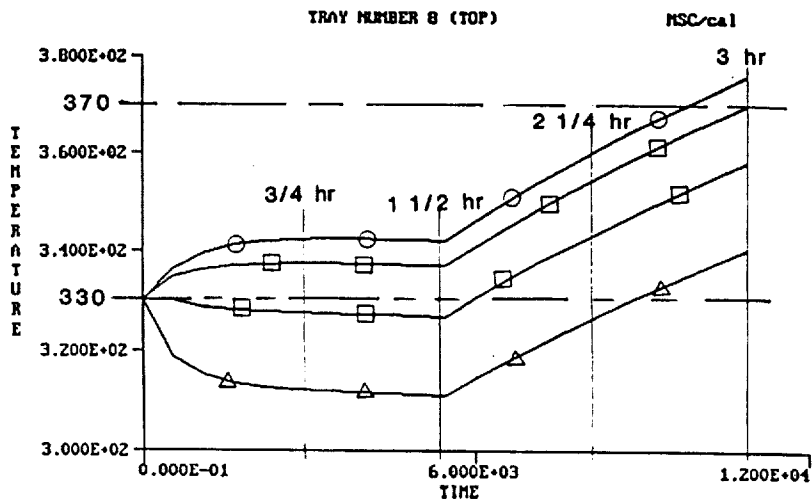


Figure 2-32. Nodal Temperature Profile LL Module FEM with 50°C Inlet, 25 cfm, Tapered Insulation

Table 2-14. Comparison of Facility Characteristics

Characteristic	Self-Contained TMS Design	Monobloc Design	Change
Plan form area of Complex	44,100 ft ²	28,100 ft ²	-36%
Plan form area of Battery Building(s)	15,318 ft ²	11,476 ft ²	-25%
Volume of Battery Building(s)	359,973 ft ³	84,560 ft ³	-76%
TMS Flow Rate	967,680 cfm	108,000 cfm	-89%
Number of TMS Blowers	42	5	-88%

Table 2-15. Recommendations for Follow-On Studies

1. Other point designs indicating:
 - Sensitivity to discharge rate (such as to a 5-hr discharge)
 - Sensitivity to air flow rate
 - Results of discharge to single-phase region only
 - Sensitivity to decrease in electrolyte thickness
 2. Specification of TMS blower system
 3. Specification of module heating control system
 4. Specification of maintenance crane system
 5. Calculation of detailed costs
-
-

stabilize the air flow so that accurate measurements could be taken during the testing to provide baseline data for future design work. The battery itself represents a significant portion of a full-sized SES module tray as defined in the 1989 SES battery design. The details are summarized in Table 2-16.

The necessary software for analyzing transient and steady-state thermal profiles in the battery was written, and includes a color contour mapping facility that allows plan and section thermal profiles of the battery to be examined. The front end of the software has been written and integrated to the data logging and alarm systems. Overall, the software design is identical to that employed on the CSPL Bank Testing Facility but additional features have been incorporated to enable more sophisticated thermal analysis to be conducted. Typical

graphical outputs from the logging program are shown in Figure 2-34. It is proposed to commence tests at the C/3 rate, and later to incorporate more typical SES cycling regimes into the program. Through December 1990, the battery had successfully completed over 100 cycles.

Technology Evaluation

Evaluations are performed at both SNL and ANL. Typically, SNL studies the performance of cells and small modules in early stages of development, working closely with the prime contractor. The work at ANL focuses on larger modules to characterize electrical and

Table 2-16. 200-Cell XPB Battery

Configuration	4-Series X 50-Parallel Strings		
Nameplate Capacity			
to 8.0 V o/c	1120 Ah		
to 7.6 V o/c	1500 Ah		
Energy			
(8.0 V o/c)	8.5 kWh		
(7.6 V o/c)	9.6 kWh		
Thermal Management	Active or Passive		
Resistance Characteristics			
	360°C	355°C	330°C
Cell	11.5 mΩ	12 mΩ	14 mΩ
String	54.5 mΩ	56.5 mΩ	64.5 mΩ
Battery	1.09 mΩ	1.13 mΩ	1.29 mΩ

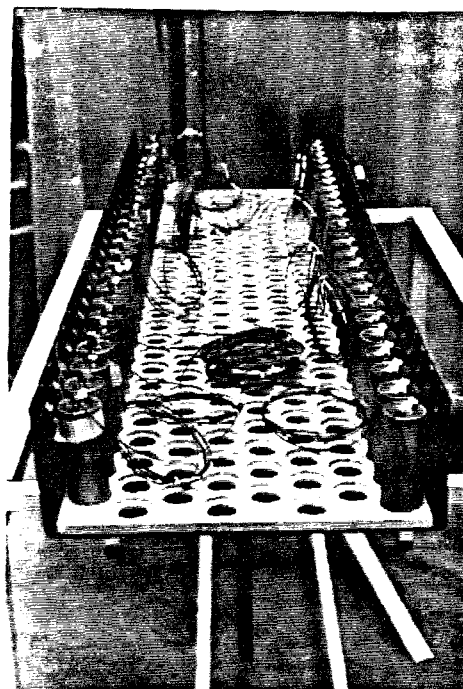
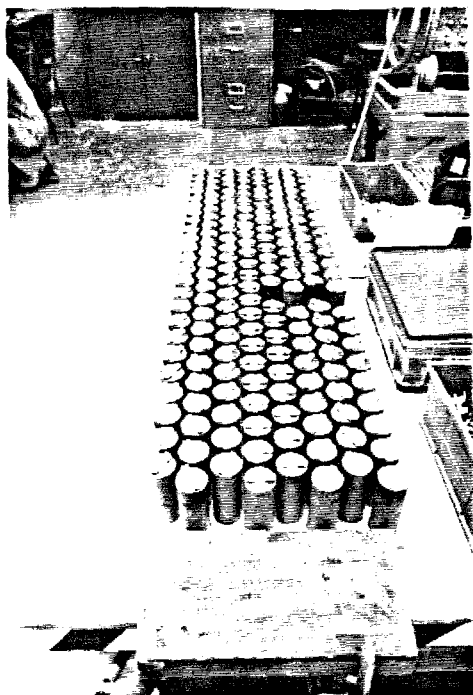


Figure 2-33. 1500-Ah 200-XPB-Cell Battery

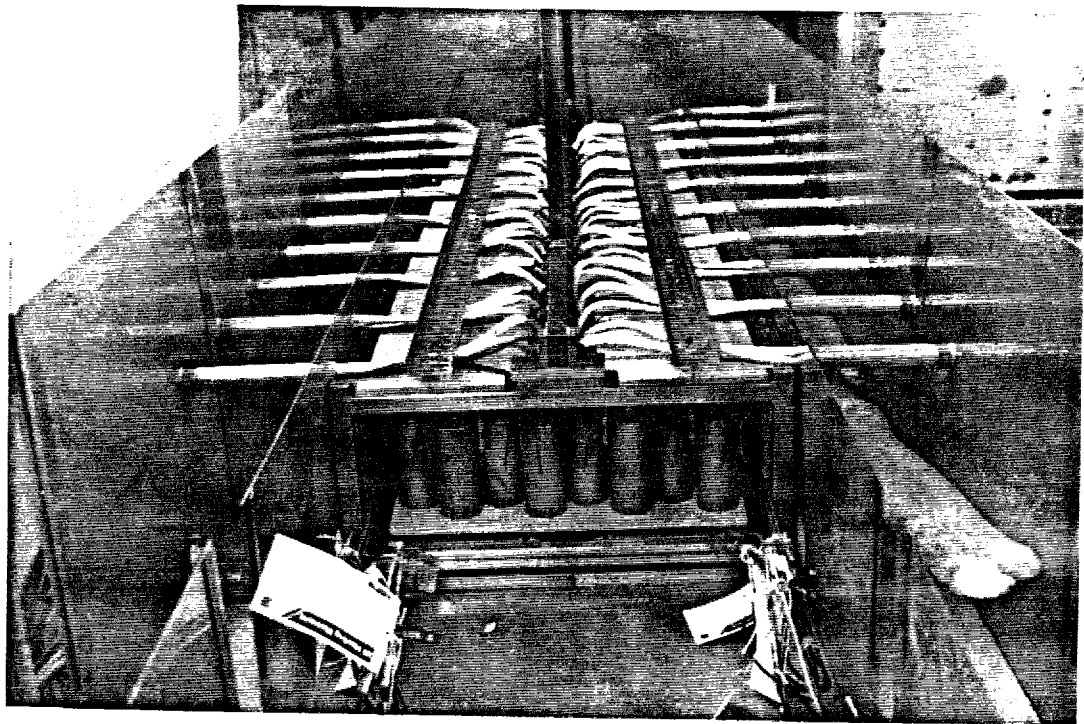
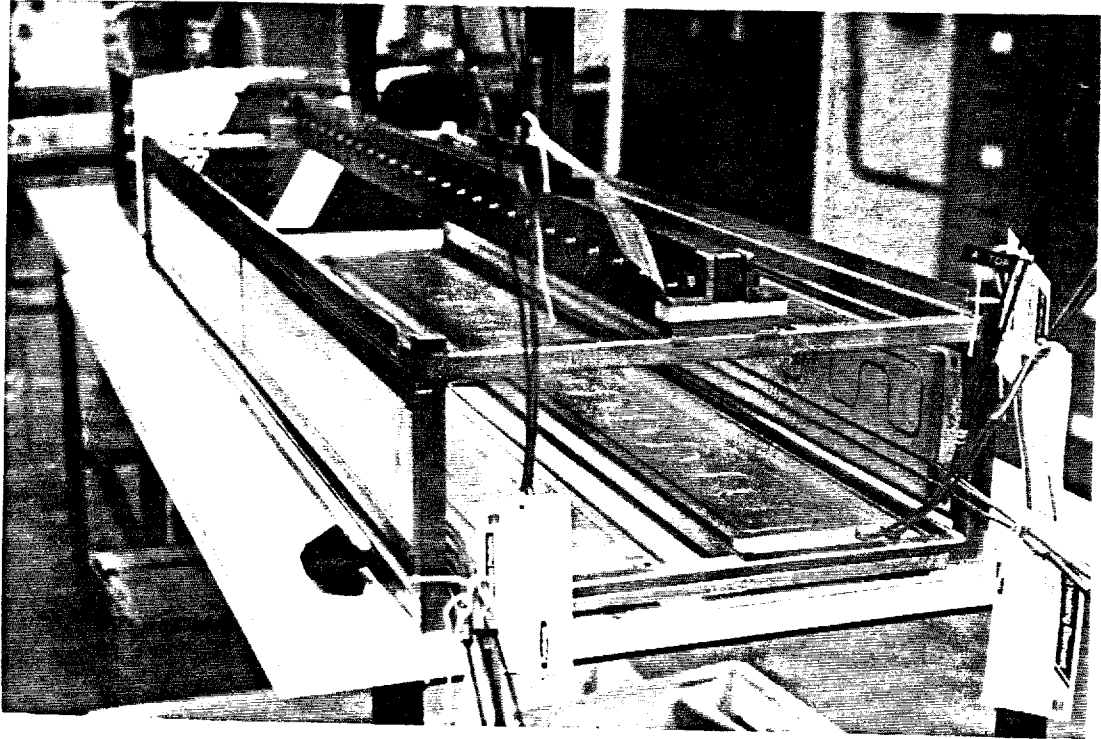


Figure 2-33. 1500-Ah 200-XPB-Cell Battery (Continued)

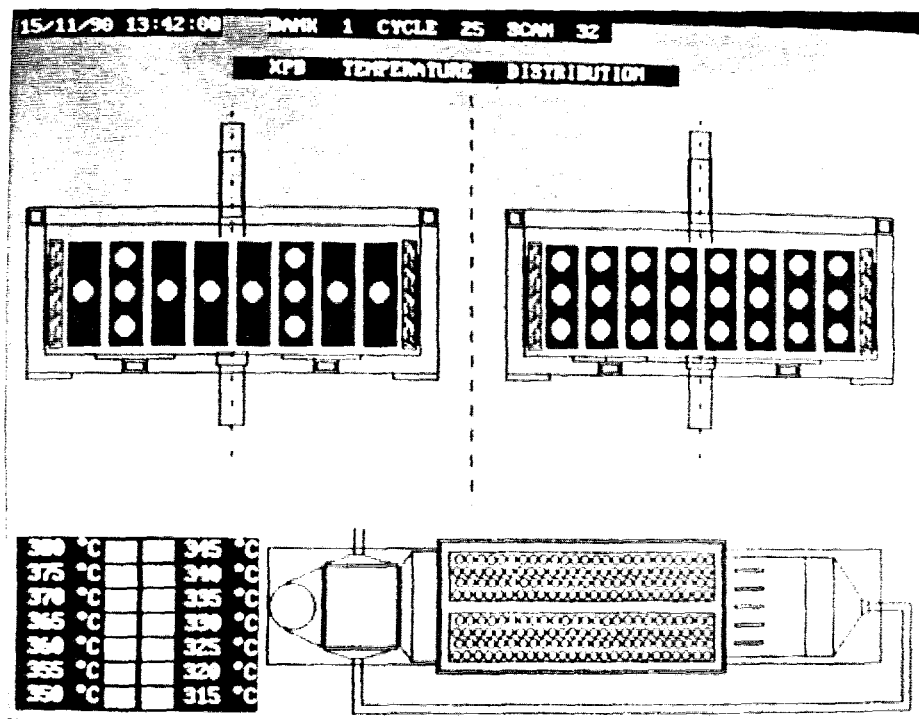


Figure 2-34. Typical Output from XPB Battery Logging System

physical properties and determine long-term performance.

SNL

A total of 11 cells and two 4-cell strings from three developers were evaluated at SNL during the year. Seven of the 11 cells and the two 4-cell strings were from CSPL. Of the other four cells that were evaluated, two cells were from Powerplex, which were provided at no cost by OPS, and two cells were from Ceramatec. The majority of the tests conducted on these cells were life cycle; however, a few of the CSPL cells did undergo peak power, constant power, and charge rate and discharge rate vs capacity tests.

CSPL Technology

During this fiscal year, SNL evaluated two groups of PB cells. The first set contained a 4-cell series string. These cells utilized the MKIII seal design, but did not employ the safety containment of the sodium electrode. A newer, second set consisted of a group of 5 cells and one 4-cell series string with the MKIII seals and the sodium safety containment device. Three of these latter cells and the 4-cell series string were previously on test at CSPL and had experienced 47 cycles before being

sent to SNL for further tests. All of the cells and strings in this second group contained a substandard glass seal between the alpha cap and beta"-alumina tube. Because of this, the life of these cells was not expected to exceed 200 cycles. The electrical performance, however, was as good as any of the other cells that CSPL had sent SNL. A summary of the testing activities conducted on the CSPL cells and 4-cell series strings is shown in Table 2-16.

The majority of the cycles placed on the first group of cells (#470 and #471) during this fiscal year were baseline capacity. The total number of cycles on these cells were 1900 and 2244, respectively. Cell #470 has been removed from test due to failure. Although normally cells are removed from test when capacity drops below 80%, cell #471 was left on test until complete failure. Figure 2-35 is a plot of cell #471's capacity vs cycle life. This behavior does not correlate with cell resistance, but can be explained with information gained from post-mortem analyses conducted at CSPL and ANL. Significant corrosion of the chromized container begins to occur around cycle 400-500 (end of plateau in Figure 2-35). Studies have shown that the iron sulfide corrosion products migrate through the sulfur electrode and precipitate on the sodium polysulfide wicking material located next to the electrolyte. This con-

Table 2-17. CSPL Cell Test Summary at SNL

SNL Number	Capacity (Ah)		Number of Cycles	Test Regimes (FY 90)	Present or Final Capacity (% of Initial)
	Rated	Initial			
470 (PB)	8.58	8.1	1900	5	54
471 (PB)	8.64	8.0	2244	1,5	52
485 (PB)	10.06	9.4	344*	1,4,5	99
489 (PB)	10.06	9.7	323*	1,3,5	#
491 (PB)	10.06	9.6	234	1,5	88
492 (PB)	10.06	10.2	224	1,3,5	#
493 (PB)	10.06	9.1	214*	1,2,5	52
474 (STR)	8.70	8.1	877	5	#
486 (STR)	10.06	10.0	436	1,3,4,5	72

Notes:

Cell Initial Capacity: Discharge @ C/3 to 1.9 VOC and Charge @ 2.0 A to 2.4 V

String Initial Capacity: Discharge @ C/3 to 7.6 VOC and Charge @ 2.0 A to 9.6 V

* Cell or String Cycled 47 Times at CSPL Prior to SNL for Testing. Thus, 47 Cycles Must be Added to Total No. of Cycles

Cell Failure Resulted in Low Capacity

Test Regimes

1. Capacity vs Charge Rate
2. Capacity vs Discharge Rate
3. Constant Power Tests
4. Peak Power Tests
5. Life Cycle Baseline

tamination retards the effectiveness of the layer, causing worsening recharge polarization with time, associated with the continued loss of capacity.

As mentioned earlier, the cells with the glass seal problem did not have a life expectancy beyond 200 cycles. All of these cells have been removed from test and the total number of cycles on these cells varied from 214 cycles to 344 cycles. Cell resistances for the majority of these cells were in the range of 33 to 36 mohms. The only cell that appeared to have a high cell resistance was cell #491. This cell had an end-of-discharge cell resistance of 44.6 mohms.

The 4-cell series string (#474) had completed the test regimes during the previous fiscal year and was on a life cycle test when at least one cell failed after completing 877 cycles. The string was removed from test

and examined; however, a posttest analysis has not been conducted.

Peak power tests were conducted on the second 4-cell series string (#486) and the results are shown in Figure 2-36. The peak power values were measured at six different depths of discharge (0%, 5%, 10%, 20%, 50%, and 80%). The maximum specific peak power for this string was approximately 195 W/kg with the string being discharged to 2/3 the open-circuit voltage. An unencumbered string weight of 520 grams was used.

Constant power tests were also conducted on 4-cell series string #486 and the results of these tests are shown in Figure 2-37. These values were determined by taking an average of the four cycles which were run at each of five power levels. An unencumbered string weight of 520 grams was used and a Ragone plot was produced.

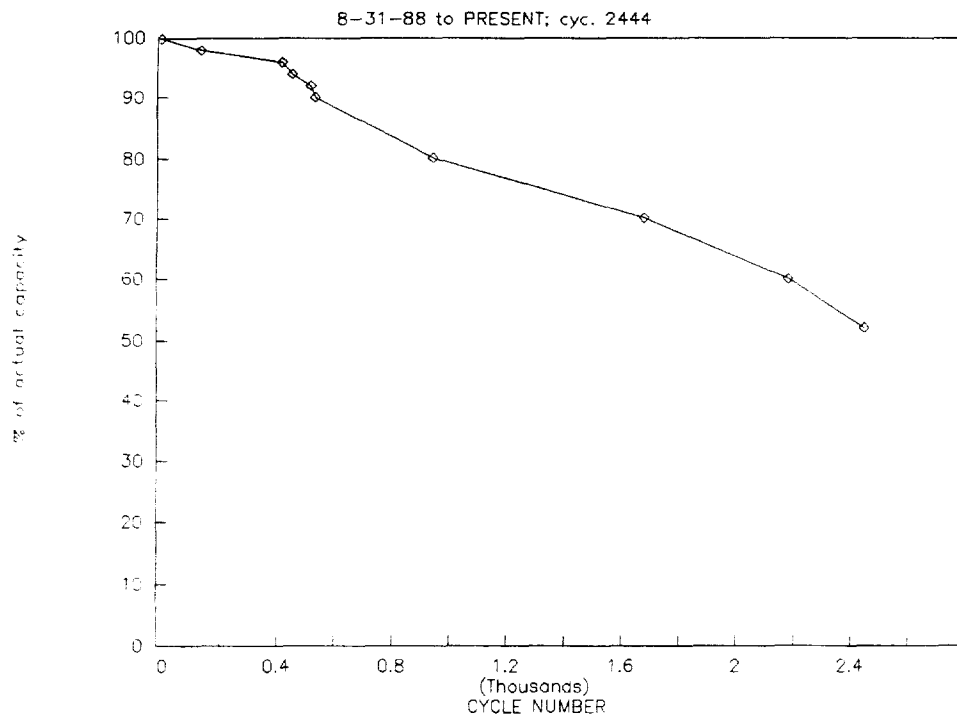


Figure 2-35. Capacity of Cell #471

ID # 486, CSPL 4-CELL STRING, Sodium/Sulfur Wt.=.520 kg

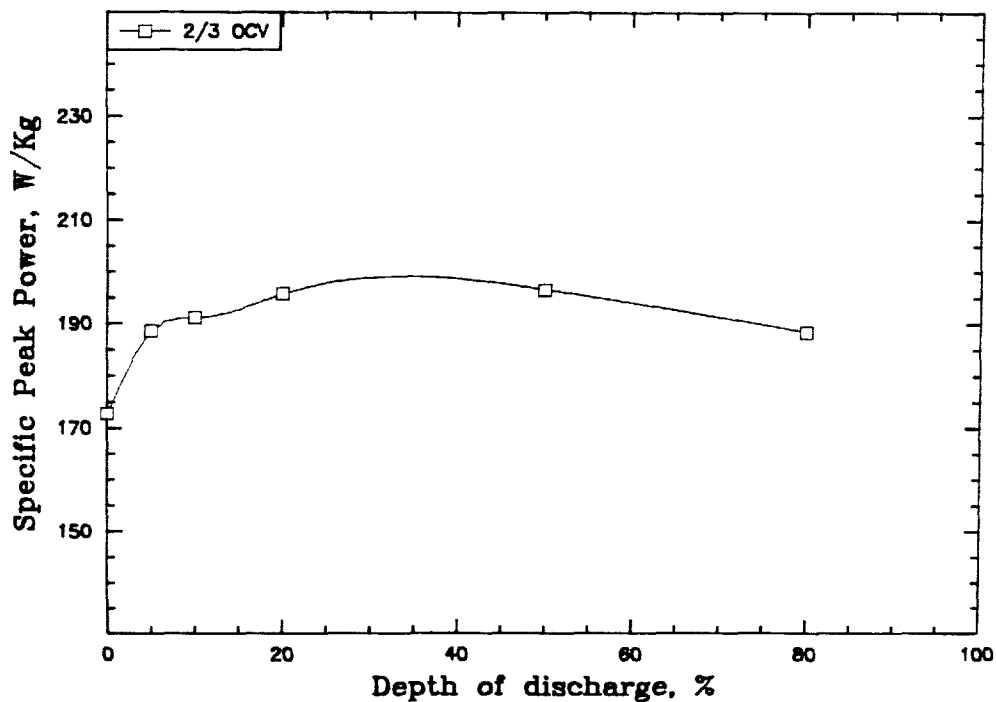


Figure 2-36. Peak Power Tests

RAGONE PLOT FOR CSPL Na/S 4-CELL STRING 486
RESULTS BASED ON UNENCUMBERED STRING WEIGHT (0.520 kg)

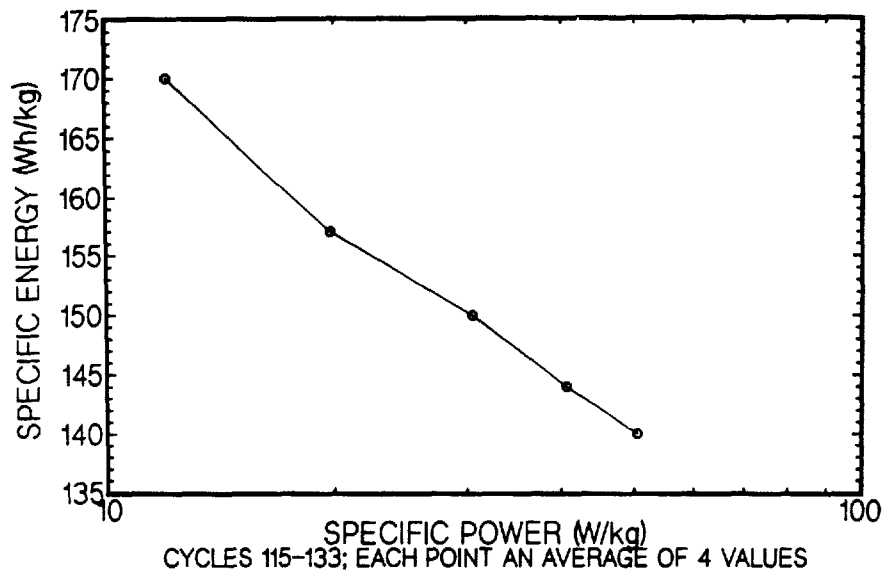


Figure 2-37. Constant Power Tests

The maximum specific energy for this string was 170 Wh/kg.

Twelve new single cells have been received from CSPL and will undergo extensive testing in the next fiscal year. All of these cells utilize the MKIII seal design with the sodium safety containment. These cells are similar to those contained in the ETX-II battery and the 120-cell module being tested at INEL and ANL, respectively.

Powerplex Technology

Only two 40-Ah sodium/sulfur EV cells from Powerplex were tested at SNL during this fiscal year. Both cells had completed the majority of the desired test regimes during the previous year and were being subjected to life cycle baseline tests. Cell #477 completed 719 cycles when the cell lost voltage and was removed from test. Cell #462 accumulated 2201 cycles before this cell failed. Upon examination, it appeared that a seal had failed. The decline in cell capacity was gradual and similar to that seen on the CSPL cell over its cell life. A gradual increase in cell resistance was observed until near the end-of-life when the cell resistance increased dramatically.

Ceramatec Technology

Two 40-Ah sodium/sulfur EV cells from Ceramatec were evaluated during this fiscal year. These cells had been on test since February and June of 1988 and had completed all the desired test regimes; however, life cycle testing was continued until failure. Cell #455 completed 1548 cycles when high temperature and low voltage alarms were activated, indicating a cell failure. The other Ceramatec cell (#454) had completed 2400 cycles before it was removed from test. A plot of actual cell capacity vs cycle life is shown in Figure 2-38. As can be seen, this cell had a much flatter capacity until the end-of-life compared to the gradual decline in capacity for the CSPL (and Powerplex) cells. Capacity started to fall off very rapidly between cycle 1800 and 2000 but then leveled off out to cycle 2400.

In comparison to that for the CSPL technology, the early-time effect of container corrosion on recharge polarization is not as significant. This factor may be due to the composition of the container or, most probably, the lack of a wicking material in the sulfur electrode. Based on post-mortem evaluations at CSPL, substantial quantities of corrosion products (chrome and iron sulfides) were observed to precipitate on the electrolyte at extended cycle time, thus reducing its effective area and increasing its resistance.

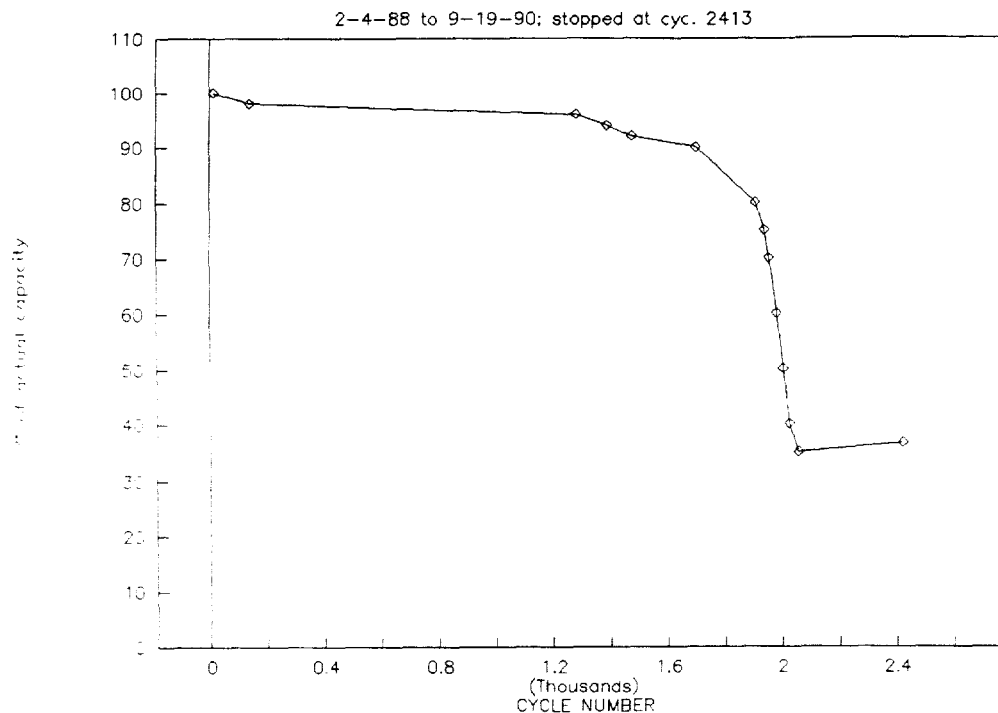


Figure 2-38. Percent Capacity of Ceramatec Cell #454

ANL

An 8-V, 300-Ah sodium/sulfur module fabricated by CSPL was delivered to ANL for performance and life characterization tests in May 1990. There are 120-cells in this module that are configured into 30 parallel-connected strings of 4 series-connected cells. Module testing was initiated in June 1990. Planned tests include performance characterization and life evaluation using SFUDS discharges to 100% DOD. Performance testing has been completed, and the module is undergoing life evaluation. At the end of FY90, the module had successfully completed 141 cycles and still retained ~100% of its initial 292-Ah capacity (3-hr rate).

The CSPL module was furnished without a thermal case and had to be installed in an existing ANL thermal enclosure that had no cooling capability. The module was heated from ambient to 150°C at a rate of <6°C/hr and then heated to its operating temperature of 350°C at a rate of <15°C/hr. Three conditioning cycles were performed at reduced charge and discharge rates because the cells had not been operated previously. After 26 cycles, the operating temperature was reduced to 330°C to allow a greater temperature rise during discharge. At this reduced operating temperature, the maximum continuous constant-current and constant-power discharge rates that could be applied without exceeding the 370°C

maximum temperature limit specified by CSPL were 150 A and 40 W/kg, respectively.

The module had a measured weight of 22.4 kg, which included power leads and thermocouple wires. The projected module weight used for the constant power and driving profile loads was 29.2 kg, which includes a weight burden for a thermal enclosure, heaters, module interconnections, etc. The burden was based on the CSPL-projected weight for the ETX-II battery (700 kg). The ETX-II battery contains 24 modules that are similar to the one being tested at ANL ($700 \div 24 = 29.2$).

Standardized tests were conducted to characterize module performance for EV applications. These tests were previously developed with aid and advise from the Standards and Procedures Subcommittee of the National Battery (ad hoc) Advisory Committee and the DOE/EHP Battery Test Working Task Force. Besides the verification of rated capacity, the tests measure:

1. Available energy as a function of constant-current and constant-power discharge rate
2. Available peak power for acceleration vs DOD level

3. Hill-climbing capability (for 45 W/kg demand) vs DOD level
4. Capacity loss (self-discharge) for stand times up to one week
5. Projected range for various driving schedules and vehicles

The standardized performance characterization tests were initiated after the module achieved stable operation. The characterization tests are discussed below.

Capacity Verification and Baseline Performance

The module was initially cycled to verify rated 300-Ah capacity using constant-current charges at the 9-hr rate (33-A) to 9.1 V and constant-current discharges at the 3-hr rate (100-A) to 100% DOD. Throughout the test program, these cycling conditions were replicated to establish a module capacity baseline. The data for these cycles are plotted in Figure 2-39.

The algorithm to determine the module discharge cutoff voltage (DCOV) at 100% DOD is defined as:

$$\text{DCOV} = 7.6 - I_b \times R_b$$

where battery current and internal resistance are I_b and R_b , respectively. R_b is derived from the change (for 5 sec) in module voltage (V_b) at the end of discharge divided by the change in I_b :

$$R_b = \Delta V_b / \Delta I_b$$

The plot in Figure 2-39 shows that there has been virtually no decline in module capacity with life. For the first 16 cycles, an R_b of 4.65 mΩ was used based on previous ANL sodium/sulfur cell data. An R_b of ~5.15 mΩ was measured initially. This value is 10% higher than that used in the DCOV algorithm, but within 0.5% of the average resistance measured for the eight modules in the CSPL 1/3-EV battery previously tested at ANL. Revision of R_b in the algorithm after 12 cycles lowered the DCOV by 48 mV and increased module capacity by 2%. After ~110 cycles, the DCOV algorithm was again revised to reflect a 5% increase in module resistance (5.15 to 5.37 mΩ). This revision resulted in a 2% increase in discharge capacity (~5 Ah).

During the 17th cycle, a blown fuse in the thermal management controller caused a large decrease in module temperature to 160°C. The fuse was replaced and the module heated to 350°C. Subsequent cycles indicated that the low temperature excursion had no noticeable effect on module performance. After 26 cycles, the operating temperature was decreased from

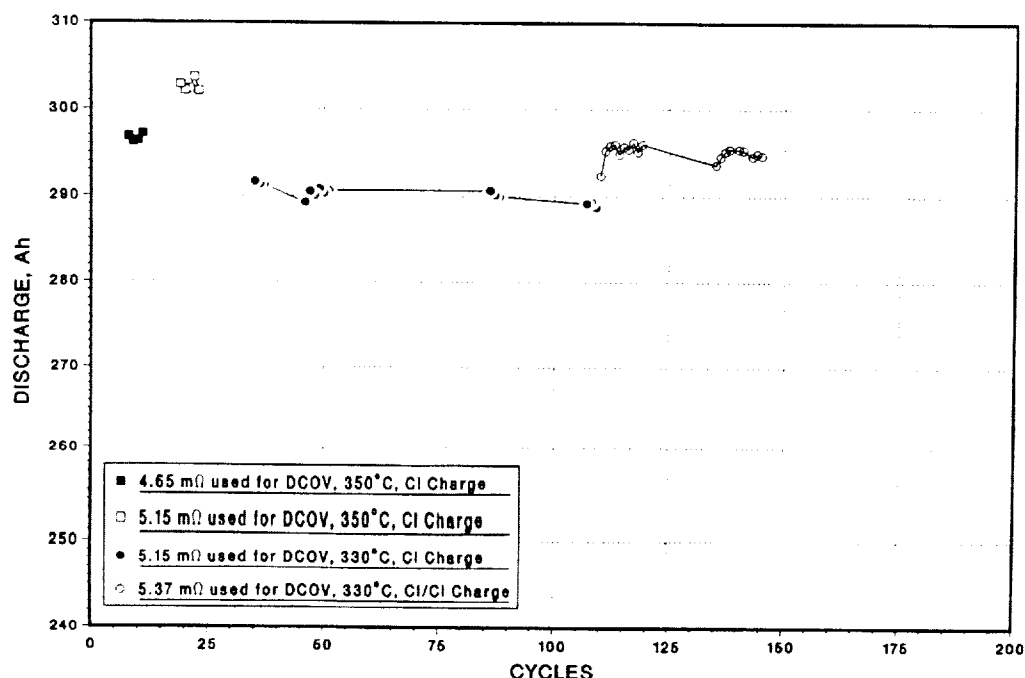


Figure 2-39. Capacity History of CSPL 120-Cell Module for 3-hr Rate Discharges

350 to 330°C, and this resulted in a module capacity loss of ~10 Ah (~3%).

Capacity and Energy vs Discharge Rate

Tests were conducted to identify the change in available capacity and energy with constant-current and constant-power discharge rates. These data, in conjunction with peak power data, allow EV range predictions for various vehicles and driving schedules. Constant-current discharges were performed at rates of 30, 100, 150, 200, and 300 A with the DCOV varied to attain the same 7.6-V open-circuit voltage at the end of discharge. At 200 and 300 A, the maximum temperature limit was reached before 100% DOD. Similarly, constant power discharges ranging from 10 to 50 W/kg were attempted. A maximum rate of 40 W/kg could be used without reaching the upper 370°C temperature limit. The resulting Puckert (constant-current discharges) and Ragone (constant-power discharges) data are plotted in Figures 2-40 and 2-41, respectively. (The projected module weight of 29.2 kg was used to calculate the discharge specific power and the specific energy.) The lowest constant-power level (10 W/kg) is representative of that needed to provide a nominal vehicle speed of ~20 mph, while the higher levels represent the powers needed for vehicle hill climbing and acceleration. Module capacity is reduced by only 7% (315 to 293 Ah) for a 30- to

150-A increase in discharge rate, but the available energy is decreased by ~14% for a 10- to 40-W/kg increase in discharge rate.

Driving Profile Discharges

After about 67 cycles, tests were performed to determine the range of various vehicles undergoing different driving schedules (see Table 2-17). The power profiles for these tests were obtained from several electric vehicle test centers. Each power profile duplicates the power demand as measured at the battery terminals of a specific vehicle while being operated according to a specific driving schedule. The power profile for each vehicle is normalized to the weight of the battery in the vehicle. To determine the fractional part of the total battery load that should be applied to the CSPL module, its projected weight (29.2 kg) is multiplied by each specific power profile. Using this methodology, the battery weight in each vehicle is unaltered. The results listed in Table 2-17 give the characteristics of each driving profile, followed by the achieved simulated miles driven and the net capacity and energy discharged. The net discharge was obtained by subtracting the capacity and energy acquired by regenerative braking (charge) from the total.

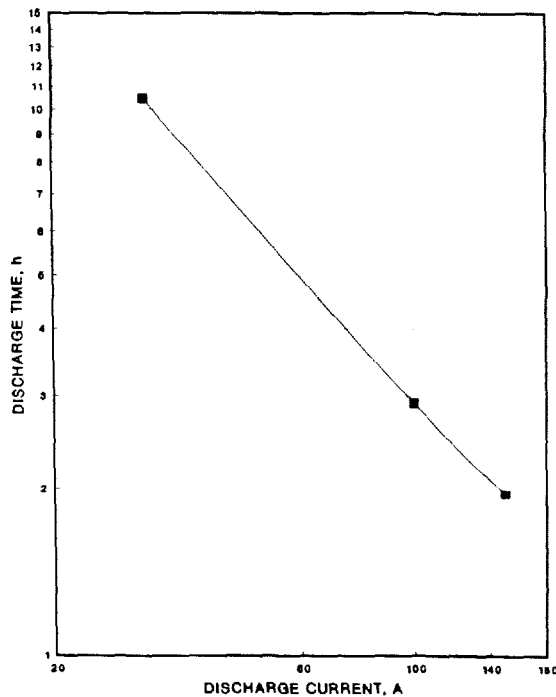


Figure 2-40. Discharge Time vs Module Constant-Current Discharge Rate

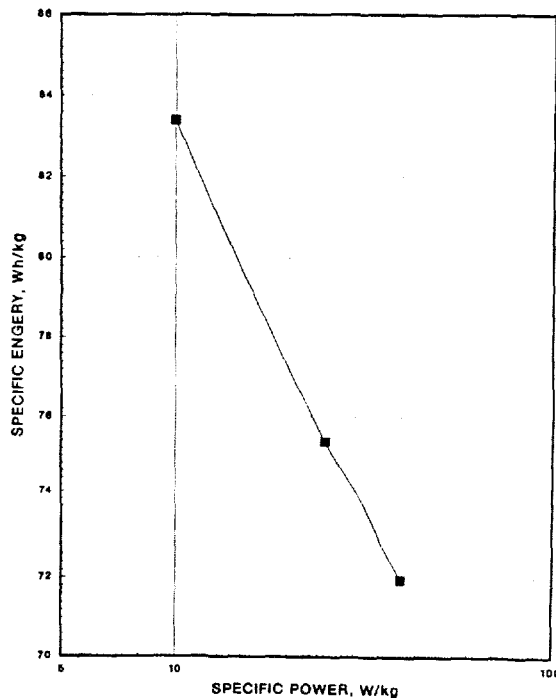


Figure 2-41. Module Specific Energy vs Discharge Specific Power

Table 2-18. Projected Vehicle Ranges Under Simulated Driving Profiles

Driving Profile Characteristics

- Driving Schedule	SFUDS79	J227aD	J227aC	J227aC
- Avg. Speed, mph	19.0	28.3	15.1	15.9
- Vehicle Type	IDSEP	IETV-1	G-Van	TEVan
- Battery Weight, kg	695	488	1180	839
- Peak Power, W/kg	79	48	36	29
- Avg. Power, W/kg	9.9	12.0	7.3	5.1

Results with 120-Cell Sodium/Sulfur Module

- Range, miles	148	174	169	263
- Capacity, Ah	295	298	304	308
- Energy, kWh	2.14	2.14	2.36	2.27

Peak Power vs DOD

Peak power tests were performed to determine the capability of the battery to deliver power for vehicle acceleration as a function of DOD. The data allow identification of the DOD at which the battery can no longer provide the power required to satisfy specific driving schedules. Module peak power (sustained for ~30-sec duration) vs DOD data are derived using acquired voltage and current data from discharges simulating the IETV-1 car undergoing an SAE J227aD schedule (J227aD/IETV-1). Module resistance (R) vs Ah of discharge is derived using the ΔV and ΔI measured between the 25- and 75-sec points of the driving profile ($R = \Delta V / \Delta I$). These data are plotted in Figure 2-42 for two module temperatures (350 and 330°C) and two module weights (22.4 and 29.2 kg) used on cycles 13 and 31. Using the resistance data and measured module voltage (V_M) and current (I_M), module internal IR-free voltage ($V_{IR-free}$) vs discharge Ah (Figure 2-43) was derived with the equation $V_{IR-free} = V_M + I_M R$. Module sustained peak power (P_{Pk}) vs discharge Ah (Figure 2-44) was then computed using the derived data and the equation: $P_{Pk} = (0.222 V_{IR-free})^2 / R$. The plotted data show that power capability is significantly reduced at decreased operating temperatures and increased battery weights (due to assembly weight burdens).

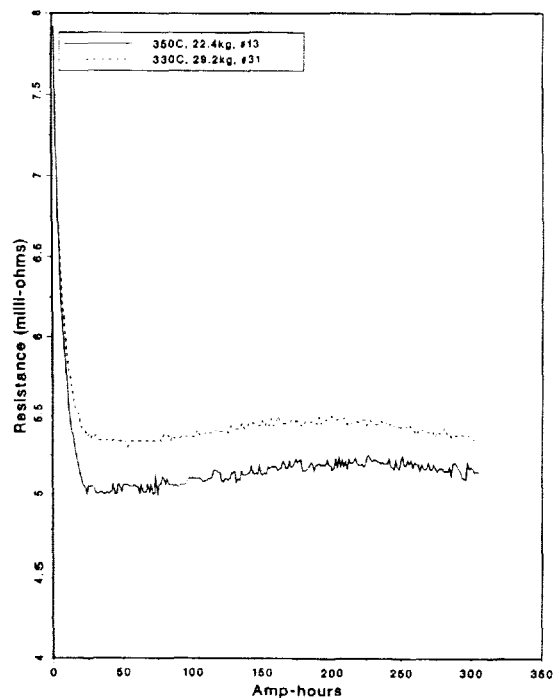


Figure 2-42. Module Resistance vs DOD During a J227aD/IETV-1 Discharge

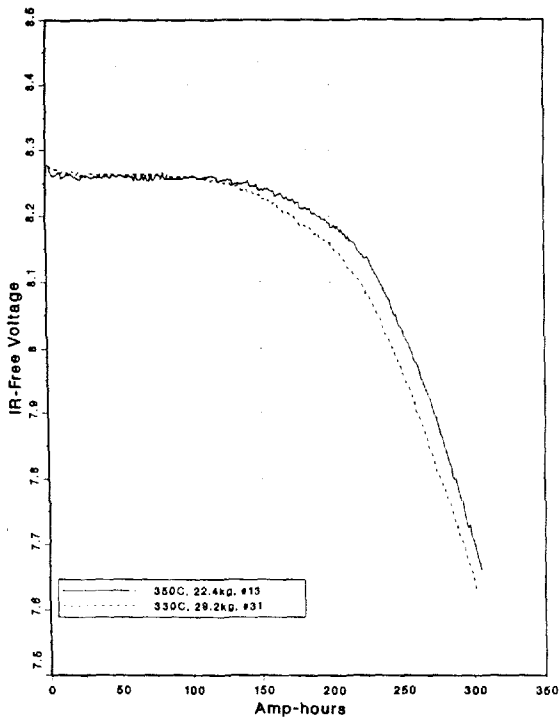


Figure 2-43. Module IR-Free Voltage vs DOD During J227aD/IETV-1 Discharge

Partial DOD Operation

Partial DOD cycles were performed after the module had accrued ~85 cycles to uncover possible “memory” effects and to verify proper charging with partial DOD operation. In this test, the module was discharged 145 Ah (~50% of the 3-hr rating) and charged per CSPL specification for 17 cycles. After the partial DOD cycles, a discharge to 100% DOD was performed to measure the available deep-discharge capacity. The capacity (286 Ah) obtained on the first deep discharge after partial DOD operation was ~1.4% less than that exhibited before partial DOD operation. Full capacity (290 Ah) was achieved on the second deep discharge.

Charge Rate/Method Evaluation

CSPL had recommended the use of constant current charges at the 9-hr rate (33-A) to 9.1 V. Module performance with this charge method was compared with that using the two-step constant-current charge regime previously used on the CSPL 1/3-EV battery. With two-step charging, a 60-A charge rate is applied until a bank voltage of 9.1 V is reached, then a reduced charge rate of 25 A is applied until the module voltage of 9.1 V is again obtained. With this method, the charge time was reduced from 9 to 5.3 hr and module discharge capacity

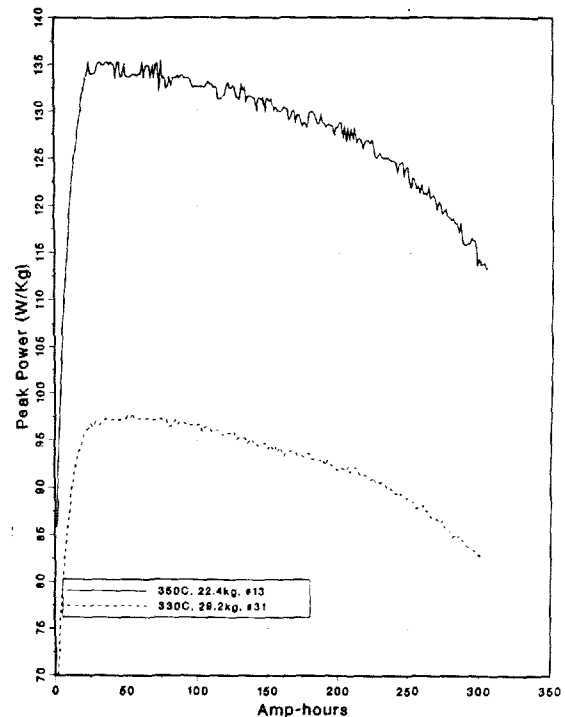


Figure 2-44. Module Peak Power vs DOD During J227aD/IETV-1 Discharge

was increased by ~2% (from 290 Ah and 2196 Wh to 296 Ah and 2237 Wh). The two-step constant-current charge method was selected for use in the remainder of this test program.

Hill-Climbing Capability

A test was conducted after about 120 cycles to determine the maximum DOD level at which the module could sustain a hill-climbing constant-power level of 45 W/kg for 6 min. This level represents that required for the ETV-1 vehicle to negotiate a 7% grade at 30 mph. In this test, the module was discharged at a 15 W/kg rate to DOD levels ranging from 70 to 90%, then a load of 45 W/kg was applied and the time to reach 100% DOD was recorded. The test data, plotted in Figure 2-45, show that the module was able to sustain the 6-min hill-climb power to a DOD of 88%.

Self-Discharge Loss

To determine the energy loss caused by an 8-day stand time, the module was fully charged and then placed on open circuit for 8 days. A discharge to 100% DOD was then conducted to measure the available capacity. The 193-Ah (2216-Wh) capacity obtained on this first discharge was 99.2% of that obtained on the

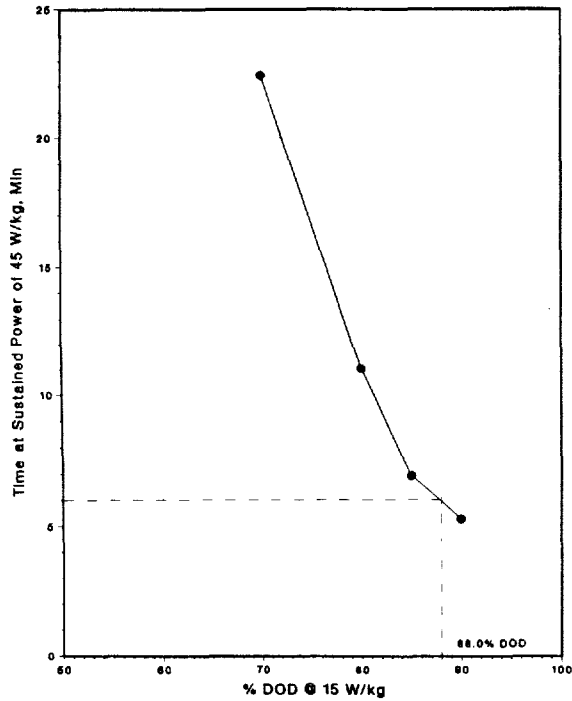


Figure 2-45. Module Sustained Hill-Climbing Capacity vs DOD

discharge (with a 0.5-hr open circuit after charge period) prior to the 8-day stand. This minimal loss is typical for sodium/sulfur systems.

Performance vs Cycle Life

Life testing of the CSPL module was started with SFUDS discharges to 100% DOD in October 1990. Testing will be continued until the module reaches end-of-life, which is defined as the inability to provide 80% of the initial driving range (148 miles). A series of reference discharges will be performed about every 50 cycles to establish the baseline 3-hr rate capacity and determine the effects of cycle life on internal resistance, IR-free voltage, and peak power capability. The variation in module R, $V_{IR-free}$, and peak-power vs DOD with life is plotted for three cycles (31, 70 and 174) in Figures 2-46, 2-47, and 2-48, respectively. The data show that after more than 140 cycles, $V_{IR-free}$ had no noticeable change, but R has increased by ~5%, which caused a similar decrease in peak-power capability.

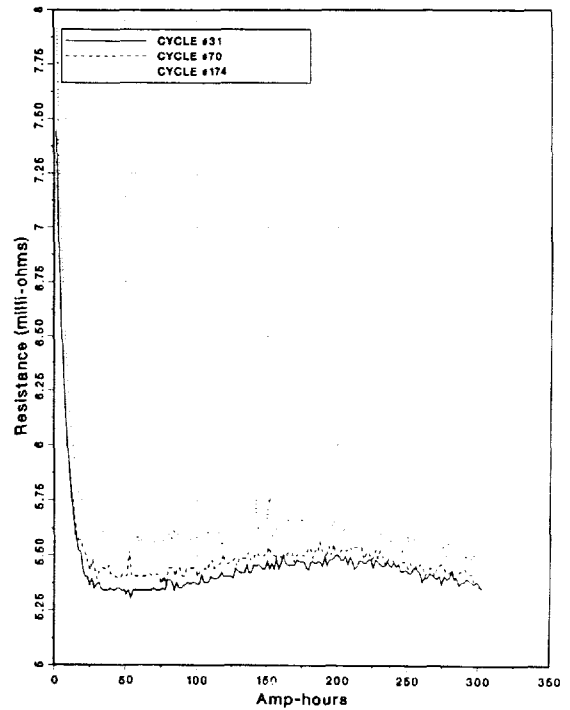


Figure 2-46. Effect of Cycle Life on Resistance vs DOD (J227aD/IETV-1 Discharge)

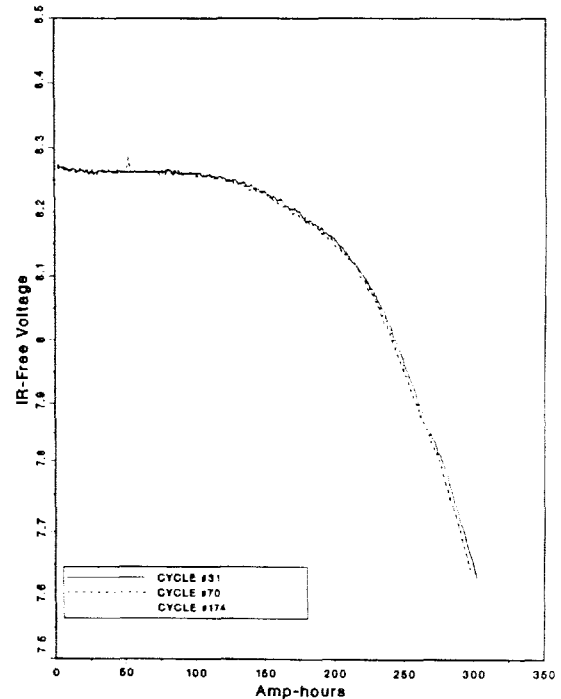


Figure 2-47. Effect of Cycle Life on IR-Free Voltage vs DOD (J227aD/IETV-1 Discharge)

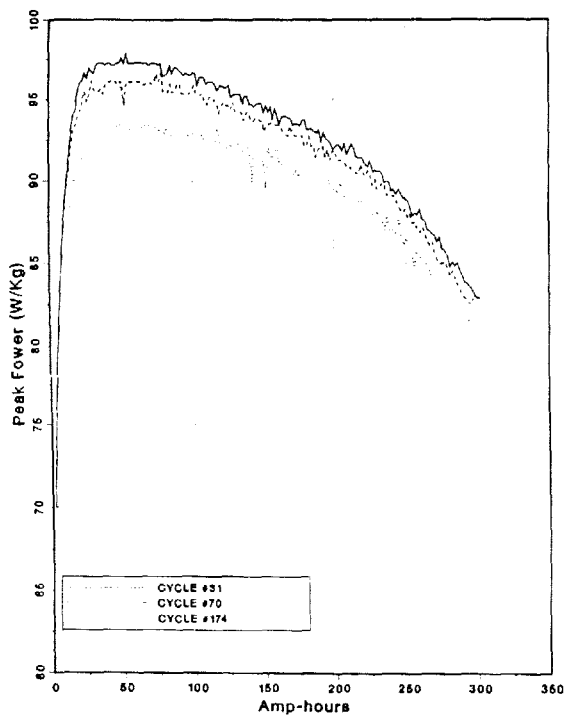


Figure 2-48. Effect of Cycle Life on Peak Power vs DOD (J227aD/IETV-1 Discharge)

Applied Research at SNL

Improved Chromium Plating of Sodium/Sulfur Cell Containers

Container corrosion remains one of the life-limiting processes for sodium/sulfur cells. The solution to this problem is difficult because the container must be very corrosion-resistant, have good electrical conductivity and mechanical properties, and yet be light weight and inexpensive. Corrosion is important not only because of its adverse effect on cell lifetime but also because corrosion products are known to affect long-term cell performance. These diverse and demanding requirements have forced developers to select and use composite materials: usually an inexpensive substrate (e.g., aluminum, carbon steel, stainless steel) that has been coated, plated, or sheathed with at least one corrosion-resistant material.

Because of its excellent intrinsic properties in molten sulfides, chromium-containing layers are usually preferred as the primary corrosion barrier. One of the candidate methods for applying chromium onto sodium/sulfur containers is by electroplating. This

process can be cost-effective and theoretically can produce deposits with good chemical, physical, and mechanical properties.

Although many sodium/sulfur developers have studied and used chromium electroplating, techniques have not yet been identified that produce reliable and effective platings. CSPL is actively pursuing a number of options to improve its current corrosion prevention scheme (thermally chromized steel). Because of this lack of a suitable technique and CSPL's immediate needs, this study was initiated to develop new techniques that improve the quality and efficiency (reduce cost) of chromium electroplating when applied to sodium/sulfur containers.

Encouraging results were obtained with an electrolyte that produces crack-free chromium deposits. This is a commercial product modified with vanadium pentoxide. Results from post-mortem analyses of actual cells plated with such a technique showed that the durability of the electroplate was superior to that achieved with cells utilizing CSPL's current corrosion protection scheme - thermal chromizing. One other electrolyte formulation was evaluated that showed promise: a commercial electrolyte that produced a highly cracked, yet impervious deposit. Based on deposit stress and quality characterizations performed, the highly cracked layers may yield the best performance of all techniques.

However, recent analyses have shown that conventional chromium electroplating techniques, including those being considered previously in this study, may not be cost-effective in sodium/sulfur applications. Furthermore, all of the processes utilize hexavalent chromium and are being increasingly subjected to many strict environmental regulations in the US. As a consequence, costs for conventional electroplating will probably dramatically increase in the near future. Finally, several developers have had success (performance and cost) with containment alternatives that utilize aluminum.

Based on the factors listed in the previous paragraph, the objectives of this task were redefined for FY90 and two techniques evaluated: 1) electroless chromium plating, and 2) electrolytic plating using trivalent chromium. Both efforts were directed at depositing a corrosion-resistant and electrically conductive layer onto an aluminum substrate. As such, a totally sound and impervious deposit may not be required. Electroless plating offers the potential of being very cost effective, and plating using trivalent chromium has little associated environmental regulations. The unknown in this effort is the corrosion resistance of such layers.

The results from the accelerated testing were very poor. The predicted lifetime for the best plating formulation is less than 6 mo in an actual cell environment. These negative results leave the "conventional" methods identified earlier in this program as the only

chromium plating options. Unfortunately, cost and the environmental aspects of using the required hexavalent chromium electrolyte are probably not acceptable. The DOE/SNL sodium/sulfur program must therefore continue to seek better containment alternatives.

3. Zinc/Bromine Project

In FY90, the zinc/bromine technology for stationary energy storage was primarily developed by industry under contracts managed by SNL. The development program at Energy Research Corporation (ERC) concluded in January 1990 with the delivery of a 52-cell, 18-kWh module. This \$5.1M development program, comprised of a \$4.7M DOE-funded contract from SNL and \$0.4M in cost sharing by ERC, began in September 1985 and was completed in January 1990. A final report was issued in May 1990. The objective of this program was to improve the core technology and perform the engineering and evaluation of a 18-kWh zinc/bromine proof-of-concept battery for stationary applications. The core technology is basic and supporting research, qualification of materials, component development, and testing of auxiliaries. In August 1990, a new \$3.6M development program, comprised of a \$3.15M DOE-funded contract from SNL and \$0.47M in cost-sharing, was initiated at Johnson Controls Inc. (JCI). The objective of the new program at JCI is to extend the JCI technology from an electric vehicle application to a load-leveling application and to design, fabricate, and evaluate a 100-kWh load-leveling system. The JCI contract is organized into two 18-month periods. Progress towards battery stack integrity and performance must be demonstrated in the first period in order to initiate the second period in February 1992.

As part of managing these development contracts, SNL accepted the final battery deliverable from ERC for evaluation during FY90, and completed testing three ERC FY89 battery deliverables. Life-cycle testing was performed in order to ascertain possible failure mechanisms. Information gained by the cycle testing program at SNL has assisted the developers with battery stack and system design. ETD supports technology improvement programs at SNL pertaining to materials of construction.

Technology Development - ERC

System Engineering and Evaluation

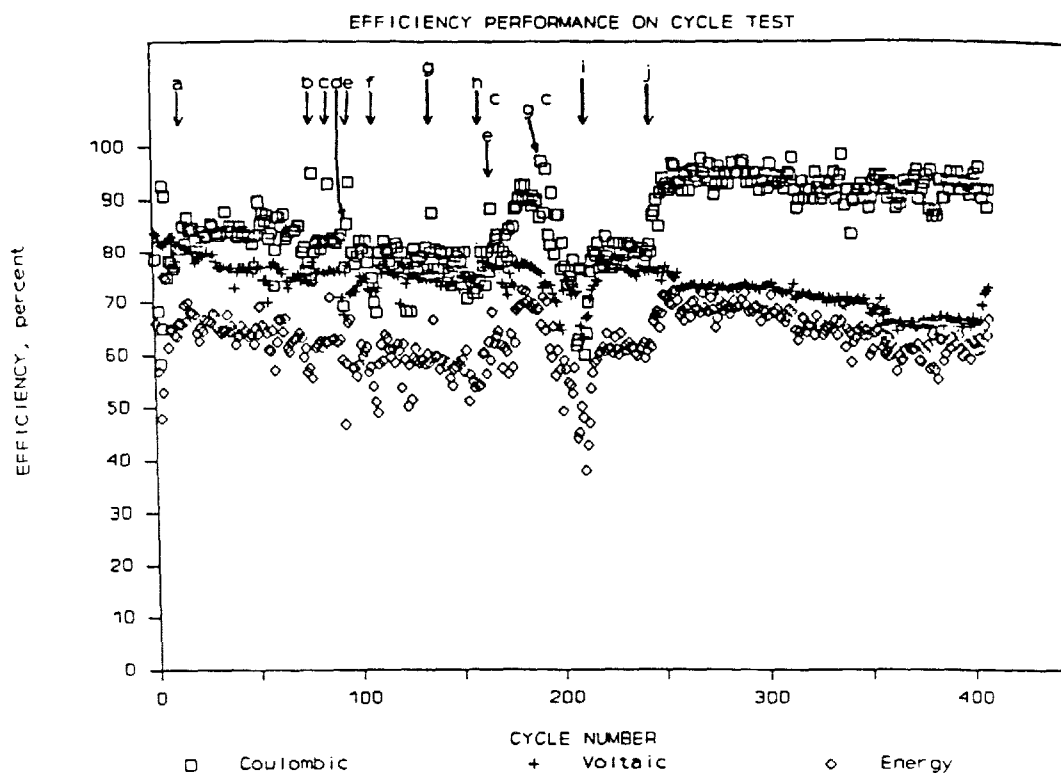
Testing was completed on the 872-cm² five-cell stack SNL-5-4. The stack used the two-flow loop system design, VLT-controlled variable frequency pump

motors, and 0.025-in-thick Daramic separators. Figure 3-1 shows efficiency data for the 408 cycle tests. All of the tests run were baseline cycles except cycle 386, in which only a 4-hr charge was used. Average coulombic, voltaic, and energy efficiencies were 92, 66, and 61%, respectively. The voltaic efficiency had been declining, possibly due to an increase in the stack internal resistance. Since cycle 250, the increase in internal resistance had led to a fall in the average discharge voltage from 7.8 to 7.1 V and a rise in the average charge voltage from 10.2 to 10.8. The probable cause was an electrolyte leak which had developed at the positive end assembly in the stack and had led to a wet end contact assembly oxidizing the positive current collector. For cycles after #394, the coulombic and voltaic efficiencies had been stabilized or increased slightly by adjusting the catholyte bypass valve to increase the mixing of the two-phase positive electrolyte in the catholyte storage tank. Figure 3-2 shows voltage data for cycle #247, in which the stack delivered 155-mAh/cm² capacity density at 68.2% energy efficiency.

Hardware Development

Fabrication of a 5-cell stack that had thicker carbon felt bromine electrodes was completed in October 1989, and was delivered to SNL. This battery module deliverable had been delayed due to problems encountered in the felt carbonization process. The retort oven used in the carbonization process had warped due to extended use resulting in a leak. The rayon felt which was normally carbonized in a nitrogen atmosphere was oxidation due to the air leak. Fabrication of the thicker felt electrodes was resumed after locating and sealing the leak. The thicker carbon felt electrodes were meant to address the issue of low voltaic efficiency in previous 1500-cm² stack tests at SNL. Component fabrication was continued to produce components for a 5-cell battery for in-house testing and a second 52-cell stack for delivery to SNL.

Test data for the first 10 cycles of battery 1500-5-4 are shown in Table 3-1. Average energy efficiency for the ten cycles of 65.7% and voltaic efficiencies as high as 81% demonstrate that the thicker felt electrode design addressed the low voltaic efficiencies observed in previous 1500-cm² stack tests.



NOTES ON SNL-5-4 CYCLE TESTS:

BASELINE CYCLE: 30 A Charge x 5 hr; 30 A Discharge to 6.0 Volts

- a. Electrolyte cleaned
- b. 1 hr charge input
- c. 4 hr charge input
- d. 4.25 hr charge input
- e. 2 hr charge input
- f. MOD-2 end electrodes installed; separators replaced
- g. 3 hr charge input
- h. Catholyte bromine level adjusted up
- i. Overnight stand temperature adjusted - low overnight temperatures were impairing performance
- j. MOD-3 end assembly (no end gasket) installed

Figure 3-1. Cycle Performance for 5-Cell Stack SNL-5-4

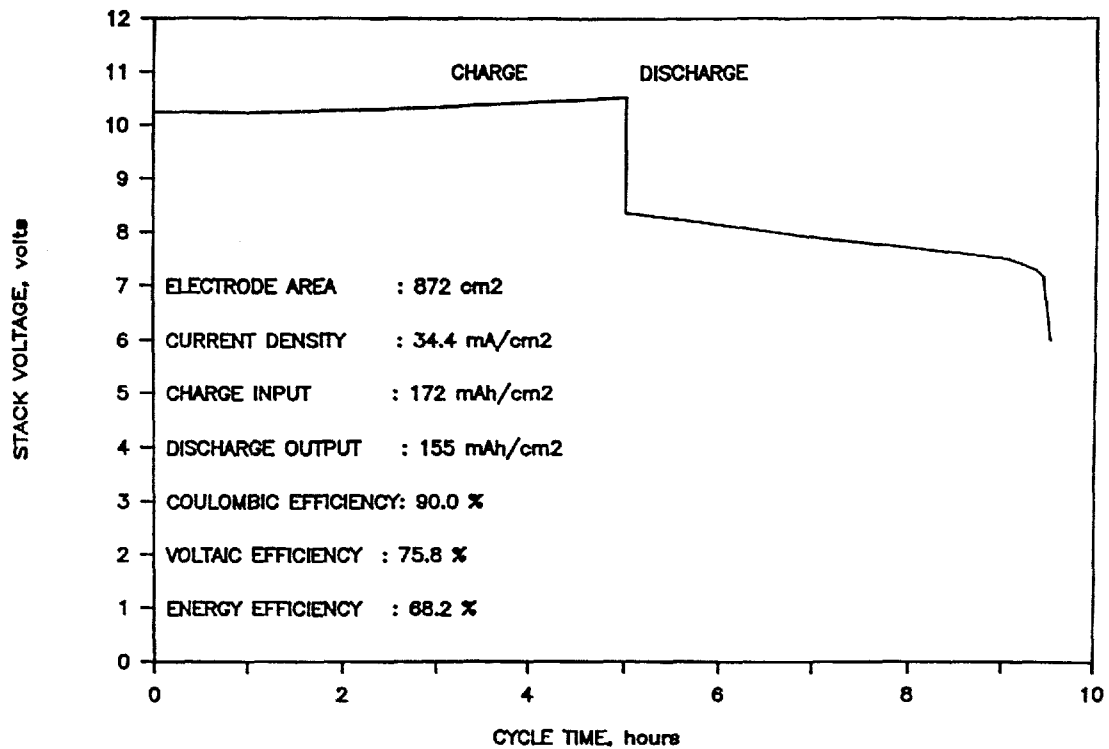


Figure 3-2. Battery Voltage During Cycle 247, Stack SNL-5-4

Table 3-1. Cycle Test Data for ERC Battery 1500-5-4

Cycle	Chg Time (Hr)	Dchg Time (Hr)	Chg Rate (mA/cm ²)	Dchg Rate (mA/cm ²)	Charge Input (mAh/cm ²)	Efficiencies		
						Coulombic	Voltaic	Energy
1	5.00	3.67	34.66	37.50	173.3	79.34	79.96	63.44
2	5.00	3.80	34.66	37.50	173.3	82.23	80.87	66.50
3	5.00	3.83	34.66	37.50	173.3	82.95	81.02	67.20
4	5.00	3.82	34.66	37.50	173.3	82.59	80.83	66.76
5	5.00	3.67	34.66	37.50	173.3	79.34	79.64	63.19
6	4.00	3.13	34.66	37.50	138.6	84.75	78.92	66.89
7	4.00	3.17	34.66	37.50	138.6	85.65	79.15	67.80
8	4.00	3.15	34.66	37.50	138.6	85.20	79.56	67.78
9	5.00	3.67	34.66	37.50	173.3	79.34	79.39	62.99
10	5.00	3.75	34.66	37.50	173.3	81.15	79.90	64.83

Hardware Testing

872-cm² Frame, 30-Cell Stack

Testing was continued on 30-cell stack SNL-30-2. This battery incorporated the two-flow loop system design, VLT-controlled variable frequency pump motors, an anolyte level detection system (which is used to automatically adjust the anolyte pump speed if cross-over occurs), and an in-line pH monitor. Efficiency data for the 409 cycle tests run on the battery are shown in Figure 3-3; coulombic, voltaic, and energy efficiencies averaged 84, 74, and 61%, respectively. All cycle testing was done on the baseline 872-cm² cycle conditions of a 5-h charge at 30 A followed by a 30-A discharge to a voltage cut off of 1.2 volts per cell.

The bromine concentration in the catholyte was lower than the desired concentration of ca. 4 g/l possibly due to evaporation over the 406 cycles that the system has been on test. As a result, the stack discharge voltage had declined slightly over the testing period. Coulombic efficiency declined from 87 to 84%, and the discharge curve shape has indicated that the stack discharge may be bromine limited.

1500-cm² Frame, 52-Cell Stacks

Testing of the first 1500-cm² 52-cell stack, 1500-52-1, was completed in FY90. The battery had exhibited a very high resistance to current flow in initial tests. It was assumed that the separators had not been completely wet, so a second wet-down procedure was done by circulating methanol through the stack, draining the stack, refilling with electrolyte, re-draining, and refilling with electrolyte. After this procedure a series of cycles was run at a lower charge time or lower current density to allow the separators to wet. An increase in the voltaic efficiency indicated that the separators were wetted properly. Test results are shown in Figure 3-4. The battery testing schedule was a 5-h charge at 52 A followed by a discharge at 56 A to a specified voltage cut off. An observation that was made in the initial testing was that the flow pressures required to achieve the design anolyte and catholyte flow rates was higher than those observed in testing of the 5-cell 1500-cm² stacks. Flow pressures were increased as the cycle testing progressed in order to determine the optimum operating conditions. By cycle 15 the electrolyte circulation pumps were being operated at relatively high pressures (16 psi catholyte / 20 psi anolyte with 13 psi anolyte back pressure). This gave a catholyte flow rate of 8 to 10 gpm (depending on state of charge) and an anolyte flow rate of 16 gpm. The design flow rates for the system are 9 gpm for the catholyte and 13 gpm for the anolyte. The 16-gpm anolyte flow rate and 13-psi

anolyte back pressure were required to balance cross-over.

On cycle 32 the electrolyte in the battery was replaced with fresh electrolyte in order to eliminate the effect of possible impurities such as residue methanol on the battery performance. The energy efficiency was actually reduced after the electrolyte change and was probably due to a loss of bromine in the original electrolyte. At cycle 39 bromine was added to the catholyte and coulombic efficiency rose to about 80% again. Coulombic, voltaic, and energy efficiencies averaged 78, 71, and 56%, respectively. A voltage curve for one of the recent cycles is shown in Figure 3-5. The stack delivered 144 mAh/cm² from the 172-mAh/cm² charge input. The initial discharge voltage was 85.2 V, or 1.64 V/cell. The average voltage over the full discharge, including the "knee" at the end of the discharge, was 74.9 V, or 1.44 V/cell.

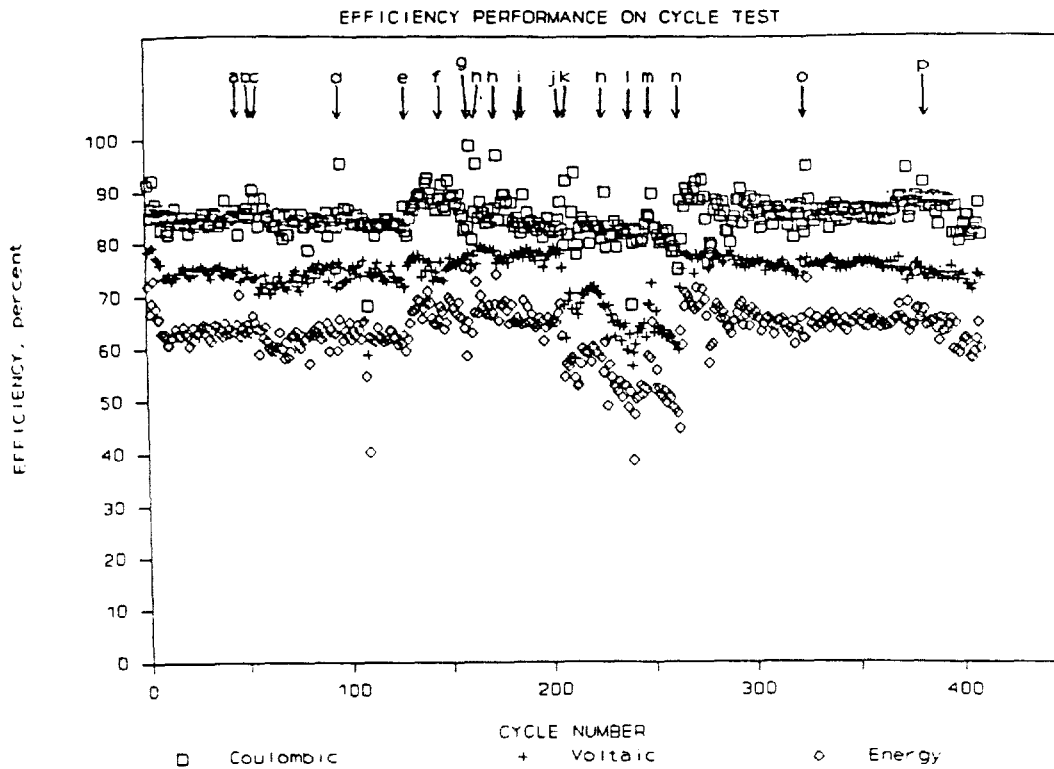
The program final deliverable (1500-52-2), a 52-cell, 18-kWh battery, was fabricated and initial evaluations completed. Performance data is shown in Table 3-2. The efficiencies for the first cycle were low due to the unusually low flow rates used. In subsequent cycle testing, the pressure was raised to 12 psig on both the catholyte and anolyte flow loops. For battery 1500-52-2, the flow restriction was less than its predecessor 1500-52-1. The design flow rates were achieved at 12 psig for battery 1500-52-2, while 15 psig and 20 psig pressures were required in the anolyte and catholyte loops, respectively, in battery 1500-52-1.

Technology Development - JCI

Battery Testing

Two 8-cell batteries, V1-35 and V1-39, were tested with shunt current protection systems. The SCP system is not required for small batteries because of the relatively low stack voltage compared to batteries with more cells. The SCP system on these 1-kWh, 8-cell batteries was installed to prove and troubleshoot the externally fed SCP electrodes. In previous testing on batteries with SCP systems, e.g., the 20-kWh Z-design battery at the Keefe facility, the battery lost approximately 3% of the usable energy to the system. When the SCP system was connected on V1-35, the energy efficiency dropped by 2%.

Initial battery testing on V1-35 showed that at the end of charge there was a 6-mA difference in current between the SCP electrodes on the anode exit manifold and the anode outlet manifold. However, there was no

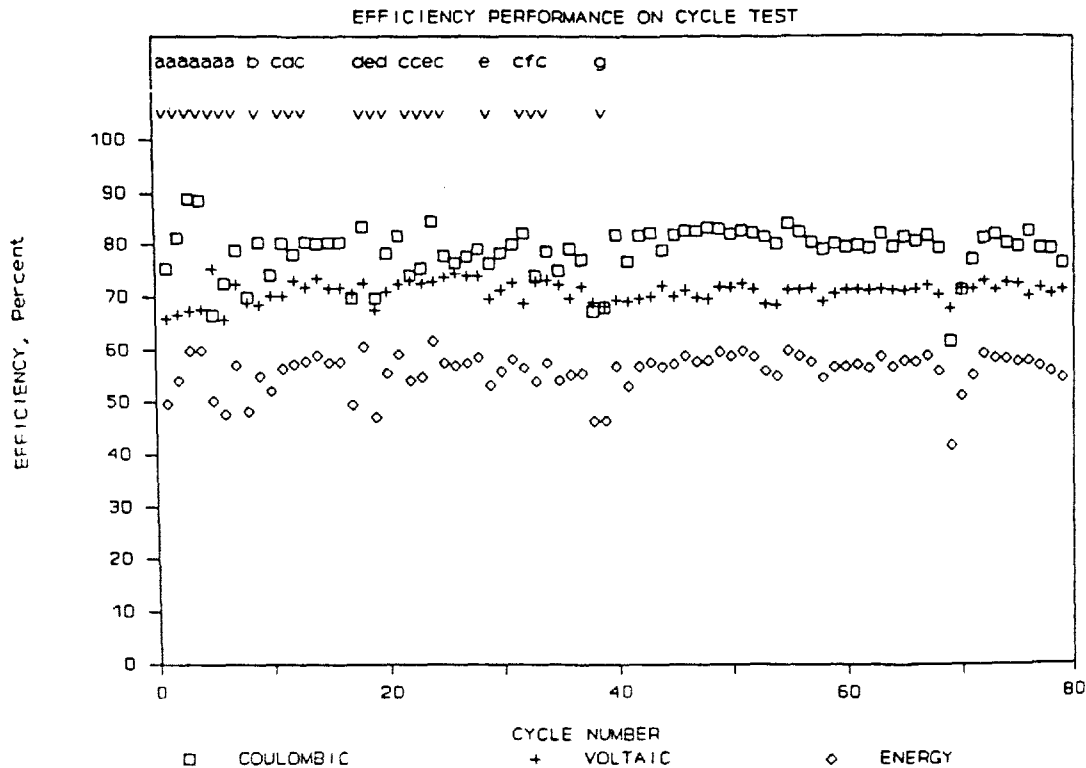


NOTES ON SNL-30-2 CYCLE TESTS:

BASELINE CYCLE: 30 A Charge x 5 hr; 30 A Discharge to 6.0 Volts

- a. Low rate cycle. Charge at 15 mA/cm² x 8 hr; Discharge at 15 mA/cm² to 36 volts. Energy efficiency raised to 70.3%.
- b. 3.9 hr charge
- c. 2.9 hr charge
- d. Hydroclone installed; 1.5 hr charge
- e. MOD-2 end assembly installed; Hydroclone removed
- f. Electrolyte cleaned
- g. 1.9 hr charge
- h. 3 hr charge
- i. 5.33 hr charge
- j. 4.5 hr charge
- k. 1.5 hr charge
- l. Electrolyte replaced with low KCl electrolyte to prevent salt-out
- m. 1 hr charge
- n. MOD-3 end assembly (no end gasket) installed
- o. 2.27 hr charge
- p. pH adjustment

Figure 3-3. Cycle Performance for 30-Cell Stack SNL-30-2



NOTES ON 1500-52-1 CYCLE TESTS:

BASELINE CYCLE: 35 mA/cm² Charge x 5 hr; 37.5 mA/cm² Discharge to 40 V

- a. Wet-down cycles. Low rate or short duration cycles to facilitate separator wetting.
- b. 2 hr charge input
- c. 4 hr charge input
- d. pH adjusted upwards
- e. 1 hr charge input
- f. Electrolyte replaced with fresh electrolyte
- g. Bromine level increased

Figure 3-4. Cycle Performance for 52-Cell Stack 1500-52-1

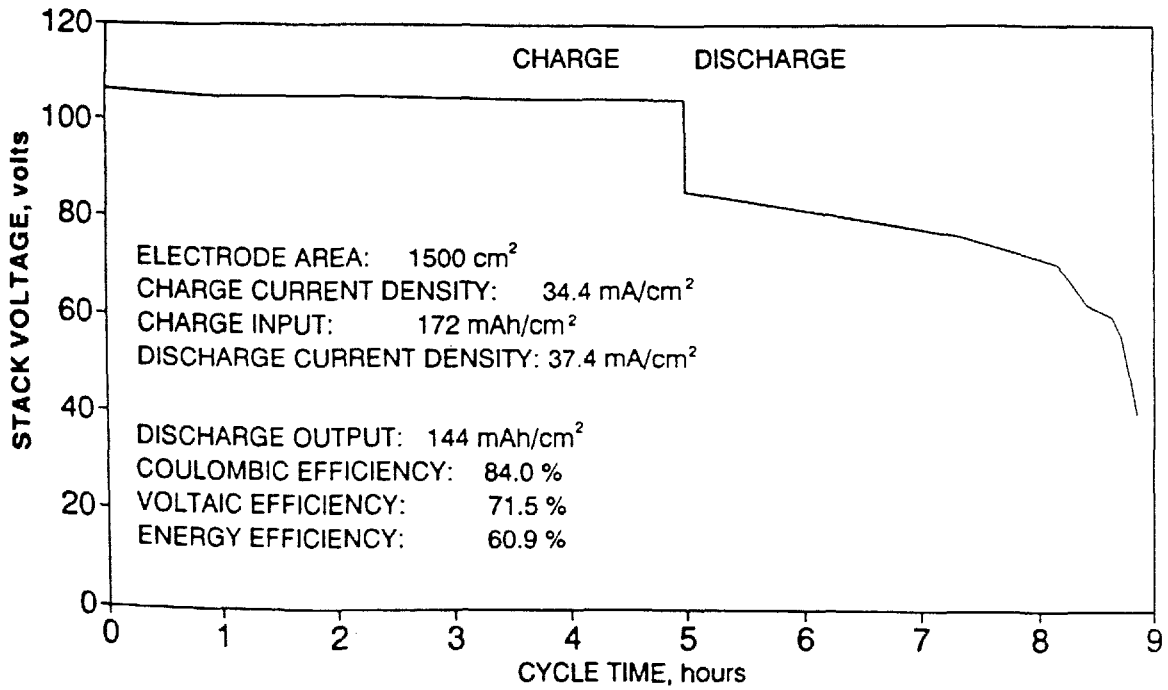


Figure 3-5. Battery Performance During Cycle 55, Stack 1500-52-1

Table 3-2. Cycle Test Data for ERC Battery 1500-52-2

Cycle	Chg Time (Hr)	Dchg Time (Hr)	Chg Rate (mA/cm ²)	Dchg Rate (mA/cm ²)	Charge Input (mAh/cm ²)	Efficiencies		
						Coulombic	Voltaic	Energy
1	5.00	3.32	34.13	36.98	170.7	71.87	69.20	49.74
2	4.00	3.15	34.33	37.33	137.3	85.63	74.14	63.49
3	5.00	3.72	34.93	37.31	174.7	79.39	75.24	59.73
4	5.00	3.63	34.80	37.33	174.0	77.96	76.15	59.36
5	5.00	3.33	34.67	37.33	173.3	71.79	74.08	53.18
6	4.00	3.42	34.40	39.20	172.0	77.87	72.91	56.78
7	4.00	3.50	34.53	37.14	172.7	75.28	73.95	55.67
8	4.00	4.00	34.20	31.20	156.0	80.00	75.19	60.15
9	5.00	3.73	34.93	37.31	174.7	79.75	74.67	59.55

difference in SCP electrode currents on the cathode side of the stack. There also was a difference in SCP electrode currents between the anode and cathode sides of the stack with the anode being 73 mA higher. Replacing the cathode side SCP electrodes with carbon-coated electrodes did not significantly effect the current required from those electrodes. Enlarging and straightening the SCP tunnels through the stack increased the draw of current (to 100 mA) by all electrodes but did not remove the offset.

Stack V1-39 has SCP with large diameter tunnels (0.1209"). Consequently, the SCP currents are much higher than the currents on V1-35. The offset between the cathodes and anodes is still present at 109 mA. The

data in the Table 3-3 illustrates 1-kWh battery efficiencies with and without the SCP system.

The bromine transport inefficiency result is higher with the SCP system active for two reasons: 1) some second phase is diverted to the anode SCP electrodes, 2) current used by the SCP electrodes appears as amhours lost to bromine transport. The residual inefficiency (zinc and bromine left in the battery when the battery reaches 1.07 V/cell cutoff) appears to be low when the SCP electrodes are connected because the amhours recorded for charge do not take into account the current that was diverted to the parasitic SCP system.

A plot of the battery voltage and SCP currents throughout a cycle on V1-39 are shown in Figure 3-6. Analysis of data points in the plot gives reason to

Table 3-3. JCI Battery Efficiency With and Without SCP

Condition	% CE	% VE	% EE	% Trans	% Res
W/ SCP system	78.3	83.1	65.0	16.5	5.4
W/out SCP system	81.4	82.4	67.1	12.4	6.3

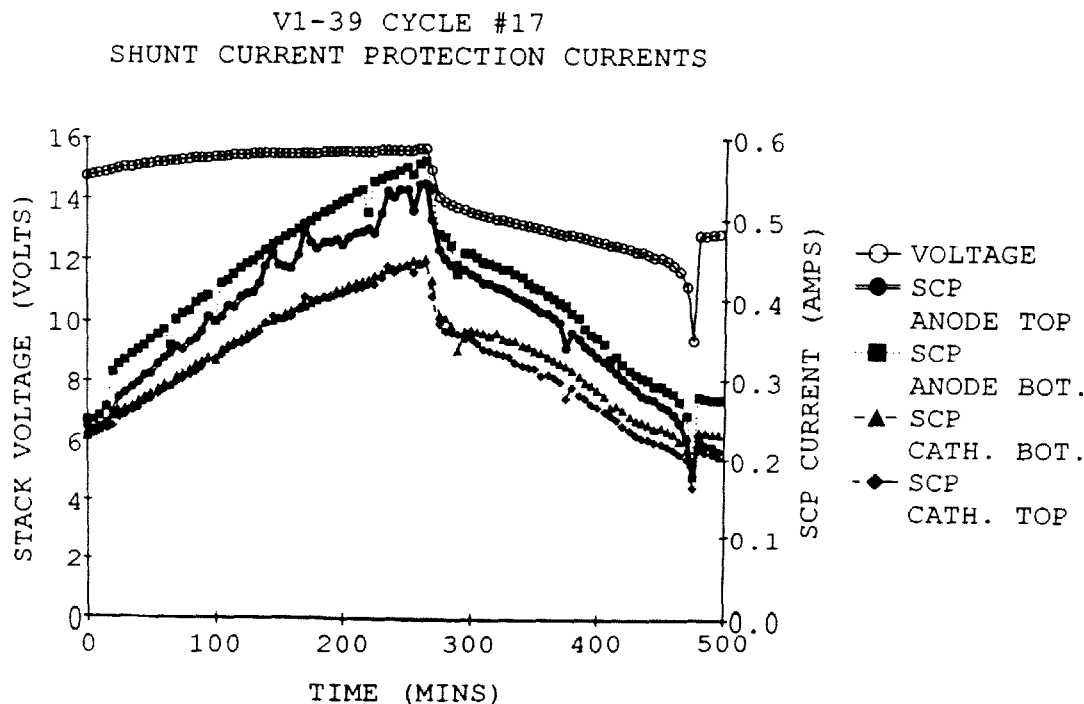


Figure 3-6. V1-39 Battery Voltage and SCP System Currents

believe that the currents are effected by the amount of second phase in the SCP system. It was noted on a cycle in which the SCP system was not active that there was flow of the catholyte from one SCP electrode to the other on the anode side of the stack and that it changed direction when the catholyte flow in the stack was reversed. This indicates that there is a pressure differential between the SCP electrodes on a side of the stack. This pressure differential may be affecting the flow of catholyte into the SCP system and could explain why there are discrepancies in the currents of these SCP electrodes.

Future tests will evaluate currents of the SCP system with regard to the quantity of second phase introduced to the system. Resistors will also be varied to determine effect on stack and SCP efficiency.

V1-38

This battery has attained over 70 cycles with unsupported electrolyte. This battery has not been switched over to the load leveling electrolyte and is currently being used to complete a study examining operating pressure. In general it has been demonstrated that with an anolyte inlet pressure 1 psi greater than the catholyte, a decrease of 2% in the bromine transport has been realized. This has resulted in a 2% increase in energy

efficiency. Figure 3-7 illustrates the efficiencies of the battery during the studies examining operating parameters.

V1-40

Constant current testing was started to establish baseline performance on this 1-kWh stack. During cycles 1-8 the battery reached the high voltage limit of 2.1 V/cell during the last 10-15 minutes of charge. Zinc utilization was determined to be 88% rather than the intended 80%. The addition of more electrolyte alleviated the flagging problem. The battery performance during the last 13 cycles is illustrated in Figure 3-8.

Materials

Frame material (3000 lb) and bipolar substrate material (1000 lb) were ordered. Quality assurance documentation and samples are at JCI for analysis. The production run of the advanced electrode material took place on September 13, 1990, resulting in 900 lb of 52" x 12" sheet. Reportedly, there were no problems with the run; thicknesses of the semi-consolidated sheet were approximately 0.050" to 0.060". Based on the measured densities, this material should be able to be consolidated (densified by hot-pressing) down to 0.025" to 0.030".

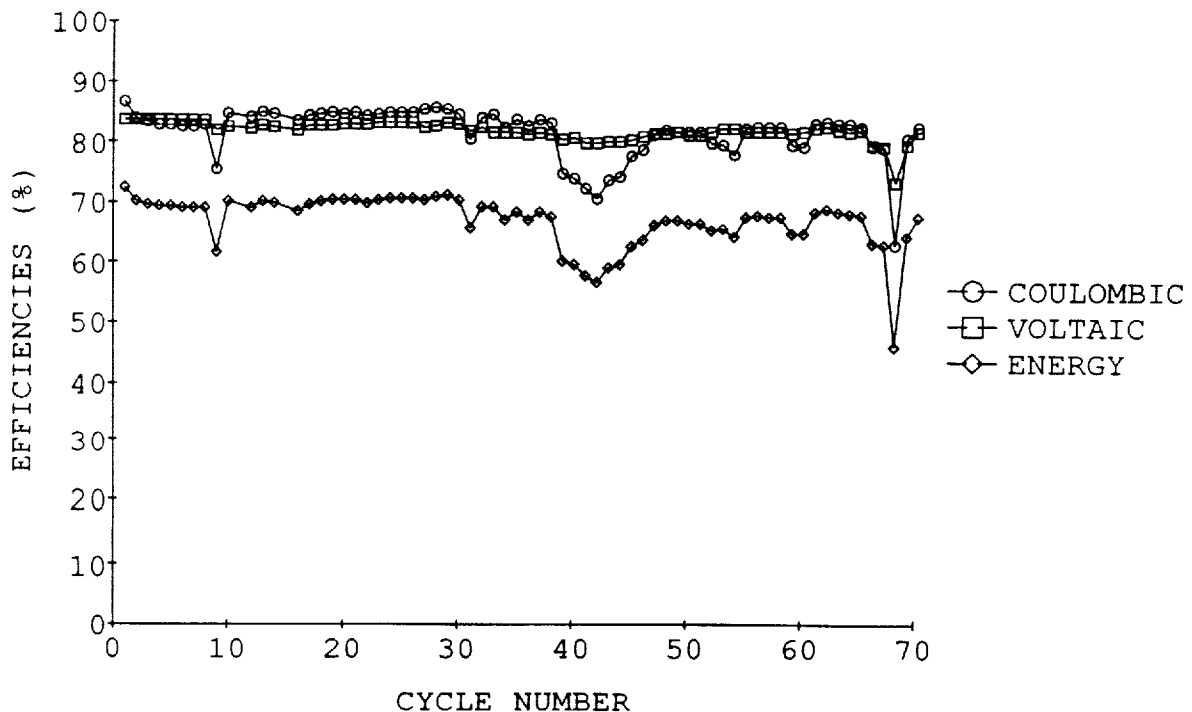


Figure 3-7. Cycle Efficiency for 8-Cell Stack V1-38

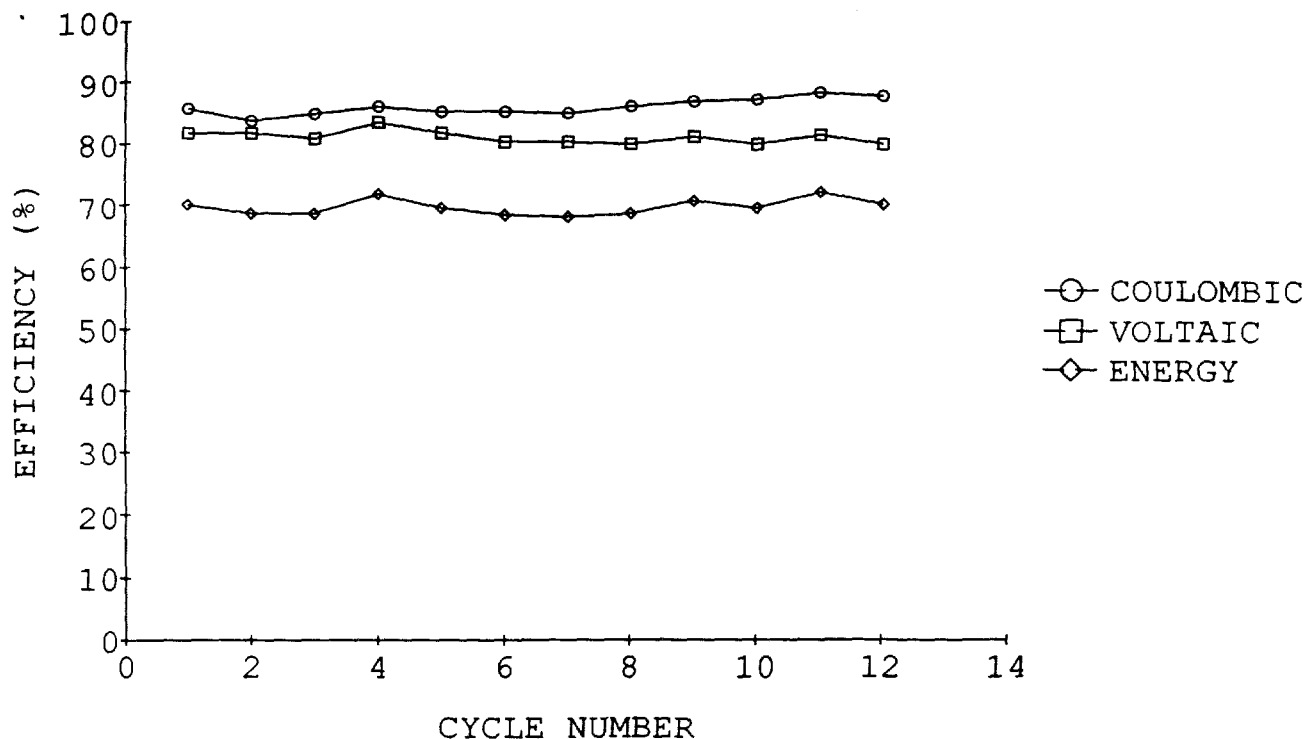


Figure 3-8. Cycle Efficiency for 8-Cell Stack V1-40

Even though the composition contained 23.5% Ketjenblack, its resistivity was 15-25 ohm-cm. This is too high for good high-rate discharge capability, but it may be adequate for lab testing of load-leveling batteries. This production run was performed to establish some process parameters and determine if the quality of electrode material would meet the JCI specifications. Previous batches were produced in the lab. By running the material on the production equipment JCI will realize an improvement in material consistency and a decrease in cost.

Technology Evaluation at SNL

During 1990, SNL evaluated two batteries from ERC. The first was a 5-cell, 1-kWh battery (SNL #494) with an electrode size of 1,500 cm². The second battery tested was a 52-cell, 18-kWh unit (SNL #497) which also had an electrode size of 1500 cm². Posttest analyses were completed on these batteries along with two other batteries from ERC which were tested earlier in the contract; a 30-cell battery (SNL #459) with an electrode size of 872 cm² and a 5-cell battery (SNL #481) with an electrode size of 1,500 cm².

Evaluation Procedures

A typical electrical cycle for the zinc/bromine batteries consisted of a timed, constant-current charge related to the theoretical zinc loading. After a 5-minute open-circuit wait following charge, a constant-current discharge was imposed until the battery voltage fell below a predetermined cut-off level, typically 1.0 V/cell. The batteries were then discharged completely (0 V).

Battery 494

A total of 127 charge/discharge cycles were performed on this battery. The majority of these cycles were baseline capacity tests; however, a set of parametric tests were also performed. Table 3-4 below was the parametric test plan used. The battery was stripped after each cycle, taking the battery voltage down to 0 V. Baseline cycles were run several times during the test plan.

Figure 3-9 is a plot showing the effect charge current had on the battery efficiencies. As the charge current was increased, the voltaic efficiency remained constant while the coulombic and energy efficiencies decreased. This decrease was also seen to a greater

Table 3-4. ERC Battery #494, Parametric Test Plan

Test Type	Zinc Loading (mAh/cm ²)	Density (mA/cm ²)	Charge		Discharge	
			Current (amps)	Time (hrs)	Density (mA/cm ²)	Current (amps)
1	138.6	46.2	69.3	3	37.4	56.1
2	138.7	34.7	52.0	4	37.4	56.1
3	138.7	27.7	41.6	5	37.4	56.1
4	104.0	34.7	52.0	3	37.4	56.1
5	104.0	26.0	39.0	4	37.4	56.1
6	103.7	20.7	31.1	5	37.4	56.1
7	110.4	36.8	55.2	3	37.4	56.1
8	138.7	34.7	52.0	4	45.0	67.5
9	138.7	34.7	52.0	4	37.3	56.0
10	138.7	34.7	52.0	4	30.0	45.0
11	138.7	34.7	52.0	4	22.0	33.0

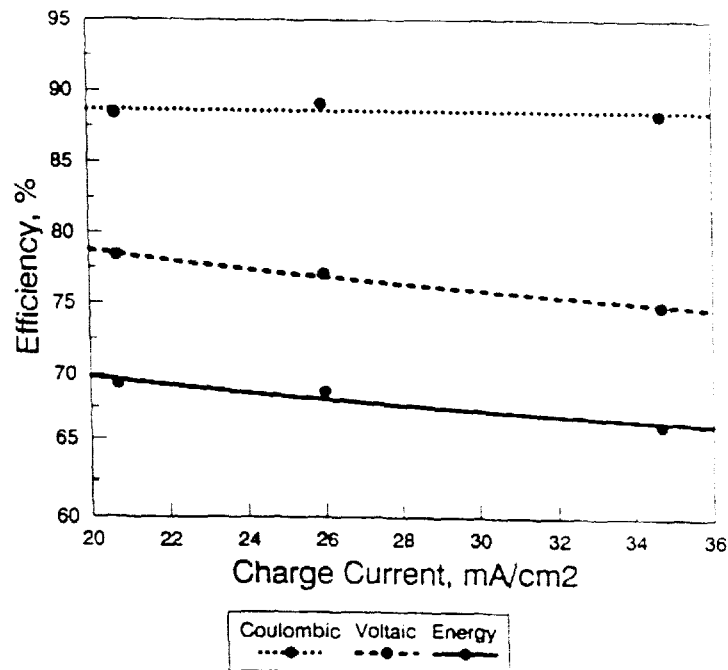


Figure 3-9. Effect of Charge Current on Battery Efficiencies

extent as the discharge current was increased. These results are shown on Figure 3-10.

The effect of increased zinc loading on battery efficiencies is shown in Figure 3-11. There was a decrease in coulombic and energy efficiency as zinc loading was increased; however, a slight upward trend was seen in the voltaic efficiency. During charge, bromine oil was concentrated and stored so on discharge, the bromine oil concentration was higher at higher zinc loadings. Therefore, the discharge kinetics overpotential was lower at higher loadings and the voltaic efficiency was higher.

Figure 3-12 is a plot showing the coulombic, voltaic, and energy efficiencies for all the cycles run on battery 494. A gradual decline of 12% in coulombic, 9% in voltaic, and 16% in energy efficiency was measured during the life of this battery.

The electrolyte level probes were cleaned daily to prevent electrolyte crossover from the catholyte tank to the anolyte tank. If this daily cleaning was not performed, a gradual decline in coulombic and energy efficiency was observed.

Several small leaks, referred to as weeping, were observed between the flow frames of this battery; however, the performance of the battery was not affected.

The battery flow system and stack were disassembled and carefully examined. Observations indicated that there was extensive leakage of the stack between the separators. Also, the cathode seal leaked, which caused the titanium current collector to become wetted with bromine. Intrusion of bromine into the RTV on both the anode and cathode ends was observed. Finally, there appeared to be no blockage of the flow channels throughout the stack.

Battery 497

A 52-cell, 18-kWh ERC battery was also evaluated during this fiscal year. A total of 61 charge/discharge cycles were placed on this battery; however, performance problems resulted in early termination of testing. Throughout the life of the battery, large amounts of bromine were added to the catholyte reservoir in an attempt to recover the efficiency losses that were experienced during cycling. The voltaic efficiency remained relatively constant over the life of the battery; however, a 20% coulombic and 10% energy efficiency decline was observed during this time.

To accomplish the posttest analysis, the battery flow system and stack were first disassembled. An analysis of the battery stack and the individual flow frames did not strongly indicate an explanation for the

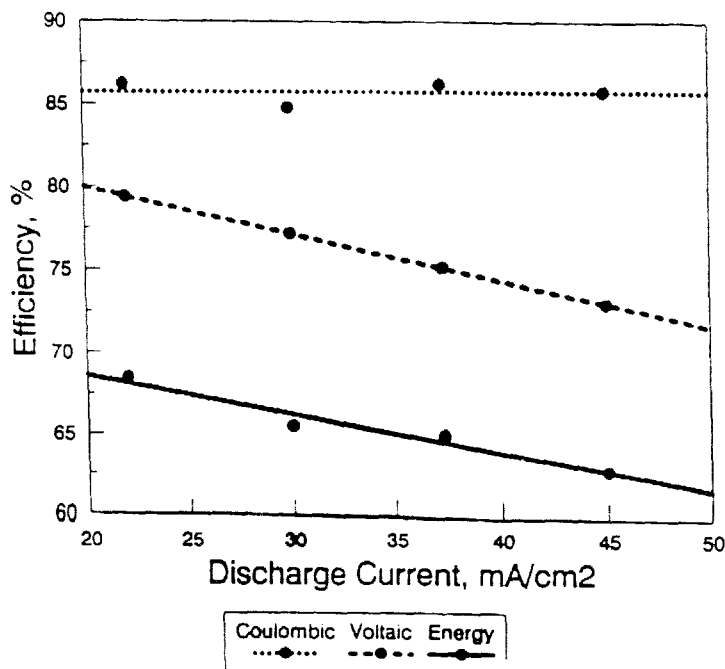


Figure 3-10. Effect of Discharge Current on Battery Efficiencies

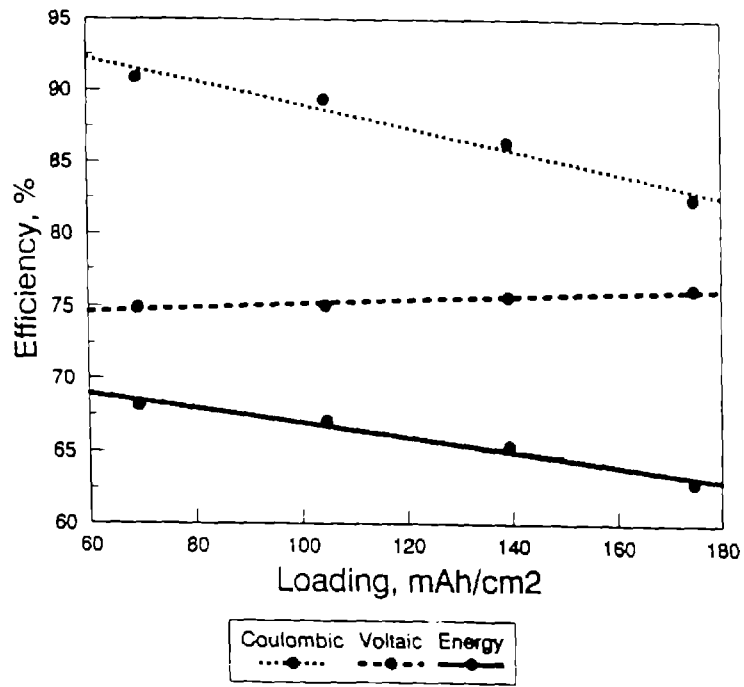


Figure 3-11. Effect of Zinc Loading on Battery Efficiencies

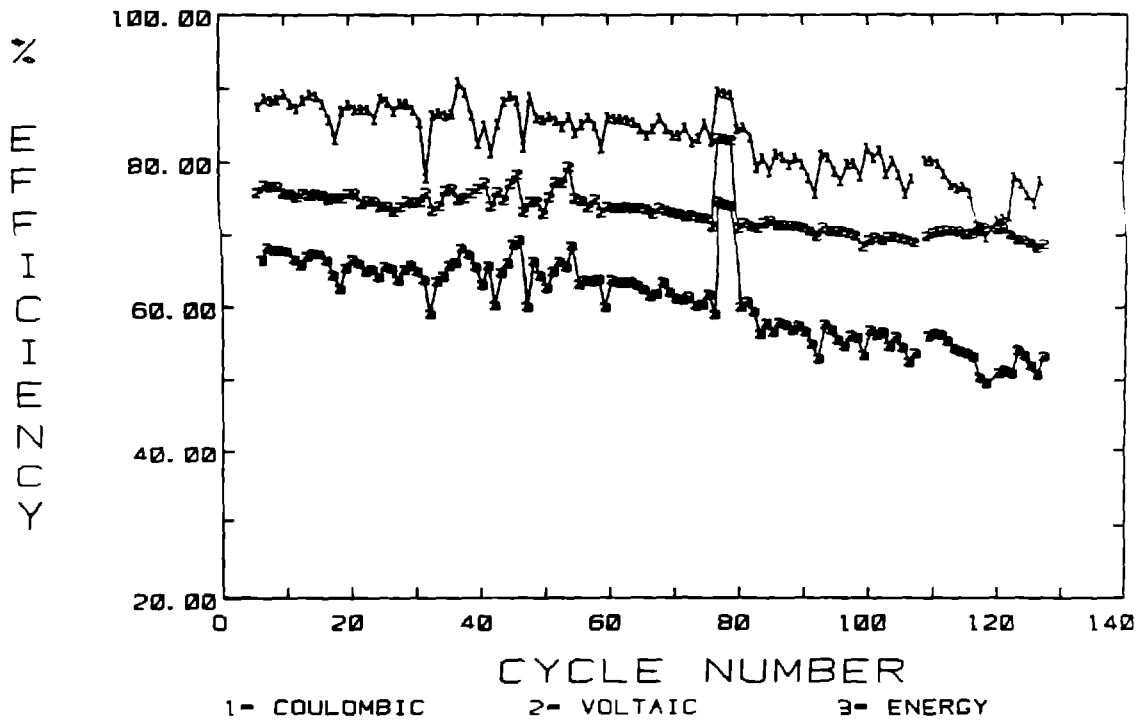


Figure 3-12. Efficiency Plots for Zinc/Bromine Battery 494

poor performance. Both titanium current collectors were found to be dry and free of bromine. There was no significant amount of foreign matter blocking the individual flow channels in the flow frames. On one flow frame, the bromine activation felt was torn, while on another flow frame, two screens, rather than one, were placed between the bipolar plate and the separator. The only evidence for the root of the poor performance was the occurrence of zinc plate on some of the bipolar electrodes when the battery had been supposedly fully charged. Obviously, the battery had experienced some degree of poor flow distribution; however, the quantitative extent that the less-than-optimal flow distribution affected the battery performance was unknown.

Battery 459

After completing 92 cycles on this battery, testing was suspended due to large fluctuations in the battery efficiencies. A tear-down of the battery stack was conducted in October 1989 and the following observations were made:

1. The negative end plate had an area of spongy black deposits approximately 6" x 6".
2. The first three bipolar plates on the negative side delaminated from the flow frames.
3. The positive end plate was cracked and the felt on the back side was wet.
4. The eighth bipolar plate had a "peanut butter" consistency material which blocked the flow channels and "filled" the felt. This material was given to C. Arnold of Sandia's Chemistry of Organic Materials Division for analysis.

Battery 481

This battery was cycled 52 times and was removed from test due to poor efficiencies. Upon tear-down, a crack was discovered near the inlet on the catholyte side. The crack extended from outside the flow frame

and across the flow channels causing the electrolyte to leak onto the current collector. The cause of the crack was the same as described above for battery 494.

Applied Research at SNL

SNL assists the program developers on specific tasks that are better suited to be addressed at SNL. During FY90, technology improvement issues concerning the materials of construction have been specifically addressed at SNL owing that these issues may have a major impact on the viability of the technology in terms of battery lifetime. Components for the zinc/bromine flow batteries are fabricated from thermoplastics. Characterization of these materials is critical for the assessment of product uniformity and battery lifetimes and to gain insight into possible failure mechanisms. During the past year, several battery materials were characterized for these purposes. The results obtained for materials used in ERC's, JCI's and Toyota's zinc/bromine batteries are summarized below.

ERC Materials

Modulus uniformity across the thickness dimension at three different locations of an unused flow frame used in the ERC battery was determined by a technique developed at SNL known as modulus profiling. In this technique, the tensile modulus of a very small area (~1 square micron) of material is determined by placing weights on a specially designed penetration probe. This technique is ideal for detecting variations in mechanical properties due to improper processing or chemical degradation. The data obtained in this exercise are summarized in Table 3-5. It is evident from Table 3-5 that there was no variation within experimental error for this virgin PVC-1 flow frame. As reported in the 1989 annual report, the variation in modulus as a function of location for a flow frame that was taken from a battery that had been cycled 100 times may have been due to

Table 3-5. Modulus Profiling of a Virgin PVC-1 Flow Frame

Location	Modulus (MPa)
Corner	1948±345
Small channel	1975±277
Large channel	1906±416

degradation. In this case, moduli taken across the thicknesses of the flow channels was significantly higher than that observed at the corners. This suggests that crosslinking of PVC may have occurred in the channel locations. Crosslinking could have occurred during processing or during cycling.

High fracture toughness is an important property for flow frame materials because of the compressive stresses that needed for stack assembly. Therefore, the fracture toughness was determined for PVC-1, PVC-4 and PVC-6, the three poly(vinyl chloride) based formulations that had been considered candidates for ERC's flow frame. This was accomplished by modifying the fracture toughness procedures used for metals (ASTM E-813). In this procedure, compact tensile specimens are precracked in stroke control. This means that the displacement of the actuator was held constant throughout the precracking allowing the load to decrease as the crack length increased. The total number of cycles for precracking of each sample was ~5000. The PVC samples were not sufficiently thick to satisfy the requirements for a valid K_{Ic} determination. This procedural variation affects only the absolute values of fracture toughness; relative values for fracture toughness are still considered valid. K_Q is the term generally used to designate fracture toughness values which do not meet all the requirements set forth in ASTM E-813. These data are listed in Table 3-6 for PVC samples whose thicknesses were the same as the flow frame material used in ERC's battery. The fracture toughness figures are in accord with other toughness measurements such as the ASTM Izod-Notched test (ASTM D-256). PVC-6, a lead stabilized PVC, is considered to be the current favored baseline flow frame material.

Current collectors of one of the problematic ERC batteries that are being evaluated at SNL were submitted for Auger analysis to determine their surface composition. These titanium plates were reported to have a 20-micron-thick ruthenium coating. It was suspected that the poor performance of this particular battery may have been a caused by loss of this coating. The composition

of the surface of these collectors as a function of sputtering time is shown in Figure 3-13. Based on sputtering rates obtained from a standard film of silicon dioxide (ruthenium standards were not available), it was estimated that maximum depth attained in these sputtering experiments were on the order of a few thousand angstroms. These data clearly show that titanium is present at or near the surface of the ruthenium film and that the titanium was oxidized. The cause for the apparent loss of ruthenium is not known.

JCI Battery

SNL is in the process of characterizing JCI's flow frame by modulus profiling and determining of the surface modulus at various locations. The purpose of this exercise is twofold: 1) to obtain baseline data for subsequent battery tear-downs; and, 2) to detect property variations which may be attributable to nonuniform processing. These flow frames are made by injection molding of polyethylene-glass fiber mixtures. The surface modulus data are summarized in Table 3-7. The surface moduli vary by a factor of two depending on location. Furthermore, these moduli were quite low. This seems to be typical of thermoplastics in general. The surface moduli of ERC's PVC flow frames were also low. Possible explanations for this observation are: 1) contamination of the surface by mold release agents; 2) surface roughness (the surface is not polished prior to the measurement of modulus).

To date, one profile was taken at middle right edge location. At this location the modulus was 1082 ± 228 MPa. This represents an average of ten measurements taken across the thickest portion of the frame (0.048 inches). There was no trend in the data; the profile was essentially flat from surface to surface. Additional moduli data at other locations are being gathered.

Table 3-6. Fracture Toughness of ERC Flow Frame Material

Sample	K_Q
PVC-1	3.3 Ksi (in) ^{1/2}
PVC-4	1.5 Ksi (in) ^{1/2}
PVC-6	5.4 Ksi (in) ^{1/2}

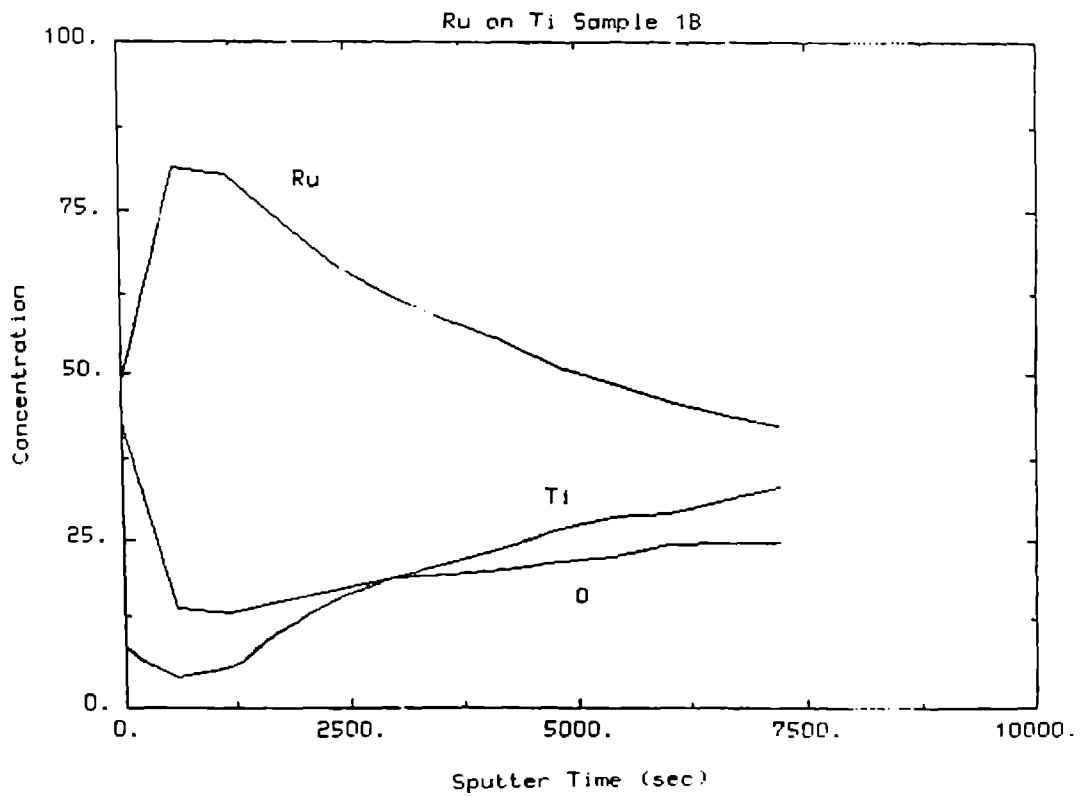
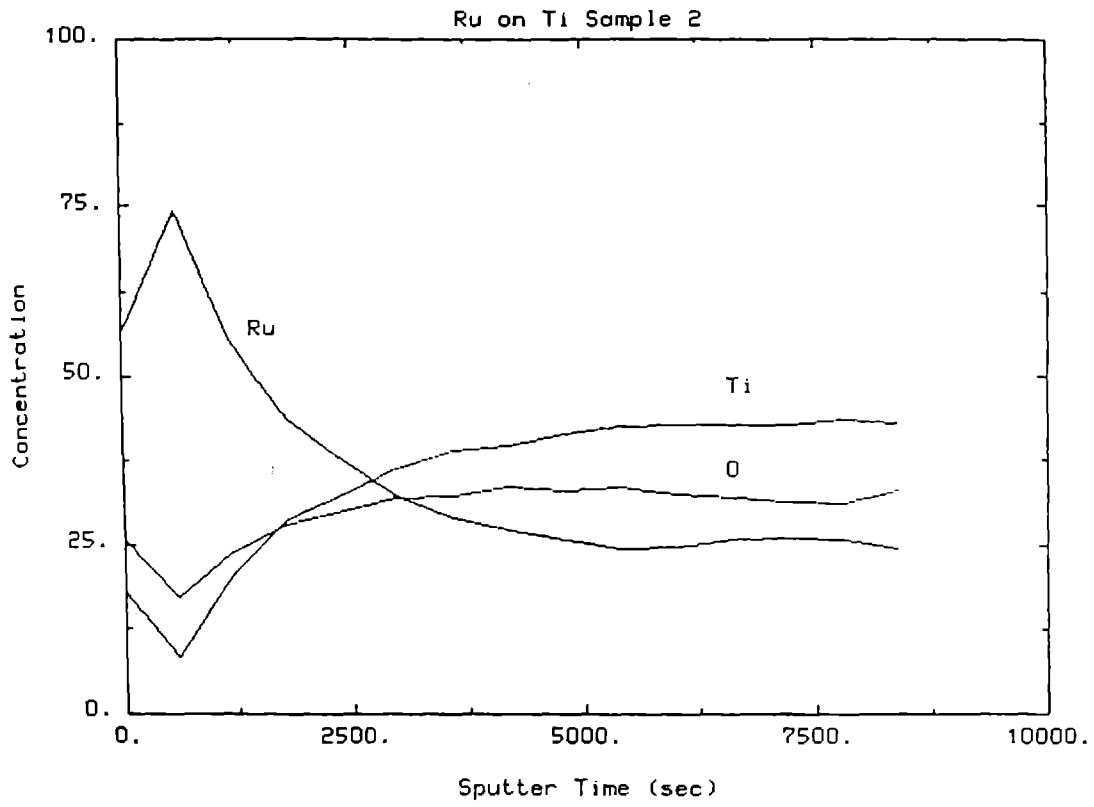


Figure 3-13. Surface Composition of ERC Current Collector

Table 3-7. Surface Modulus of JCI Flow Frame

Location	Modulus (MPa)	Comments
Middle left edge	165±30	Smooth surface
Middle right edge	241±14	Smooth surface
Middle right edge	187±19	Mottled surface
Left middle between ridges	134±17	Smooth surface
Right middle between ridges	126±8	Smooth surface

Toyota Battery

Separators from two torn-down Toyota batteries were sent to Sandia by JCI for analysis. Both of these batteries, designated JCI-2 and JCI-3, were 65-cell batteries and were normally cycled by charging at 18 A for 4.5 h followed by a discharge at 18 A. JCI-2 was cycled 144 times. During the later cycles this battery gave evidence of electrolyte shorting and the coulombic efficiency fell rather sharply. The teardown indicated that the short occurred through the separator next to the terminal anode. JCI-3 was cycled 70 times. On cycle 68 there occurred a pump failure during charge which resulted in a temperature excursion estimated to be as high as 70°C. After this event the battery was defunct. To determine the extent of degradation of the separator, which was a microporous silica-filled polyethylene (Asahi SF-600), we characterized both virgin and used separators by FTIR, modulus profiling, area resistivity and bromine permeation rate. The results are sum-

marized in Table 3-8. The following points can be made with regard to this data:

1. Chemical or thermal degradation, if it occurred at all, was minimal as evidenced by no changes noted between the virgin and the aged separators by FTIR.
2. No change was observed in the modulus of the separator taken from the JCI-2 battery within experimental error.
3. Decreases in modulus ranging from 46 to 84% for separator taken from the JCI-3 battery were observed. This suggests that degradation did occur which was not detectable by FTIR; mechanical properties are generally more sensitive to changes in molecular architecture than are spectral properties, i.e., small changes in chemical or thermal degradation can lead to large changes in molecular weight which, in turn, affect mechanical properties.

Table 3-8. Postmortem Characterization of Toyota Separators

Separator	FTIR	Modulus (MPa)	Area Resistivity (W·cm ²)	Bromine Permeation Rate (moles Br ₂ /sec·cm ²)
Control	NC	107±8	0.84	2.1 K10-9
JCI-2-10	NC	104±14	1.29	2.7 K10-9
JCI-3-65	NC	68±14	1.23	2.6 K10-9
JCI-3-46	NC	86±10	1.55	2.7 K10-9
JCI-3-47	NC	45±12	1.35	2.6 K10-9

NC = No change

4. The electrochemical properties of the separator, i.e., area resistivity and bromine permeation rate, deteriorated somewhat (a 46 to 84% increase in resistivity and 24 to 28% increase in bromine per-

meation rate) but not as much as might have been expected based on visual observations, especially for separator 47 of the JCI-3 battery. This separator was very brittle and badly discolored.

4. Nickel/Hydrogen Project

A project to design and develop a nickel/hydrogen battery for photovoltaic and other terrestrial applications was concluded under a cost-sharing contract between Johnson Controls, Inc. (JCI) and SNL. Nickel/hydrogen batteries have been successfully used for many years with satellite photovoltaic systems and are noted for their long life, reliable performance, and maintenance-free operation. The primary challenge of this project was to dramatically reduce the first-cost of the battery to make it economically competitive on a life-cycle cost basis with other energy storage batteries, without compromising these favorable characteristics.

In a previous contract with SNL, #53-8334 completed in March of 1988, a 7-kWh nickel/hydrogen battery using a common pressure vessel (CPV) design was delivered to SNL for testing at the photovoltaic facility. The CPV design represented a radical departure from standard aerospace designs which required a separate "individual" pressure vessel (IPV) for each cell. The delivered battery was composed of four nominal 1.75-kWh, 10-cell stacks, each encapsulated in its own stainless-steel boilerplate vessel. This battery was coupled to a photovoltaic array and successfully tested at SNL for two years before recently being returned to JCI for continued testing. In addition to developing further cost reductions, one of the key objectives of the contract was to duplicate the excellent performance of the 7-kWh deliverable while demonstrating a practical field-deployable pressure vessel.

Technology Development - JCI

Component Improvement, Cost Reduction, and Evaluation

A summary of the performance status of several cells which were on test at JCI to evaluate various design improvements is provided in Table 4-1. Cell #140, a standard cell with asbestos separator and 10% platinum/carbon (Pt/C) catalyst, has now completed over 2400 deep discharge cycles at room temperature. Cell #165, a cell with no LiOH in the electrolyte, also continues to perform well after over 1100 cycles. Cells #186 and #187 contain two variations of a negative electrode with a modified catalyst layer and no hydrophobic teflon backing. These cells have now sur-

passed 700 full discharge cycles, demonstrating the potential for an additional cost reduction. Cell #188, which contains a lower cost binary catalyst, also continues to perform well after over 600 deep discharge cycles. In addition to these cells, several others were built and tested in support of the 2-kWh battery fabrication effort.

All laboratory cells except cell #165 were removed from test as the technical development portion of the contract wound down and emphasis was shifted toward completion of the 2-kWh battery deliverables. They are being stored in a discharged state in a nitrogen-purged cold box.

Cell P003, which contains the rolled-process negatives being used in the 2-kWh deliverables, was delivered to SNL for their testing. Previously, all electrodes for the program were made using a cast process which could not be economically adapted to larger scale production runs.

Hydrogen Storage

One of the key elements of a practical terrestrial nickel/hydrogen battery is the pressure vessel. Design efforts have focused on safety and low cost. The JCI design approach has been to use fiber-wound vessel to provide the required strength, with a metal liner to retain the hydrogen. The metal liner consists of a cylinder which is adhesively bonded to two hemispherical end domes. This design provides a controlled failure mechanism which allows the domes to pull free from the cylinder and vent the enclosed hydrogen.

The successful burst test qualification with an initial series of vessels was encouraging. However, inconsistent curing of the epoxy used for the dome-to-sleeve bond was observed in follow-up tests. A concentrated effort was pursued with the full support of the epoxy manufacturer and the Materials Research Group at JCI. The incomplete cure was traced to an excess of one of several sulfide species contained in the epoxy hardener. The non-stoichiometric ratio allowed a delayed reaction of the excess sulfide with oxygen, leading to a degradation of the material properties. Initial attempts to alter the original epoxy to provide a stoichiometric ratio resulted in a cured product which was believed to be too stiff to provide the required joint expansion. Finally a new epoxy was developed which appeared to be an

Table 4-1. Status of Laboratory Test Cells

<u>Cell Number</u>	<u>Number of Cycles</u>	<u>Amp-Hour Nominal</u>	<u>Capacity Latest</u>	<u>Effic. (%) Coulombic</u>	<u>Mid-Disc. Energy</u>	<u>Charge Voltage</u>	<u>Discharge Amp/Hour</u>	<u>Design Amp/Rate</u>	<u>Features</u>
140	2381	120	112.5	93.7	69.4	1.159	20/6	31/0.25C	Standard Cell
165	1317	120	115	95.5	78.0	1.227	16/7	30/0.25C	No LiOH
186	726	160	164.6	97.5	83.0	1.251	27.2/62	34/0.21C	No Negative Backing
187	730	160	163.0	97.2	81.5	1.264	27.2/6	34/0.21C	No Negative Backing
188	616	160	159.1	97.8	82.2	1.249	27.2/6	34/0.21C	Binary Catalyst

excellent alternative based on laboratory tests. Larger batches of the epoxy were produced and used to fabricate test vessels which produced excellent results in burst tests but exhibited creep failure during extended pressurization.

The initial designs had emphasized a high adhesive ductility to avoid shear failure. As the fiber winding is stretched during vessel pressurization, relative movement will occur between the domes and cylinder. The coupling adhesive must be ductile enough to maintain the bond through repeated cycles. However, vessel tear-down analyses revealed that this high ductility was a contributing factor in a different failure mechanism at the adhesive joint. Subsequent measurements of vessel expansion during pressurization indicated that the ductility requirement had been significantly overestimated, indicating that a less ductile adhesive could be used. This improved understanding of the required bond properties allowed the consideration of several alternative adhesives including modified versions of the original epoxy.

A test fixture, which was designed to simulate the type of loading that the epoxy would undergo in the pressure vessel joint, was set up to help screen new adhesive candidates. Two tests were applied: 1) constant pressure vs time and 2) pressurization while being thermally cycled between -18 and 65°C. A total of five adhesives were evaluated using this procedure. Based on the results of the fixture tests, a new acrylic adhesive was selected for the fabrication of a series of prototype pressure vessels, including test vessels and subsequent battery vessels.

One of the test vessels was hydrostatically burst-tested to failure at the Milwaukee School of Engineering (MSOE) Fluid Power Institute. The vessel began to leak at a hydraulic pressure of 1810 psig providing a safety factor exceeding the required 5:1 above the maximum allowable working pressure (MAWP) of 350 psi. The vessel failed in a non-catastrophic manner as it did not fragment, explode, or break apart in any way. The safety factor of 5:1 is required by the ASME Boiler Code for filament-wound pressure vessels.

In subsequent tests involving pressure cycling between 0 and 350 psi, 30,000 pressure cycles were achieved at room temperature without failure. At one cycle per day, 30,000 cycles would exceed 82 years of service life. The test temperature was then raised to 150°F. A leak was detected after 294 additional cycles. When the vessel was cooled to room temperature, no further evidence of leakage was observed so cycling was reinitiated. Another 961 room temperature cycles were completed before a leak was once again detected. Tear-down of the vessel indicated that the leak occurred in the

primary sleeve-to-cylinder bond area and most likely resulted from a poor initial fill of epoxy.

Based on the excellent results from the test vessels, vessels for each of the four 2-kWh battery deliverables were sequentially fabricated. Prior to their delivery, each of these battery vessels passed the SNL required proof test which consisted of pressurization to 1.5 times the MAWP. The vessels were held at this pressure using helium for a minimum of 30 minutes. They were then vented to the MAWP and held there for a minimum of 24 hours. Examination for leaks was performed with a gas leak detector which is capable of detecting helium leaks at a rate of 10^{-5} cc/sec based on the difference between the thermal conductivity of helium and air. Secondary examination was also made visually with a soapy water solution, and by monitoring the vessel pressure over time. No evidence of leaks was observed in any of the four vessels throughout the tests.

Deliverable Design

With the exception of the vessel design, the 2-kWh battery design closely parallels that successfully demonstrated in the 7-kWh battery previously delivered to, and tested at, SNL. Cell modules, Figure 4-1, employ the back-to-back positive design. Nine modules are connected in parallel and slipped into a polypropylene case (Figure 4-2) to form a nominal 160-Ah cell. Ten cells are assembled in a compression fixture and coupled electrically in series to form the nominal 12-V, 2-kWh stack (Figure 4-3). Finally the stack is encapsulated in the fiber-wound vessel, shown in Figure 4-4. Both sets of batteries are identical with the exception of the negative catalyst. The batteries delivered to the New Mexico site have standard Pt/C catalyst while the batteries delivered to the Florida site have the new binary catalyst.

Deliverable Fabrication

Two significant technical problems complicated the assembly of the four 2-kWh batteries. High scrap rates due to nonuniform loading were observed in the impregnation process. The problem was traced to the degradation of the platinum coating on the process counterelectrodes. It was the first failure of impregnation counterelectrodes ever observed at JCI. Once the problem was identified, it was easily resolved by replacing the entire set of counterelectrodes. Subsequent impregnation runs produced the most uniform loading ever achieved with the 70 mil positives.

The second problem was indirectly related to the vessel processing. Popping was observed in the 2-kWh

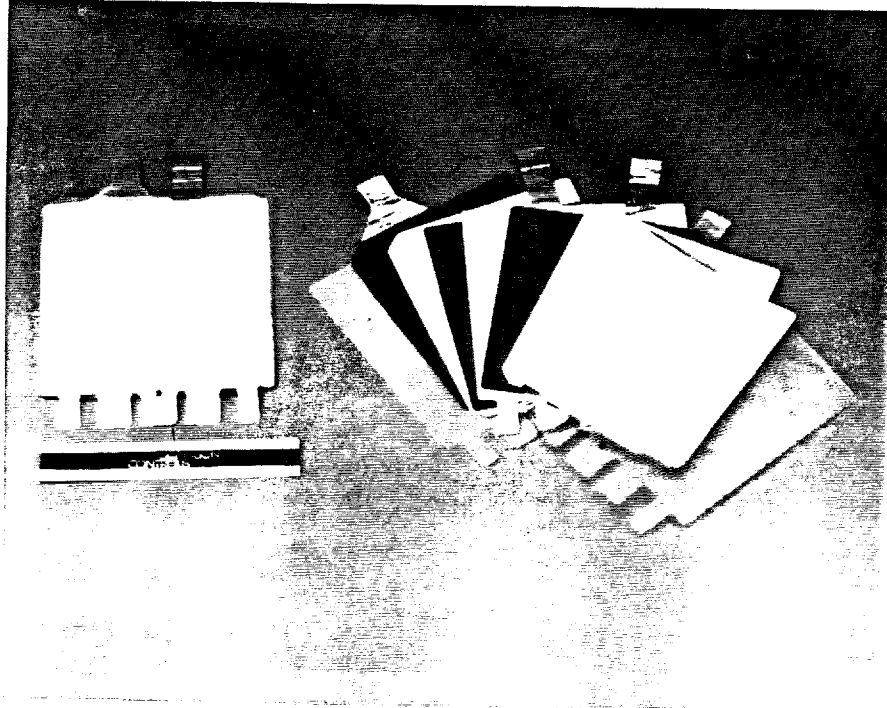


Figure 4-1. Cell Module with Back-to-Back Positive Design

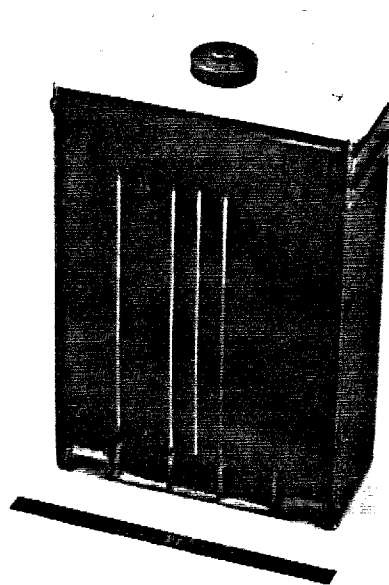


Figure 4-2. Nominal 160-Ah Cell in Polypropylene Case

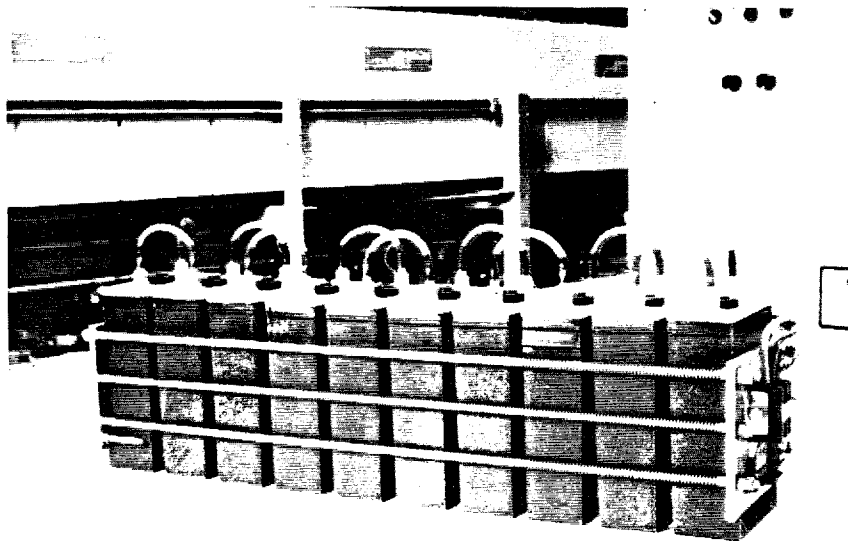


Figure 4-3. 10-Cell, Nominal 12-V Battery Stack in Compression Fixture

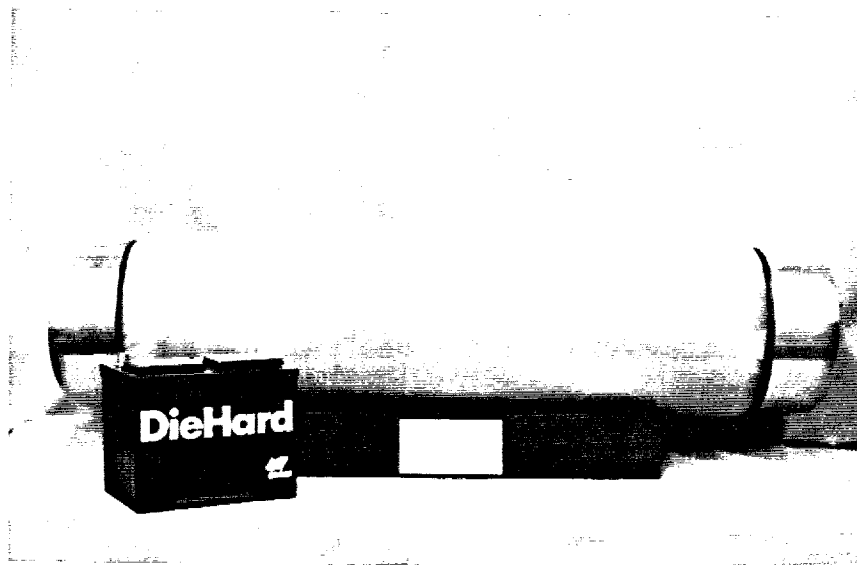


Figure 4-4. 2-kWh Battery in Fiber-Wound Vessel

batteries during their initial activation cycling. Popping is caused by the rapid concentrated recombination of oxygen and hydrogen, causing a high heat generation rate which damages the cell components. It occurs in areas of liquid-gas interface where the oxygen produced during overcharge tends to concentrate. Popping had been previously observed in some aerospace design cells when excessive amounts of electrolyte were used, but had never been observed in the terrestrial design cells. The key difference in the terrestrial design is that excess electrolyte is contained in the mud rest area of the cell case, below the cell components. However, with the new vessel fiber-winding process, that excess electrolyte has an opportunity to become trapped among the cell components since the cells are inverted during the winding operation. In this case, several damaged cells and cell cases had to be replaced, which required removal of the cell stacks from the vessel. Excess electrolyte was removed from the cells prior to insertion into the new fiber-wound vessels, to eliminate the problem during reprocessing of the batteries. Process changes were also adopted in the activation cycle to avoid those conditions in which popping occurs.

Deliverable Testing

Following the successful resolution of the technical problems encountered in the fabrication of the four prototypes, and their subsequent qualification testing at JCI, the batteries were delivered to two test sites. One set of the 2-kWh units was delivered to the Florida Solar Energy Center in Cape Canaveral, while the second set was delivered to the New Mexico Solar Energy Institute in Las Cruces.

Both sets of batteries were put through a series of baseline cycles prior to being coupled with the photovoltaic arrays. Initial series cycling of the Florida batteries showed evidence of low capacity in one battery. However, following an on-site activation cycle, performance improved and both batteries now appear to be well matched, delivering 3.8 kWh. The batteries have now been connected in parallel in line with the photovoltaic array and are proceeding through a series of 80% depth-of-discharge daily cycles, simulating a lighting application.

One of the two New Mexico batteries appears to have lost a cell due to a short. The short is most likely a residual effect from the popping problem discussed previously. Cursory attempts to eliminate the short through cycling procedures were unsuccessful. The batteries have been configured in series to minimize any battery-matching effects of the shorted cell, and testing is continuing. Despite the short, the battery pair is

delivering the rated 4-kWh capacity. The batteries have now been coupled with the photovoltaic array, and testing on a low 15-25% depth-of-discharge daily cycle, simulating a vaccine refrigeration application, is proceeding.

Related Efforts

As the CPV technology was developed for terrestrial applications, its potential advantages for aerospace applications became better understood. The CPV configuration offers the potential for up to a 50% improvement in specific energy and a 3:1 reduction in volume for aerospace applications as compared to the current IPV Nickel/hydrogen aerospace technology. Several additional design features unique to the advancing terrestrial design may also lend themselves to ultimate application in an aerospace battery. Examples include the effective application of the thick (70 mil or thicker) electrochemically impregnated nickel electrodes and the use of improved hydrogen electrode catalysts. In an independent effort, a 26-cell, nominal 24-Ah prototype aerospace CPV battery was designed and fabricated by JCI and COMSAT. The battery has completed more than 7,000 low earth orbit (LEO) cycles at a 44% depth-of-discharge.

Conclusions

The ongoing demonstration of the terrestrial CPV nickel/hydrogen battery in a practical field-deployable vessel has overcome the last significant technical design hurdle for the system. Design modifications that reduce the mass-production cost of the system to a level that is competitive with lead-acid and other emerging terrestrial battery technologies have been demonstrated at the cell and/or battery level. However, further demonstration of the systems capabilities and reliability is required to gain technological and economic acceptance.

Technology Evaluation at SNL

Contracts for the development of nickel/hydrogen batteries at JCI provide for periodic delivery of cells and batteries to SNL for evaluation purposes. Typically, these cells consist of several modules and represent state-of-the-art technology or contain experimental components modified to reduce cost or improve performance. Four nickel/hydrogen cells were on test during this period. Table 4-2 lists their configurations and the test conditions.

Table 4-2. Configuration and Test Conditions

Cell S/N	Cell Mods	Positive Th. (in)	Add.	Negative Type	KOH (%)	°C Cool	Current (A) Chrg/Disch.	Cycle Type
#23	7	0.070	Li	Gortex	33	10	20/20	Conserv. ¹
#144	9	0.070	Li	Gortex	24	None	25/25	Std.*
#185	9	0.070	Li	TFE Film	24	None	25/25	Conserv. ⁺
#P003	9	0.070	Cd	Rolled	24	27	25/25	Std.*

Notes:

*Standard life-cycle: discharge to 1.0 V/cell followed by a charge until the pressure-time slope drops to 75% of the linear value.

¹Conservative cycle: discharge to 1.0 V/cell followed by a charge to an input of 130 Ah.

+Conservative cycle: discharge to 1.0 V/cell followed by a charge to an input of 160 Ah.

Cycle Tests

Cell #23—Cycling continued with this cell which represents 1986 technology. Capacity maintained a steady rate of 124 Ah using the conservative 130-Ah charge cycle. High voltage (1.7 V) was observed occasionally and then became a frequent problem. Testing was discontinued after a total of 1700 cycles and the cell was subsequently returned to JCI for further evaluation.

Cell #144—This cell, with a Gortex backing on the negative electrodes, represents the baseline design used in the 3.5-kWh battery. It is being subjected to the standard cycle test and has now accumulated 1757 deep cycles. During its life cycling, it was observed that the EOC pressure would gradually increase resulting in a high pressure alarm at 330 psig. Each time this occurred, pressure was reduced to a level of 50 psig at EOD and then testing was resumed.

The pressure reached 330 psig at cycle 1472. After the pressure was reduced, it was noted that the capacity was gradually diminishing. EOD pressure was still showing an upward trend, but EOC pressure was not increasing at the same slope. At cycle 1658, the cell was subjected to an activation cycle consisting of charging at a low rate with the cell vented to the atmosphere followed by discharging while connected to a hydrogen bottle at a constant 50 psig. When cycling was resumed, the capacity continued to drop and is now 150 Ah, considerably below the baseline value. See Figures 4-5a and 4-5b.

Cell #185—The negative electrodes of this cell have the lower cost JCI fluoroplastic film as a hydrophobic backing. During initial testing using the

standard cycle, the EOC pressure increased an average of 0.42 psig per cycle such that the high limit of 330 psi was reached several times. Also, on discharge, the temperature reached the high limit of 40.0°C several times.

To overcome these problems, charging has been terminated after an input of 160 Ah. Using this conservative test plan produces a steady coulombic efficiency of 98.4%. The cell has now accumulated 825 cycles. This type of cycling still produces a gradual increase in EOC pressure necessitating an occasional reduction of EOD pressure to 50 psig.

Cell #P003—This is a nine-module cell of the same construction as the cells used in the 2-kWh batteries being delivered to other testing facilities. The design varies from other cells on test at SNL in the use of a rolled-process negative film with a catalyst loading of 0.4 mg Pt/cm². The nominal capacity rating is 160 Ah. While cycling at JCI, it showed a capacity of 170 Ah.

This cell also has a tendency to show a rise in EOC pressure. After accumulating 135 cycles using the standard cycle test, a series of parametric tests was conducted, first at room temperature and then with a cooling jacket installed on the pressure vessel.

The tests consisted of:

- 25-A discharge, 25-A charge - baselines
- 25-A discharge, 35-A charge
- 25-A discharge, 15-A charge
- 35-A discharge, 25-A charge

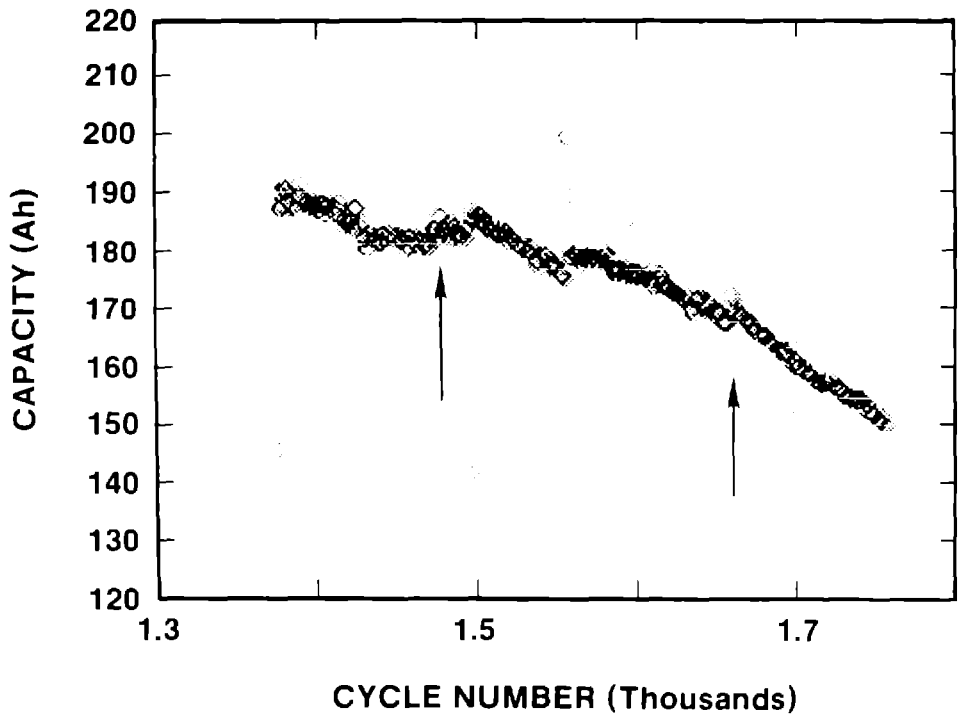


Figure 4-5a. Capacity vs Cycle Number (Cell #144)

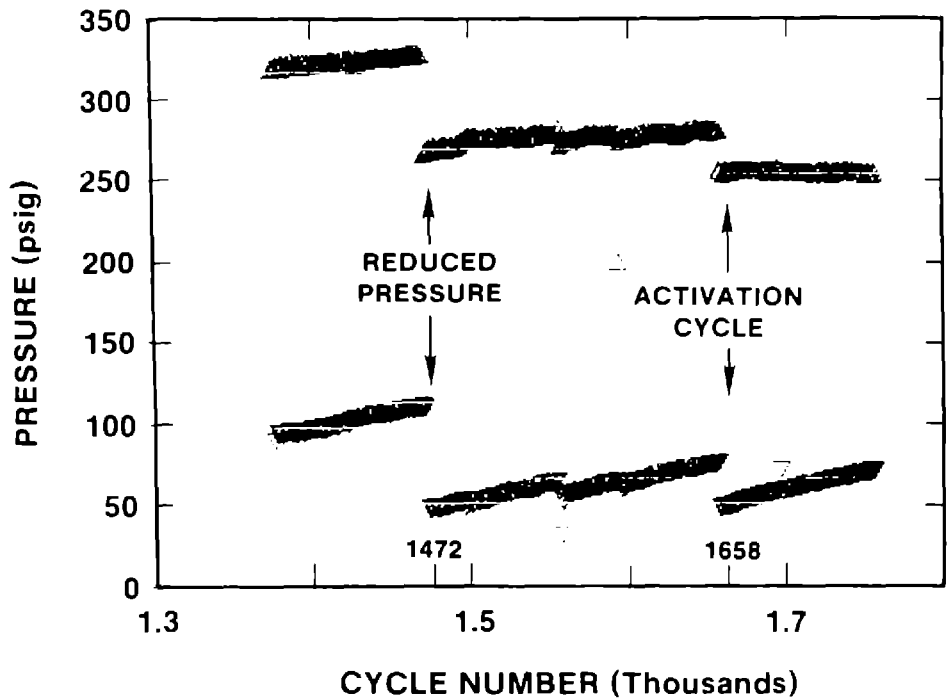


Figure 4-5b. Pressure vs Cycle Number (Cell #144)

15-A discharge, 25-A charge.

The 35-A discharge without cooling reached the high temperature limit. A 30-A discharge without cooling also resulted in a high temperature alarm. A comparison of the capacities showed an increase of 6 Ah

when the cell temperature was being controlled by the cooling jacket (Figure 4-6).

Table 4-3 lists the results of the three cells currently on test up to September 30, 1990.

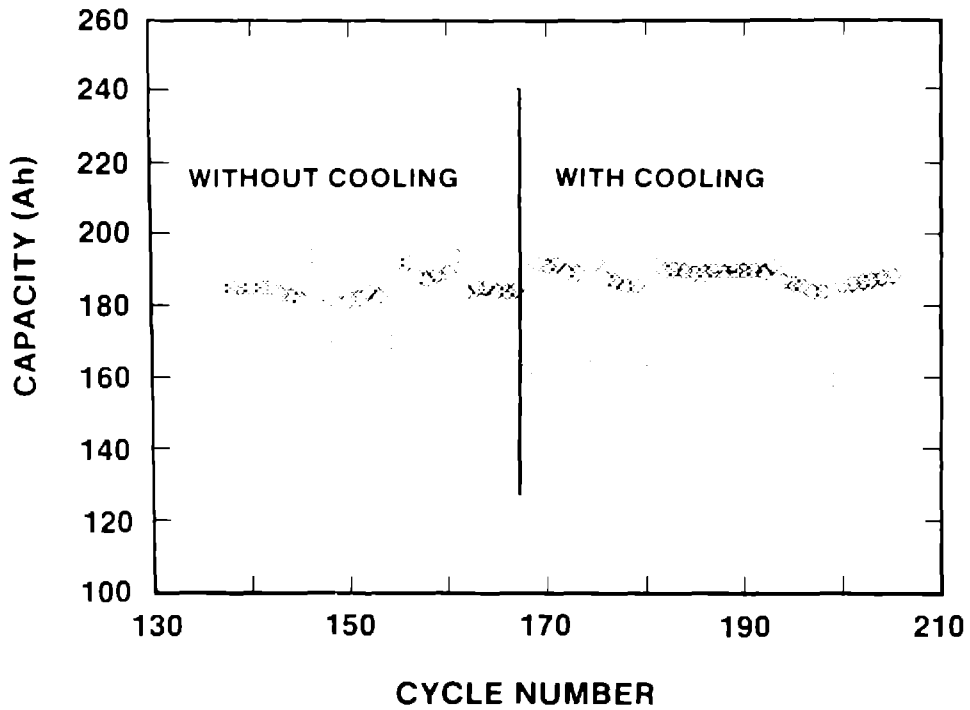


Figure 4-6. Capacity vs Cycle Number, Cell #POO3 Parametric Tests

**Table 4-3. Summary of Test Results
September 30, 1990**

Cell	Cycles	Capacity (Ah)		Effic. (%)		Mid Point Disch. V/c	Pres. (psig) EOD/EOC
		Nominal	Latest	(Ah)	(Wh)		
#144	1757	150	150.3 (176.0)	92.9 (91.6)	75.0 (77.8)	1.231 (1.266)	71/255
#185	824	160	157.3 (177.2)	98.4 (92.5)	85.3 (78.0)	1.282 (1.264)	62/294
#P003	206	160	188.6 (171.3)	94.9 (94.2)	83.1 (82.3)	1.282 (1.287)	81/308

Notes:

Baseline performance in parentheses

Cell #144—Pressure reduced to 50 psi after HPA at cycle 1472. Activation cycle at cycle 1658.

Cell #185—Pressure reduced to 50 psi after HPA at cycle 473.

Cell #P003—Pressure reduced to 50 psi after HPA at cycle 122. Parametric testing.

5. Aluminum/Air Project

In August 1987, SNL contracted with Eltech Research Corporation to develop the aluminum/air battery technology for electric vehicle applications. Case Western Reserve University, Helipump Corporation, and Kaiser Aluminum have subcontracted some of the program tasks. The objective of this program was to improve the technology and to engineer and evaluate an advanced aluminum/air battery. The 3-year, \$2.57M development program, comprised of a \$1.93M DOE-funded contract from SNL and \$0.64M in cost-sharing from Eltech, was completed in September 1990.

Technology Development

Background

An alternative to a secondary battery as the power source in an electric vehicle is a fuel cell, i.e., a cell that generates power by consuming a mixture of a fuel and oxygen from the air. Metals such as lithium, aluminum, zinc, and iron may be used in a fuel cell; however, aluminum is a particularly attractive candidate. Aluminum offers high energy and power densities, is environmentally acceptable (as are the products of the cell reaction), is easy to handle, and has a large industrial base for production and distribution.

In an aqueous electrolyte, aluminum corrodes forming hydrogen gas which must be safely handled within the battery system. In operation, aluminum is dissolved to form a soluble aluminate species, consuming alkali metal hydroxide. Hence, as the battery operates, the conductivity of the electrolyte decreases until precipitation of aluminum trihydroxide occurs to replenish the electrolyte in terms of free hydroxide.



Thus a "steady state" condition may be achieved with respect to the composition and conductivity of the electrolyte, at which time the electrolyte will contain crystals of aluminum trihydroxide.

The reaction at the cathode is the electroreduction of oxygen, which can only be sustained at practical rates

by using a gas diffusion electrode. A three-phase boundary between the catalyst, electrolyte, and reactant oxygen must be established and this demands a unique electrode structure. It is known that the presence of carbon dioxide in the air feed stream can lead to loss of performance and, therefore, the battery system must include technology to reduce the levels of carbon dioxide in the air feed stream or, ideally, to remove it entirely.

The aluminum/air battery is, therefore, a multi-component system and may be represented schematically as in Figure 5-1. The project to develop this battery system has focused upon several challenges:

1. The need for high performance electrodes.
2. The separation of crystals of aluminum trihydroxide from the electrolyte and control of the composition of that electrolyte.
3. A cell design that allows replacement of the anode.
4. The removal of carbon dioxide from the air feed to the battery.
5. The safe handling and/or disposal of hydrogen gas.

Jointly funded contracts to develop an aluminum/air battery, involving DOE and Eltech, began in 1980 and were administered by Lawrence Livermore National Laboratory. At first, emphasis was placed upon the cell components, particularly upon the development of the air cathode. Later both electrolyte management technology and the design of the cell were also addressed. In 1987 the contract to develop the aluminum/air battery was extended, again jointly funded by DOE and Eltech, but administered by SNL. The objective of Phase 1 of the project, requiring approximately three years to complete, was to optimize the battery and auxiliary systems. A longer term objective would be to design, construct, and install a system in an electric vehicle.

The Phase I contract, which combined both experimental studies and mathematical modeling, addressed:

1. Design and optimization of the aluminum/air cell.
2. Design and optimization of the auxiliary systems, i.e., the heat exchanger, solids separation, control of carbon dioxide, and disposal of hydrogen gas.

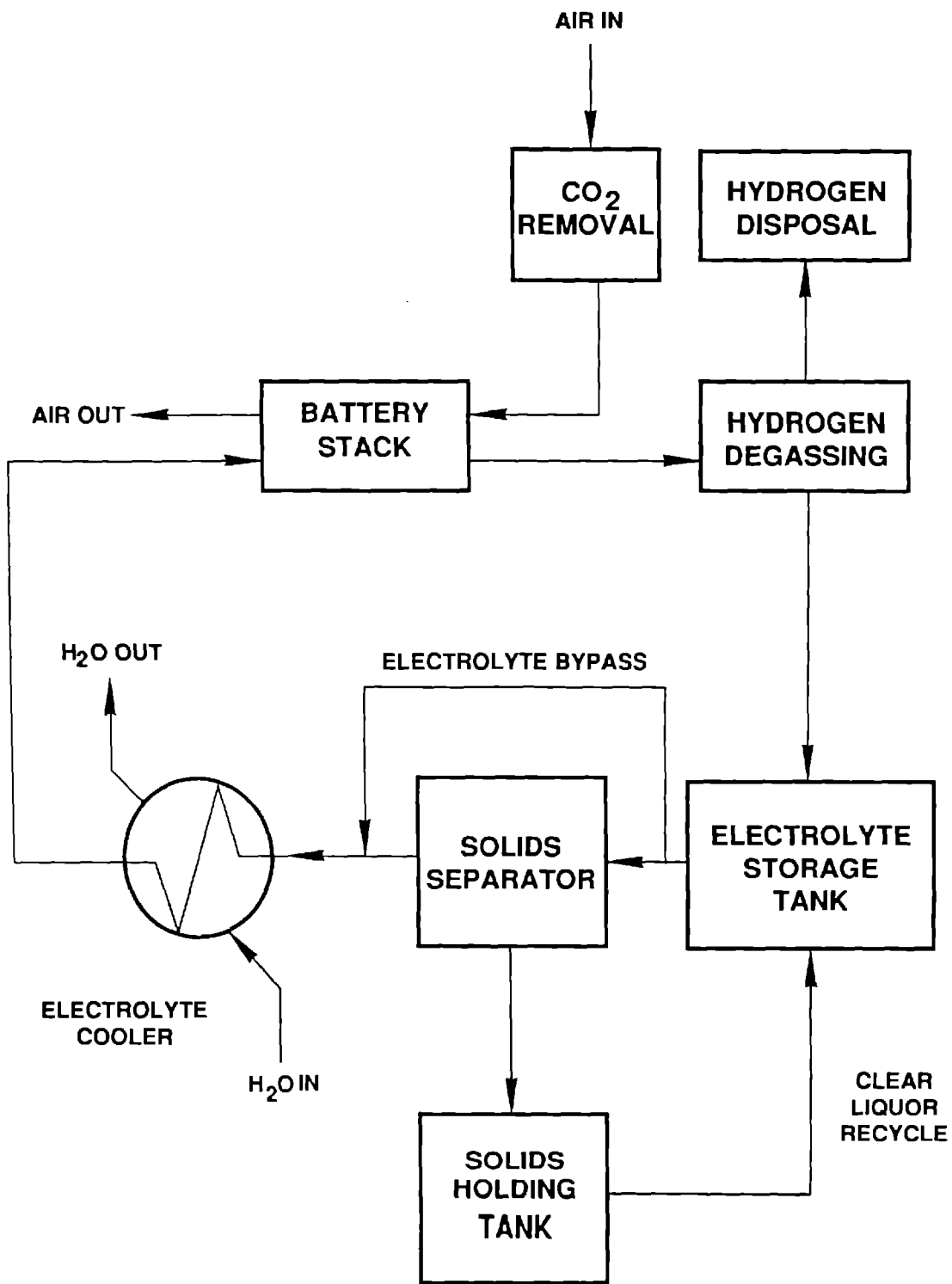


Figure 5-1. Aluminum/Air Process Schematic

Specific research objectives were subcontracted by Eltech to Case Western Reserve University, Helipump Corporation, and the Kaiser Center for Technology:

1. Development of a mathematical model of the B-300 cell was undertaken by Dr. R. F. Savinell of Case Western Reserve University. This subcontract included an experimental study to provide support data for the model.
2. A study of the feasibility of the acoustically aided separation of aluminum hydroxide solids in an aluminum/air battery system was completed by Dr. D. L. Feke of Case Western Reserve University.
3. The development of high-performance aluminum alloys at a pilot scale, i.e. 100-200 lb ingots, was carried out at the Kaiser Institute of Technology.

Status of the Project

Cell Design

Initially, the B-300 cell was selected for use in the contract and a multi-cell battery (12-V) based upon this design was fabricated, assembled, and successfully operated. However, it was evident that the weight and volume of an array of B-300 cells were too large to be considered viable for use in a vehicle. Independent programs at Eltech had focused upon the development of a smaller aluminum/air cell, with dissolution from both sides of the anode plate and therefore requiring external current collection (Figure 5-2). This new cell (AT400) was considered for the ongoing SNL program. Concepts were developed for a multi-cell array, with modularized busswork and refined electrolyte distribution (Figure 5-3). The sealing arrangement for the anode plate was modified to use a clamp arrangement, consisting of a split polyvinylchloride collar and EPDM foam gasket material.

The AT400 single cell was operated repeatedly: a) to demonstrate stable, acceptable performance from the cell and system, b) to determine the electrochemical behavior of aluminum alloys fabricated at Kaiser, and c) to demonstrate the stability of the performance of the air cathode through the test period. The cell was operated using a simplified federal urban drive schedule (SFUDS) (Figure 5-4) over approximately five hours, with an overnight period at open circuit, the electrolyte then being drained from the cell. Fresh electrolyte (5M KOH, 60°C) was used for each individual test. Thus, if a polarization scan is recorded with a new anode plate, the cell voltage reflects the performance of the air cathode since the anode polarization and electrolyte resistance remain essentially constant. A summary of

cell performance over two months (Table 5-1) shows stable and reproducible behavior for both the cell and the air cathode.

Overall, the experience with the AT400 in terms of assembly, operation and replacement of anode plates (refuelability) has been satisfactory. The projected weights and volumes of a 55 kilowatt battery, based upon B300 and AT400 cells, clearly shows the advantages of this new cell (Table 5-2). This data is developed using performance obtained with an aluminum alloy as the anode plate.

Materials and Energy Balances (System Analyses)

This study was initiated in December 1988 with the objective to generate materials and energy balances, process flow diagrams, and to allow analyses of the aluminum/air battery system. The initial efforts focused upon the evaluation of the two modes of operation.

1. "Batch" Operation—at a constant current density of 400 mA/cm², allowing metal dissolution to continue to the point at which solids begin to form and then replacing the electrolyte, and
2. "Steady state operation"—also at a constant current density of 400 mA/cm² where crystallization of aluminum trihydroxide occurs and the composition and conductivity of the electrolyte attain a steady state.

A complete set of calculations and documents were generated for each case and a spreadsheet developed. A more realistic mode of operation is represented by the SFUDS and, therefore, a summary of operation of the battery system under such a schedule was generated (Figure 5-5).

Early in 1990, Dr. P. Symons (Electrochemical Engineering Consultants, Inc.) modified the material and energy balance spreadsheet to create a first-generation system model. This early version was transferred to Eltech, where additional improvements to the model were effected. These modifications allowed rapid and extensive evaluation of the performance of the aluminum/air battery system.

Eight steady-state and six batch operation mode options were evaluated, giving consideration to the total weight and volume of the system, as well as to the predicted range. The electrolytes used in these cases were either 5M or 7.5M potassium hydroxide and estimates of the maximum attainable current densities were based upon available experimental data. In each of the steady-state options it was assumed that the crystallizer would contain 10 wt% seed crystals, that a

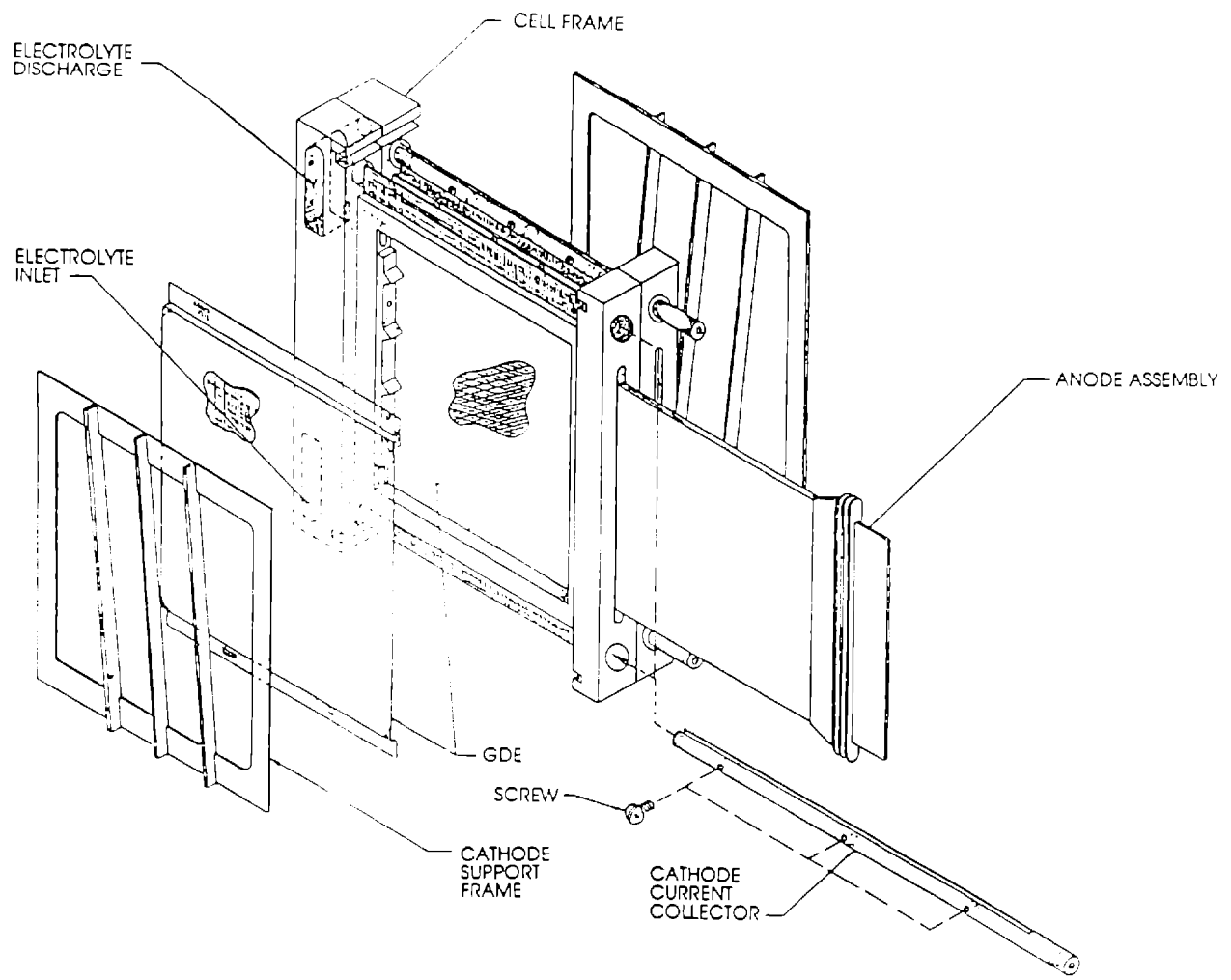


Figure 5-2. Exploded Diagram of AT400 Cell

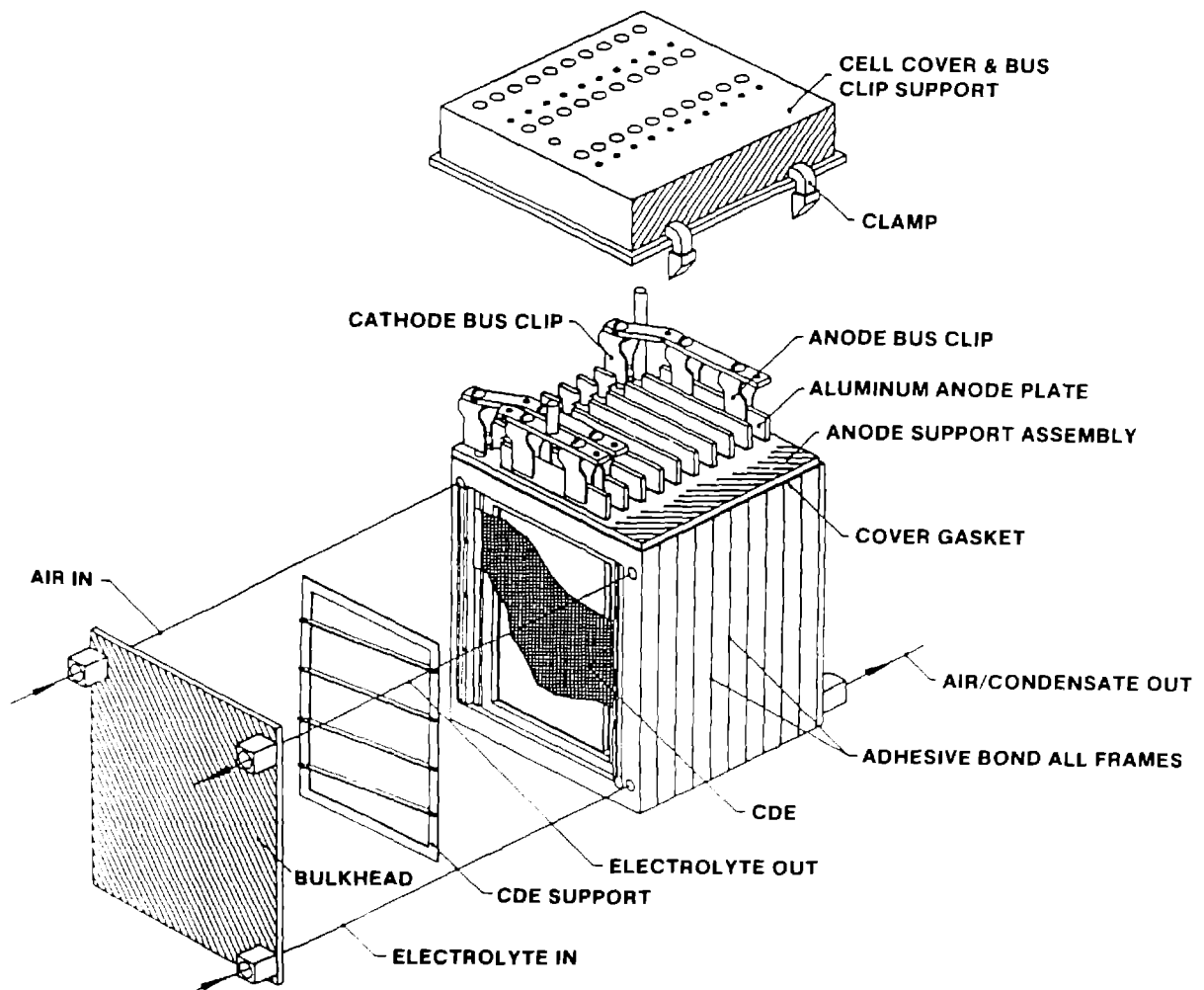
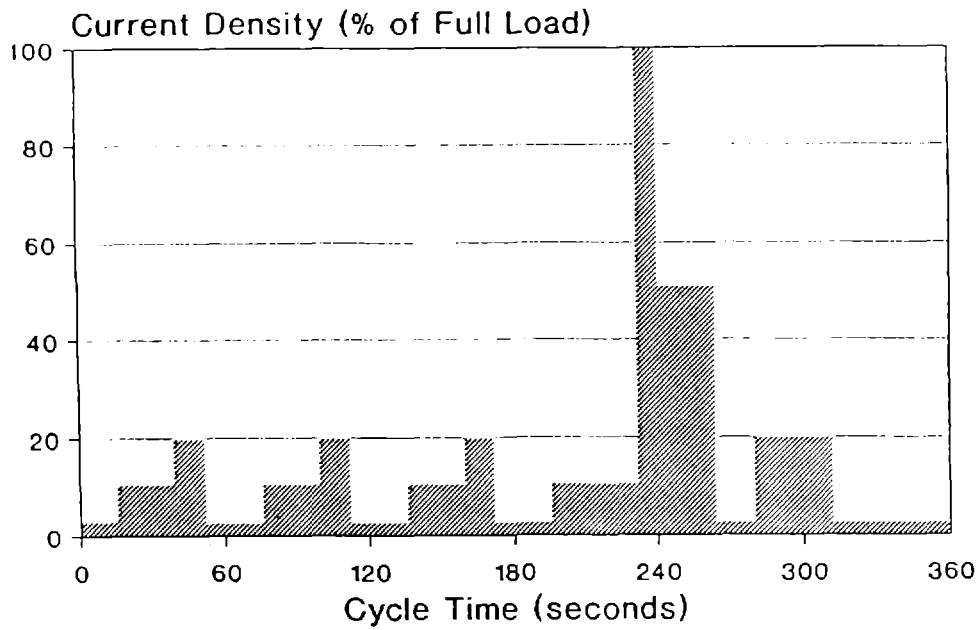


Figure 5-3. 10-Cell Module Based on AT400 Cell

Al/Air Battery - Current Density Profile



Al/Air Battery - Velocity Profile

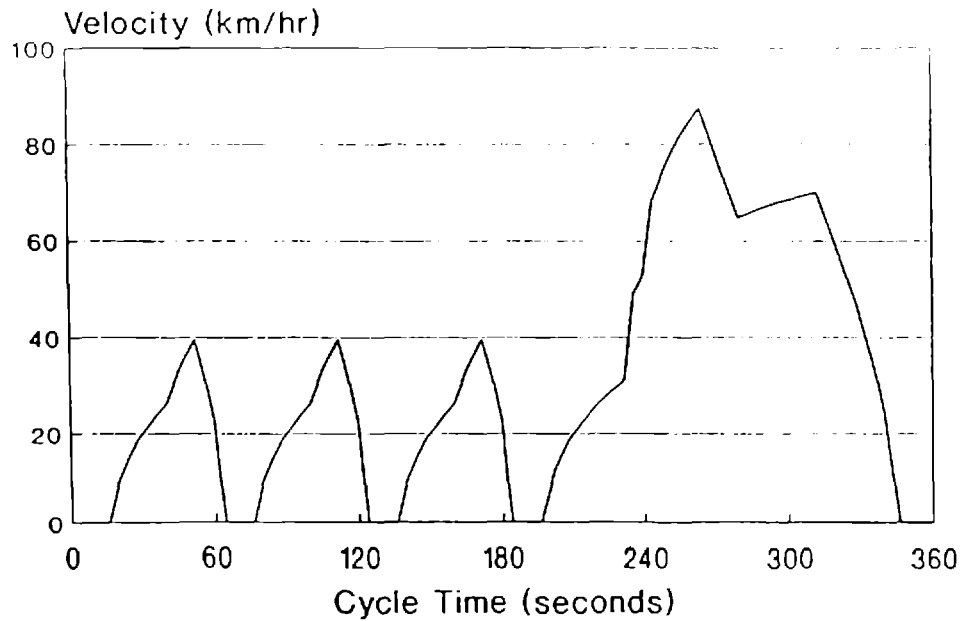


Figure 5-4. SFUDS for AT400 Single Cell

Table 5-1. Polarization Behavior in the AT400 Cell

Date	Open Circuit	Cell Voltage (volts)				
		100 mA/cm ²	200 mA/cm ²	300 mA/cm ²	400 mA/cm ²	450 mA/cm ²
6/25/90	1.86	1.46	1.31	1.17	1.05	1.00
6/27/90	1.82	1.47	1.34	1.20	1.09	1.05
6/29/90	1.78	1.46	1.34	1.22	1.11	1.07
7/3/90	1.89	1.49	1.35	1.23	1.12	1.07
7/6/90	1.88	1.47	1.34	1.21	1.10	1.05
7/11/90	1.88	1.47	1.34	1.22	1.10	1.06
7/19/90	1.81	1.46	1.32	1.18	1.06	1.00
7/26/90	1.85	1.48	1.34	1.21	1.09	1.03
8/15/90	1.84	1.47	1.33	1.19	1.04	0.97
8/20/90	1.88	1.49	1.34	1.21	1.08	1.01
8/28/90	1.80	1.47	1.34	1.20	1.08	1.02

Anode Material: 99.99% Aluminum
 Electrolyte: 5M KOH, 60°C

Table 5-2. Comparison of Aluminum/Air Cells

Single Cell	B300 Cell	AT400 Cell
Active Area (cm ²)	273	400
Weight (kilograms)	3.66**	0.5**
Volume (liters)	3.1	1.1
Anode Weight (kilograms)	0.35	0.30
55 kW Stack*		
Weight (including anodes) (kilograms)	1450	200
Volume (liters)	1140	275

* Based upon a single cell voltage of 1.14 volts at 480 mA/cm² (the estimated peak current density for SFUDS operation) which is readily achieved with an aluminum alloy (see Table 5-8).

** CPVC as the material of construction

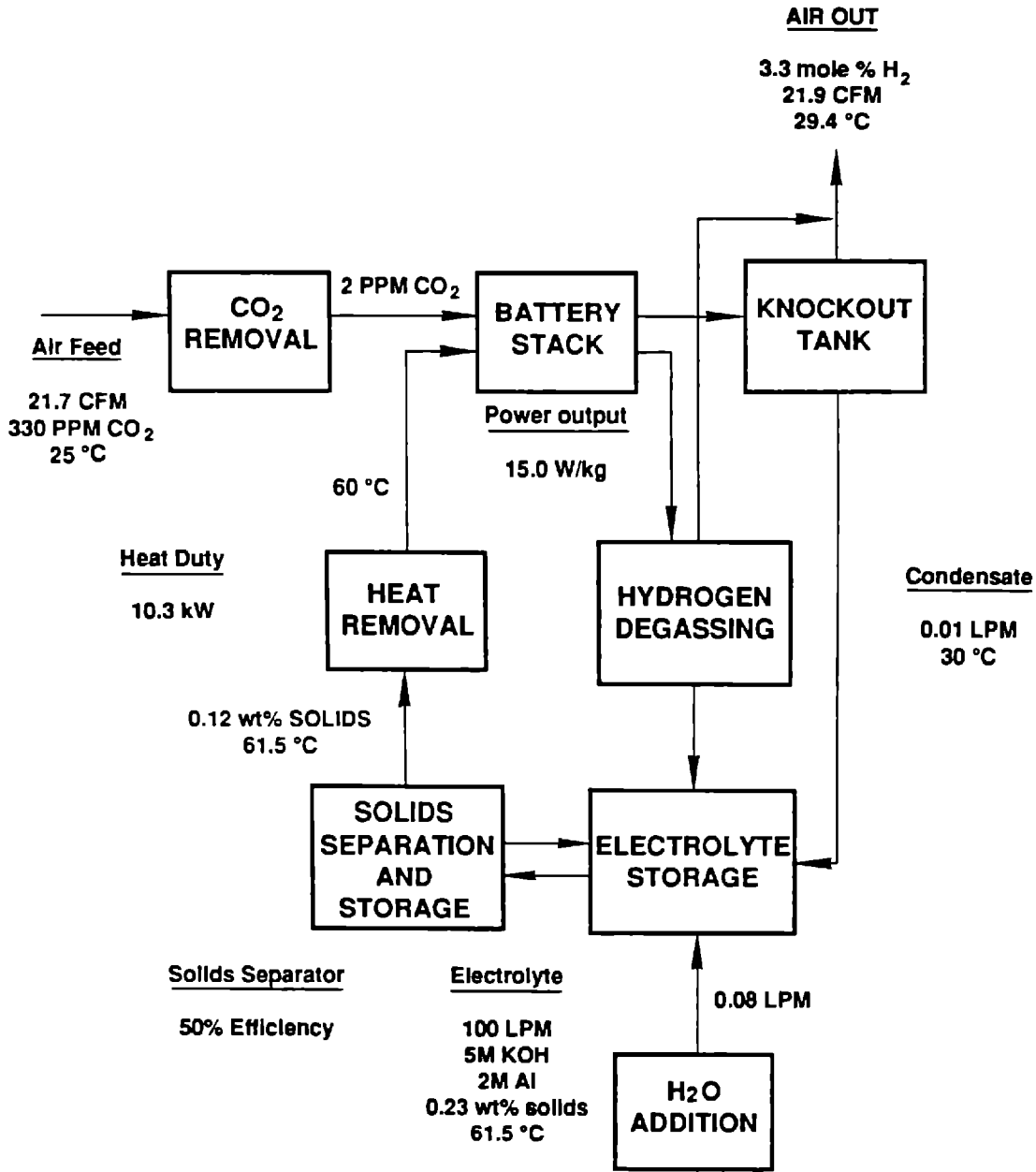


Figure 5-5. Aluminum/Air Battery System for SFUDS Base Case

separation efficiency of 50% would be achieved, and that a solids cake content of 50 wt% was yielded. Range calculations assumed that the electrolyte composition was at steady state at the beginning of each mission and are thus conservative. A summary of several of the options is presented as Table 5-3.

Options 2 and 10 were selected for further analysis and a summary of the projected battery system and performance specifications is shown as Table 5-4. The peak power and average power requirements are those given for the IDSEP van.

Table 5-3. Summary of Operating Options Used in Systems Analysis

Option	KOH Initially (moles/liter)	Al Steady-State (moles/liter)	Peak C.D. (mA/cm ²)	Cell Area* (cm ²)	Volume (liters)	Weight (kilograms)	Range (miles)
<u>Steady State Operation</u>							
1	5.0	2.5	400	475	1195	1090	390
2	5.0	3.0	280	590	1095	935	390
3	5.0	3.0	280	565	910	700	165
4	7.5	5.0	270	610	1110	945	425
<u>Batch Operation</u>							
5	5.0	2.15	480	435	800	700	100
6	5.0	2.90	300	560	825	700	105
7	7.5	3.0	450	440	800	700	125
8	5.0	3.0	280	590	1010	930	135
9	7.5	3.0	450	440	965	930	185
10	7.5	5.0	270	610	1010	930	230

* Based upon 280 cells in the battery stack.

Table 5-4. Projected Battery System and Performance Specifications

	"Steady State"	"Batch"
Electrolyte: KOH (molar)	5.0	7.5
dissolved Al (molar)	3.0	5.0*
Weight (kilograms)	935	935
Volume (liters)	1045	1115
Number of Cells	280**	280**
Area per Cell (cm ²)	565	870
Peak Power (kilowatts)	55	55
Average Power (kilowatts)	8.3	8.3
Peak Current Density (mA/cm ²)	280	175
Average Current Density (mA/cm ²)	40	30
Average Parasitic Power (kilowatts)	1.0	3.4
Energy Density (watt-hours/kilogram)	205	100***
Range (miles)	380	180***

* at end of mission

** 2 stacks each of 140 cells

*** Based upon "end-of-life" due to electrolyte saturation.

It should be noted that the peak power and peak current density values shown in Table 5-4 are achievable under "worst case" operating conditions, i.e., high aluminate concentrations, low conductivity, and inter-electrode gap approaching its maximum value.

A sensitivity analysis was performed to determine vehicle range under SFUDS operation as a function of battery system weight (Figure 5-6). It can be seen that the predicted ranges for steady-state and batch operation converge as the system weight approaches 700 kg, but as the battery weight increases the advantage of the steady-state system becomes evident.

Development of Aluminum Alloys

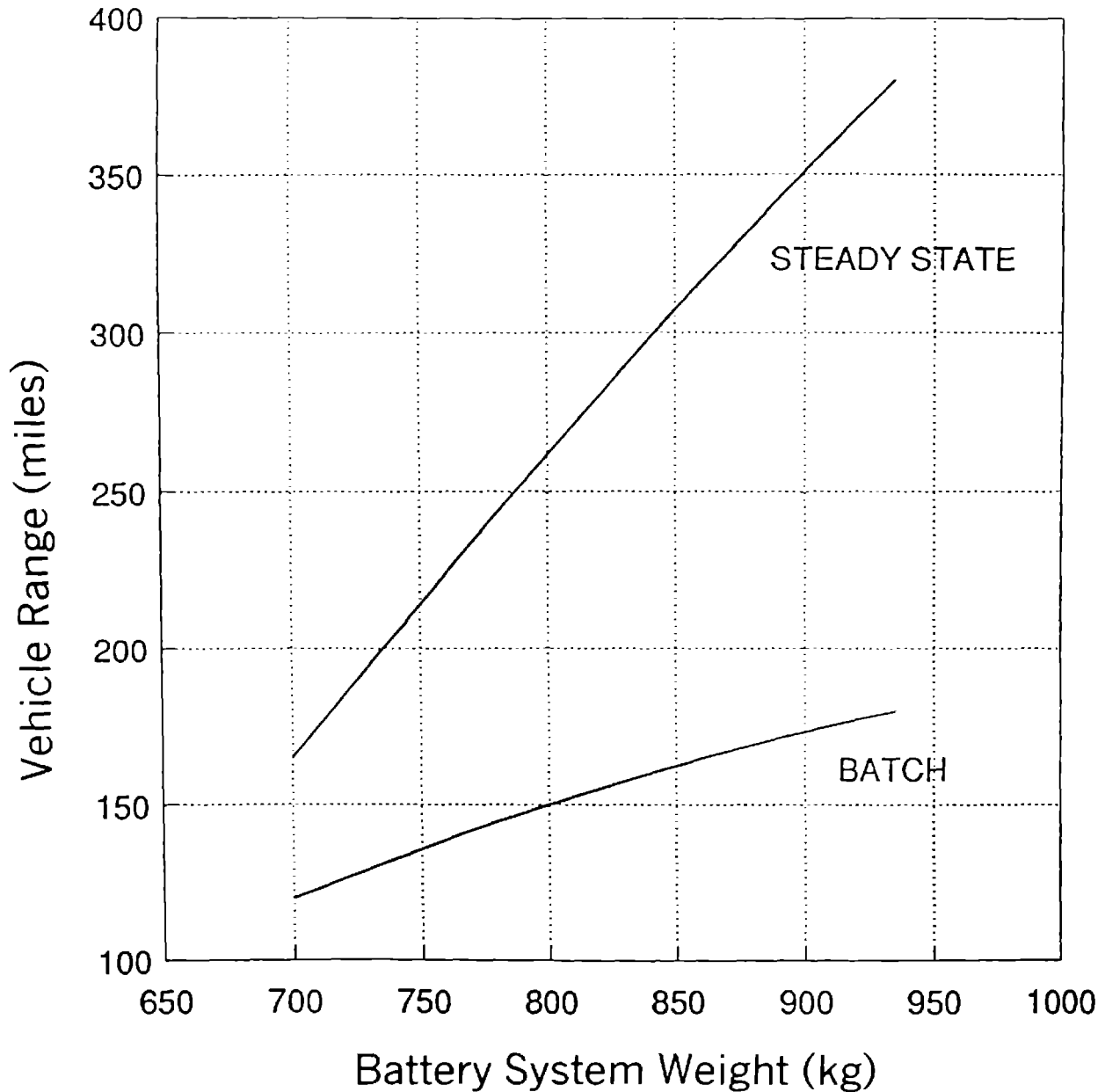
This task was initiated to address the production of pilot-scale quantities of aluminum alloys. Experience has taught that high-performance aluminum alloys have shown inconsistent performance, particularly when fabricated as larger ingots (100-200 lb). It would appear that control and understanding of the fabrication prac-

tice is important and that the development of a relationship (albeit empirical) between the metallurgy and electrochemistry may be necessary.

The program at the Kaiser Center for Technology included:

1. A forensic study, the examination of available materials where inconsistent performance has been observed.
2. Casting, the fabrication of selected alloys into book molds (1"x3"x5", 1.5 lb) and an ingot (3"x9"x50", 130 lb).
3. Thermal and mechanical processing.

Sets of small plates (approximately 1.5"x1.5"x0.1") of a manganese-indium-magnesium-aluminum alloy, that had been subjected to various thermomechanical processes, were used to obtain information regarding surface characteristics, grain structures, microstructures and electrical conductivities. The results of this work



IDSEP Van - SFUDS

Figure 5-6. Vehicle Range vs Battery System Weight Development of Aluminum Alloys

were used to select the processing steps for the alloy plates to be fabricated as part of the task.

Four alloys were fabricated as both bookmolds and ingots using direct chill casting procedures. The casting station was relined with an alumina-filled titanium diboride ceramic prior to fabrication of the four alloys.

The chemical compositions of the cast ingots, determined by quantometry, are shown as Table 5-5.

A section of the ingot and two bookmolds of alloy #3 were processed to give sheetstock of thickness 0.183". Four different combinations of microstructures and grain structures were then developed using various

Table 5-5. Chemical Composition of Base Aluminum and Alloys (ppm)

	Si	Fe	Mn	Mg	In	Sn	Ga
Base Alum.	26	19	5	1	<0.1	<0.1	<0.1
Alloy 1	29	19	1080	2	1000	<0.1	<0.1
Alloy 2	35	19	280	750	500	<0.1	<0.1
Alloy 3	25	21	1080	1060	940	<0.1	<0.1
Alloy 4	29	21	5	4970	<0.1	95	490

thermomechanical processes. The structural combinations are shown as Figure 5-7 and the processing steps involved are shown as Figure 5-8.

The electrochemical behavior of the processing combinations for alloy #3 was determined. The data is presented in Table 5-6, and it can be seen that the performance of the ingot and bookmold materials were generally very consistent. The polarization behavior of the materials with the alloying elements "in solution," i.e., from processes 1A and 2 as a consequence of the solution heat treatment and rapid quench, is superior although the difference is not as marked at the lower current densities. On the other hand, lower rates of corrosion are observed when the alloying elements are not "in solution" (processes 1B and 1C).

Overall it was considered that the alloy material from process 2 gave superior performance and, therefore, sections of alloys 1, 2, and 4 were also processed following that sequence. The electrochemical behavior of the alloys is summarized as Table 5-7, the data being obtained in the laboratory test cell using 5M KOH as the electrolyte. Alloy plates were also used in the AT400 single cell, completing an initial polarization scan before cycling in an SFUDS mode over five hours. The AT400 cell data is presented as Table 5-8.

Alloy #3 is clearly superior in terms of the electrochemical behavior, particularly showing low corrosion rates through the SFUDS operation. The performance of this alloy, produced as an ingot and processed by conventional technology, closely approaches the target levels established for the program.

Acoustically Aided Separation of Aluminum Hydroxide Solids

The basis for any acoustically aided separation using suspensions is that the suspended solids and heat

fluid have different mechanical properties. Thus, the liquid and solid may be expected to respond differently to the application of sound waves. The suspended solids will experience different time-averaged forces and these forces can promote migration of the particles to fixed positions within the acoustic field.

A series of experiments were completed initially using either a stationary standing-wave or a coincidence resonance field. Suspensions of particles of aluminum hydroxide (average diameter 2.5 microns) in 5M potassium hydroxide at 60°C were circulated through an acoustic cell. Analyses indicated that a high separation efficiency (ca. 95%) was achieved with low electrical power requirements. However, the cell quickly became saturated with solids and it was evident that a continuous process, rather than a "batch" approach, was required.

The acoustic cell was readily operated in a continuous mode and it was observed that the separation efficiency was markedly dependent upon the flow rate of the electrolyte (Table 5-9). The use of a series arrangement of acoustic cells was considered but the efficiency of separation decreased markedly during a second pass with the electrolyte.

There are several areas in which improvements in the processing capability of the acoustic cell could be made, e.g., cell configuration, cell size, and cell materials. A unit was considered (Figure 5-9) containing 10 internal chambers separated by a fluoropolymer composite, which is acoustically transparent. Such a unit would be the basis of an acoustic separator for an aluminum/air battery.

Disposal of Hydrogen Gas

A parasitic corrosion reaction occurs simultaneously with the dissolution of aluminum in aqueous

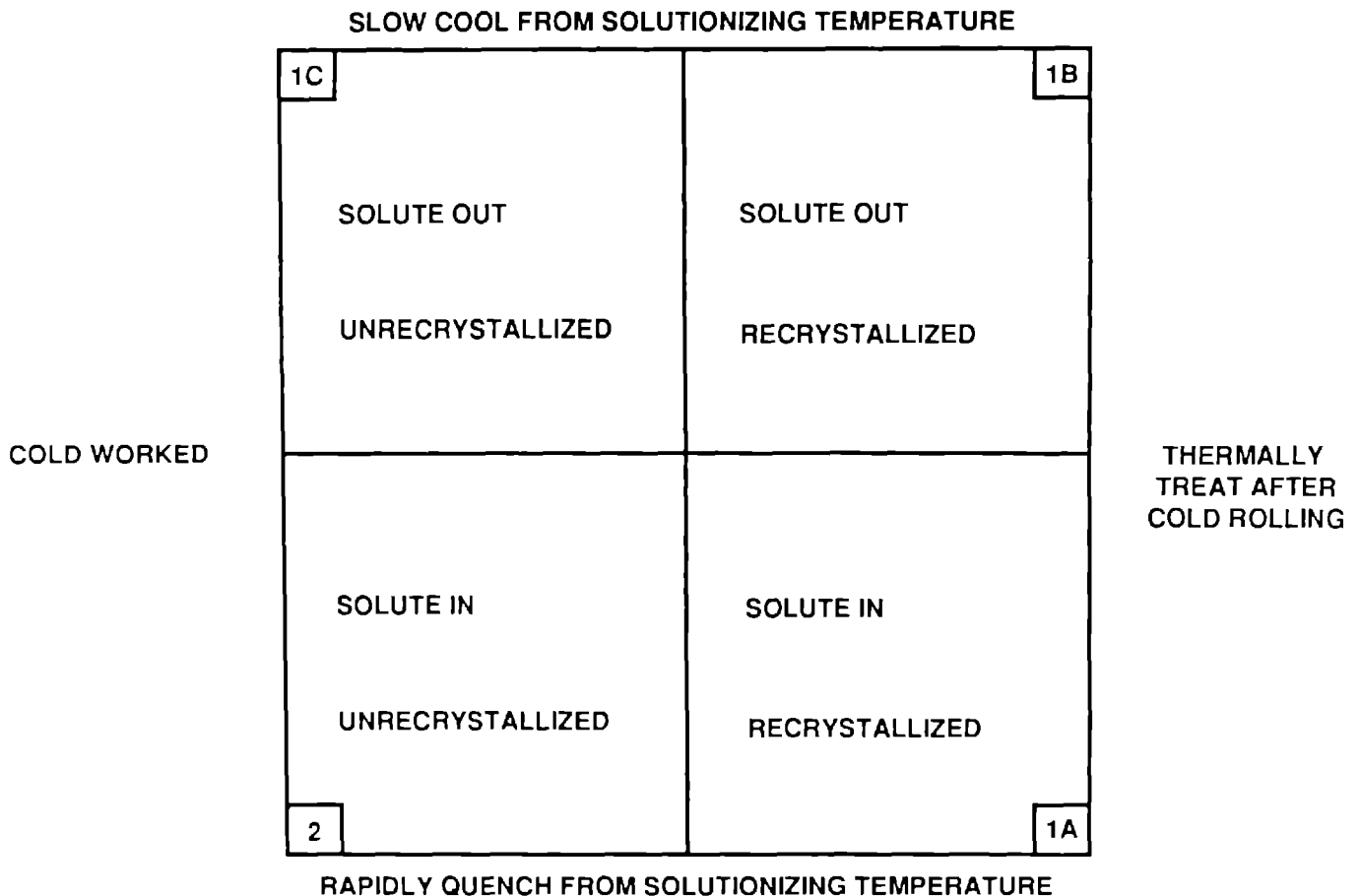


Figure 5-7. Alloy Processing Combinations

electrolytes to generate hydrogen gas. While the amount of hydrogen generated may be minimized by use of aluminum alloys and/or corrosion inhibitors, it cannot be entirely eliminated. The gas must therefore be handled safely within the battery system, with a technique or unit that is compact, relatively simple, reliable, and economical.

To provide electrical power to an IDSEP van, for example, it is projected that the battery stack would consist of 280 cells each of active area 565 cm². The total hydrogen flow rate as a function of current density in 5M KOH at 60°C is shown as Figure 5-10, with a high performance aluminum alloy as the anode material, e.g., an indium-magnesium-manganese-aluminum alloy. The hydrogen disposal unit must be designed to treat the maximum hydrogen flowrate, i.e., for 99.995% aluminum, 90 l/min generated at the peak current den-

sity of 280 mA/cm². Four methods for disposal of the hydrogen gas were considered:

1. Dilution with air is the simplest approach, the hydrogen gas being diluted to less than 4% by volume (the lower flammability limit). The preferred approach is to include a small, lightweight blower in the system as an auxiliary air source.
2. Catalytic Recombination requires dilution of the hydrogen gas stream to allow efficient recombination.
3. Direct Combustion would require substantial engineering to safeguard against fire and/or explosion.
4. The use of a fuel cell would provide additional electrical power to the system but is a complex problem needing dehumidification and pressurization of the reactant gas and a control system to

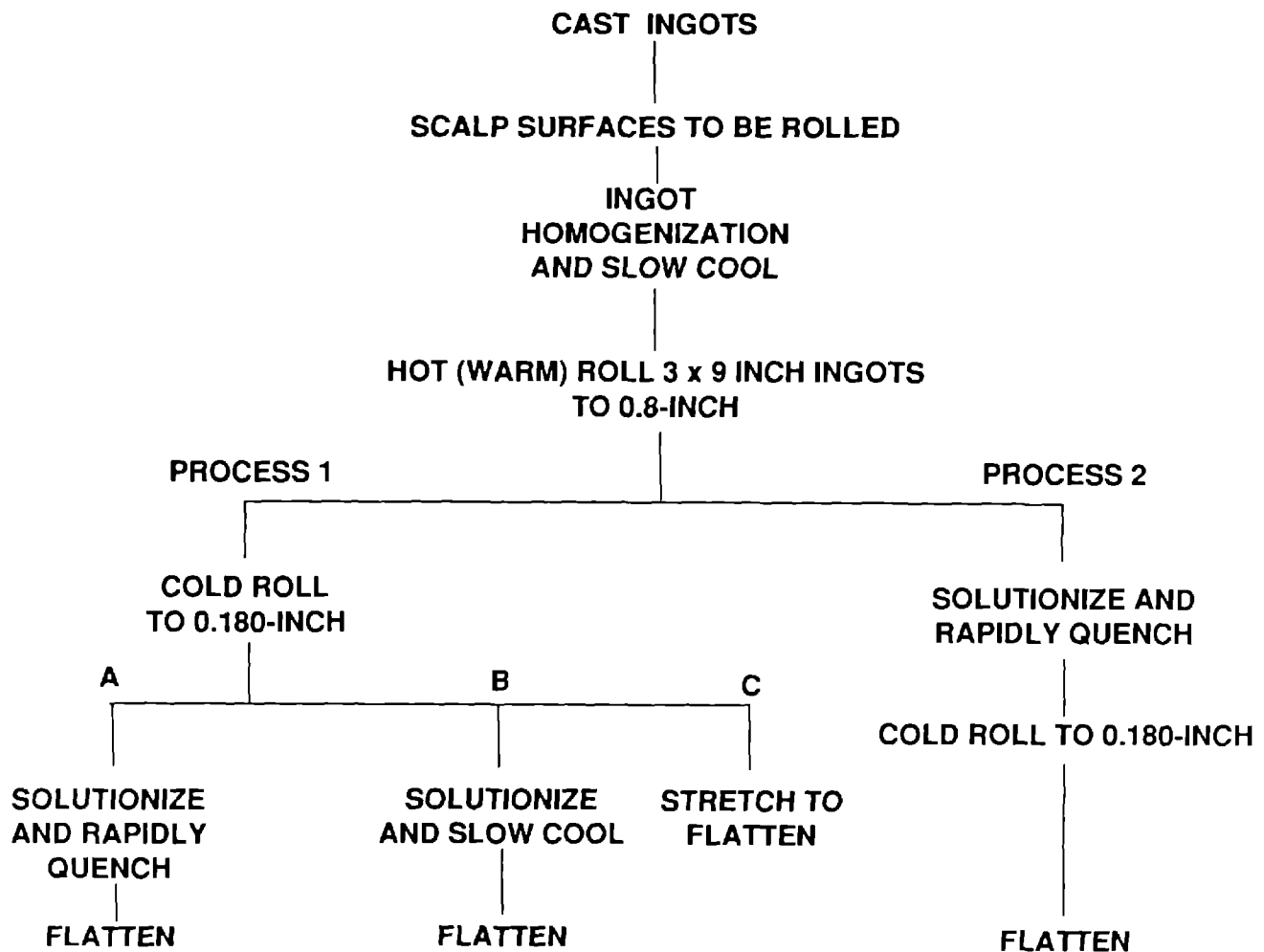


Figure 5-8. Alloy Processing Steps

integrate the power produced with that of the main battery.

Mathematical Modeling Studies Experimental Support

A program was undertaken to provide experimental data related to the dissolution and corrosion of aluminum metal in alkaline electrolytes. The effects of

a) the concentration of hydroxyl ions, b) the concentration of aluminate ions, c) mass transfer and d) temperature were determined using a rotating cylindrical electrode fabricated from high purity aluminum.

The current-potential curves for the dissolution of aluminum at 60°C are exponential (favoring Butler-Volmer kinetics) and therefore linear Tafel relationships were obtained. The high values, ranging from 460 to

Table 5-6. Electrochemical Behavior of Alloy #3

	Ingot Material											
	Open Circuit		At 100 mA/cm ²		At 200 mA/cm ²		At 300 mA/cm ²		At 400 mA/cm ²		At 500 mA/cm ²	
	Potent.	Corr.	Potent.	Corr.	Potent.	Corr.	Potent.	Corr.	Potent.	Corr.	Potent.	Corr.
From Process 1A	-1.72	51	-1.70	15	-1.71	70	-1.66	58.5	-1.60	65	-1.60	73.8
From Process 1B	-1.77	38.1	-1.74	69	-1.56	20	-1.41	22	-1.27	10	---	---
From Process 1C	-1.75	27.7	-1.67	31.9	-1.50	20.6	-1.38	17.5	-1.25	14	-1.16	4.9
From Process 2	-1.76	30.4	-1.71	41	-1.69	47.4	-1.65	58	-1.60	60.9	---	---
<u>Electrolyte:</u> 5M KOH, 60°C												
<u>Potential</u> (volts) vs. Hg/HgO reference												
<u>Corrosion</u> as current density (mA/cm ²)												
Ingot and Bookmold Material												
1A, Ingot, heat treated	-1.72	51.7	-1.7	15.0	-1.72	70.1	-1.66	58.5	-1.60	65.3	-1.60	73.8
1A, Bookmold, heat treated	-1.76	11.6	-1.7	17.1	-1.71	34.1	-1.66	46.0	-1.63	62.5	-1.59	71.0
1C, Cold Rolled	-1.75	27.7	-1.67	31.9	-1.50	20.6	-1.38	17.6	-1.38	14.0	-1.16	4.9
1C, Bookmold, Cold Rolled	-1.80	16.4	-1.72	23.3	-1.52	16.9	-1.40	12.7	-1.28	---	-1.13	1.4
<u>Electrolyte:</u> 5M KOH, 60°C												
<u>Potential</u> (volts) vs. Hg/HgO reference												
<u>Corrosion</u> as current density (mA/cm ²)												

Table 5-7. Electrochemical Behavior of Aluminum Alloys

Alloy No.	At Open Circuit		At 100 mA/cm ²		At 200 mA/cm ²		At 300 mA/cm ²		At 400 mA/cm ²		At 500 mA/cm ²	
	Potent.	Corr.	Potent.	Corr.	Potent.	Corr.	Potent.	Corr.	Potent.	Corr.	Potent.	Corr.
1	-1.77	87.5	-1.71	82.2	-1.71	152.9	-1.69	146.5	-1.65	185.4	-1.61	151.0
2	-1.74	69.7	-1.72	76.1	-1.71	108.7	-1.69	114.1	-1.64	96.5	-1.60	91.6
3	-1.74	32.7	-1.74	28.7	-1.73	64.9	-1.70	87.3	-1.66	97.1	-1.59	56.7
4	-1.71	77.7	-1.65	125.4	-1.58	60.6	-1.54	82.6	-1.51	69.9	-1.48	82.8

Potential, volts vs Hg/HgO
Corrosion, mA/cm²

Table 5-8. Performance of Alloy Plates In the AT400

Alloy	Cell Voltage at						Average Corrosion Over SFUDS
	O.C.	100	200	300	400	450	
	[Current Density (mA/cm ²)]						
1	1.85	1.61	1.54	1.46	1.38	1.34	429.6
2	1.83	1.60	1.53	1.45	1.38	1.33	79.5
3	1.85	1.59	1.52	1.45	1.37	1.32	15.5
4	1.77	1.50	1.41	1.32	1.24	1.21	253.9

Electrolyte 5M KOH, 60°C
Corrosion as mA/cm²

Table 5-9. Acoustic Separation Continuous Filtration Experiments

Electrolyte Flowrate (cc/min)	Collection Efficiency (%)
6-7	97-5
10	82
27	50-55

660 mV/decade, indicate that a surface film is formed at the aluminum electrode. The formation of a film also explains the absence of dependence of the rate of dissolution upon the rate of rotation of the electrode. At lower temperatures (30-40°C), the current-potential relationships become distinctly linear, suggesting that the thickness of the surface film is quite strongly dependent upon the temperature.

It was shown that the rate of dissolution is sensitive to the presence of dissolved aluminum in the electrolyte and the overpotential at the anode increases with increasing concentrations of aluminate ions. This is further illustrated in Table 5-10 in terms of the reaction

order, Tafel slope and activation energy for the dissolution process.

Technology Evaluation at SNL

An Eltech aluminum/air cell was installed at SNL during the week of June 25, 1990. The unit consisted of a single cell based on the AT400 design, an electrolyte reservoir with the associated plumbing station, and a carbon dioxide scrubber. Solid separation equipment was not included. Refueling was accomplished mechanically by replacing the depleted aluminum anode. As opposed to the previous B-300 design, replacement of the AT400 anode was uncomplicated.

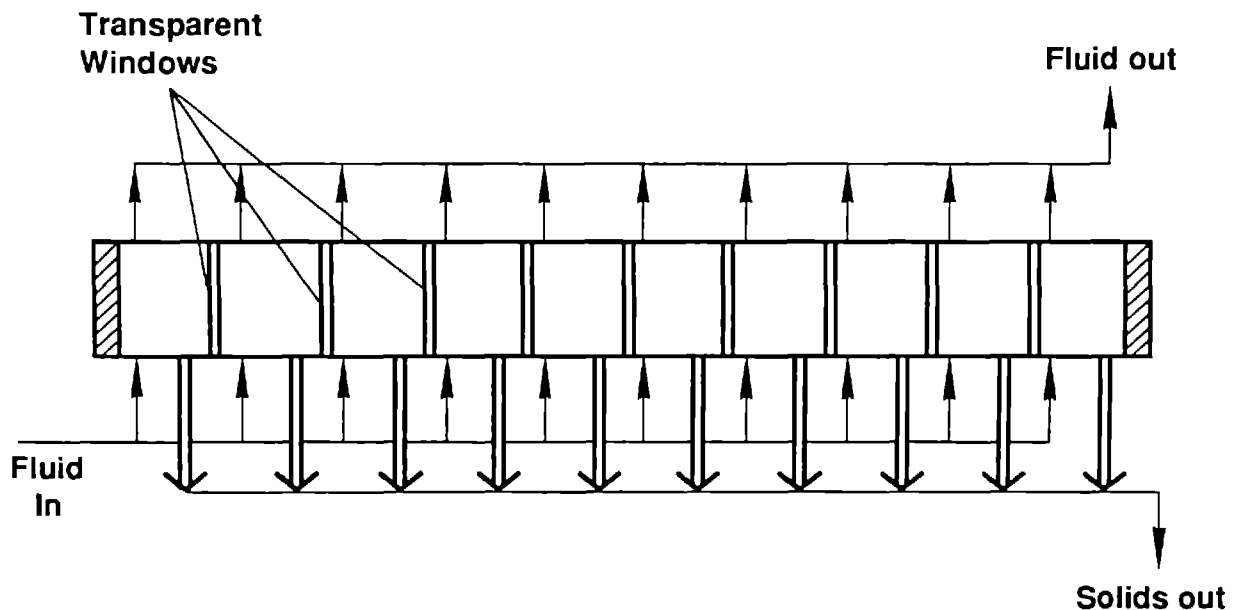


Figure 5-9. Design of Multiple Chamber Acoustically Augmented Aluminate Separation Cell

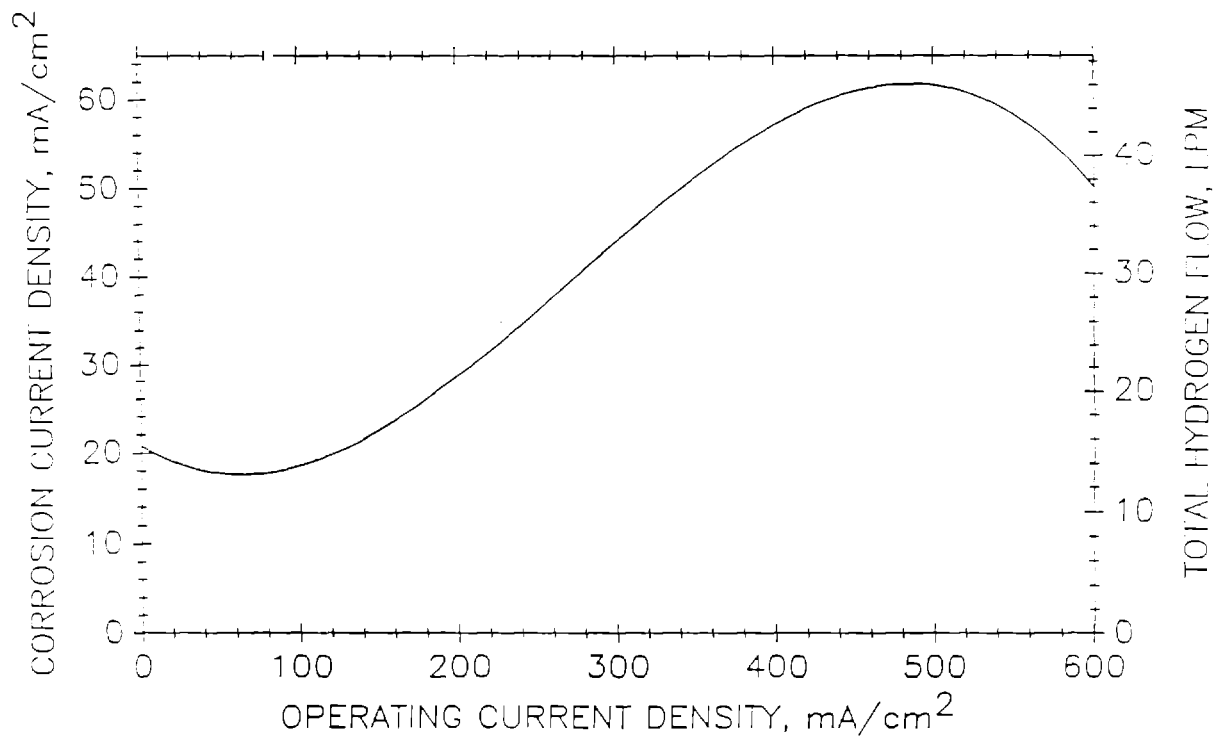


Figure 5-10. Predicted Hydrogen Produced as a Function of Battery Current Density for Advanced Alloy in Full-Sized Battery

Table 5-10. The Effect of Aluminate Ions Upon the Dissolution of Aluminum

Aluminate Conc. in 5M KOH, 60°C (moles/liter)	Activation Energy for Dissolution (k cal/mole)	Tafel Slope (mV/decade)	Reaction Order
0	12-14	460	0.95
1.0	15	490	---
2.0	24-8	540	0.5

When fully charged with a new anode, the cell had a theoretical capacity of approximately 975 Ah. Tests were run with pure aluminum anodes (99.995%) and with a advanced aluminum alloy (alloy #3, see above) at imposed current densities of 100, 200, 300, 400, 450 mA/cm², in addition to a stand test at 0 mA/cm². All tests were initiated with 5M KOH with no dissolved aluminum. Approximately 6.5 liters of electrolyte were used. All tests were run with an electrolyte flow rate of 400 ml/min.

Test results are shown in Table 5-11. Six runs were made with the advanced alloy while 18 runs were made with the 99.995% aluminum anodes. Polarization data for the 6 alloy runs and 17 of the 99.995% aluminum runs is shown in Figure 5-11. Polarization data was taken prior to the initiation of the constant current experiments. As Figure 5-11 shows, the performance of the cathode was stable throughout the runs. The on-line time for the runs was approximately 65 hours. Near the end of this set of experiments, the condensate increased

Table 5-11. Test Results of Pure Aluminum and Alloy Anodes

Test #	Anode Type	Elapsed Time (min)	Discharge Current Density (mA/cm ²)	Al Efficiency Fara/Total Wt. Loss (%)	Average Corrosion Rate (mA/cm ²)	Anode Utiliz. (%)
1	99.995%	253		75.5	66.7	40.4
2	99.995%	240	200	78.0	49.6	32.7
3	99.995%	240	300	87.1	37.8	48.6
4	99.995%	240	100	44.2	119.7	17.9
5	99.995%	240	300	74.9	83.5	46.3
6	99.995%	240	200	72.8	64.4	31.9
7	99.995%	216	400	81.2	78.3	56.3
8	99.995%	60	400	82.7	69.1	16.0
9	99.995%	53	450	82.9	73.6	19.0
10	99.995%	120	200	69.9	74.0	16.5
11	99.995%	80	300	71.9	97.3	20.8
12	99.995%	120	0	6.9	138.5	1.0
13	99.995%	60	300	81.2	57.8	13.3
14	99.995%	90	300	80.5	60.9	24.2
16	99.995%	120	300	77.3	73.1	29.7
17	ALLOY	120	200	84.1	32.8	15.7
18	99.995%	240	100	52.9	80.1	32.7
19	99.995%	80	300	84.8	46.3	15.8
20	ALLOY	240	100	63.4	51.4	14.0
21	ALLOY	80	300	89.3	30.6	15.3
22	ALLOY	60	400	91.2	31.2	14.6
23	ALLOY	120	200	75.5	56.8	18.7
24	ALLOY	53	450	91.5	34.0	17.6

in pH and rate; however, the performance of the cathode did not degrade.

Figure 5-12 shows the corrosion rate and the faradaic efficiency of the advanced alloy. Comparing Figure 5-12 with Table 5-11, the corrosion rate of the

advanced alloy is a clear improvement over the corrosion rate of the pure aluminum anode which was typically 75-100 mA/cm² at an imposed current density of 100-450 mA/cm². Both the corrosion rate and the faradaic efficiency improve with increased current den-

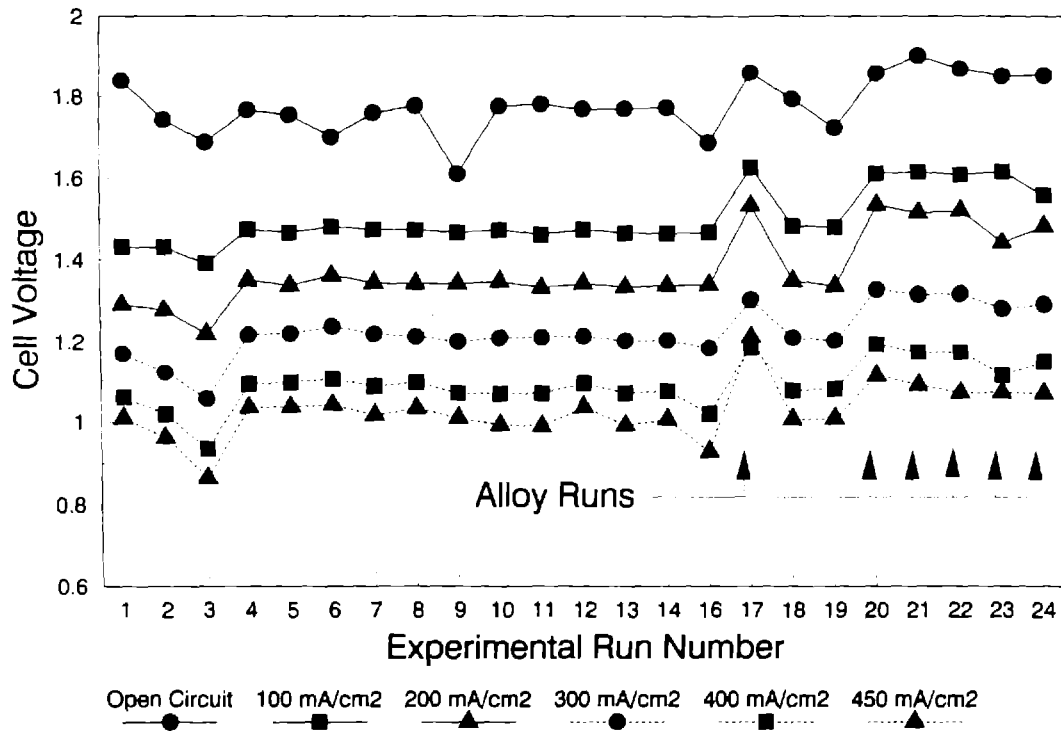


Figure 5-11. Cell Polarization Data

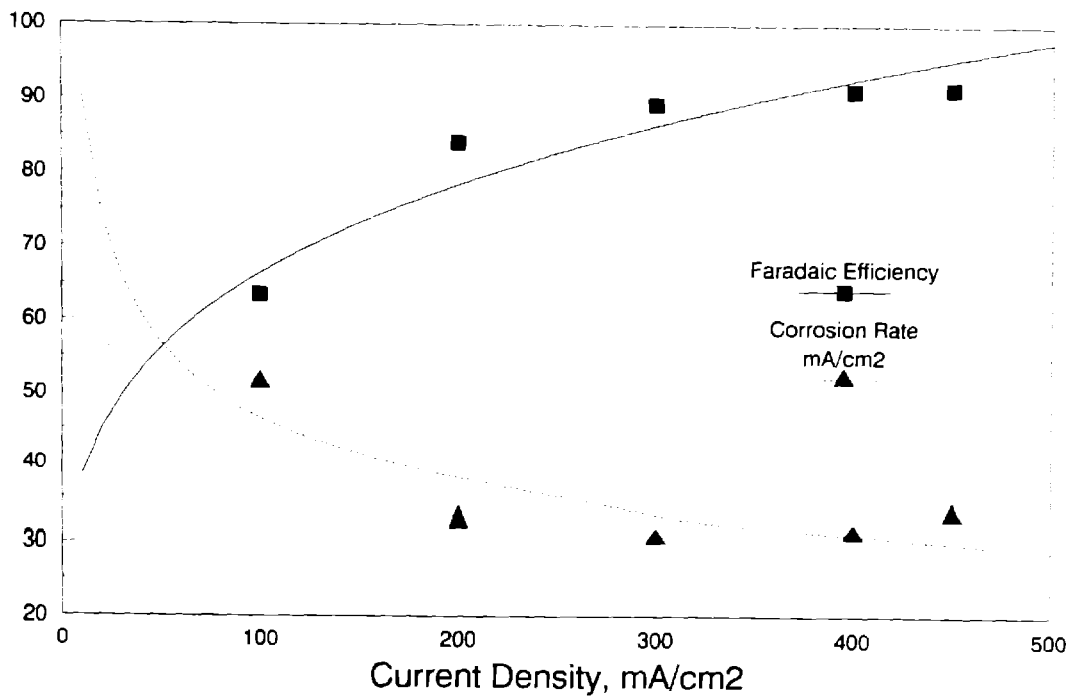


Figure 5-12. Corrosion Rate and Faradaic Efficiency of the Advanced Alloy

sities due to the relative kinetics of the hydrogen reduction and the aluminum oxidation reactions. Although the advanced alloy displayed a corrosion rate of 30 mA/cm², which is an improvement compared to the 99.995% aluminum anodes, 30 mA/cm² still represents a hydrogen production rate of 5 l/hr for a 400 cm² electrode.

Figure 5-13 compares the faradaic efficiency for the advanced alloy with the 99.995% aluminum anode. At all imposed current densities from 100 to 450 mA/cm², the advanced alloy was superior in performance. For an imposed current density greater than 300 mA/cm², the faradaic efficiency loss of the advanced alloy was approximately half of the 99.995% aluminum anode.

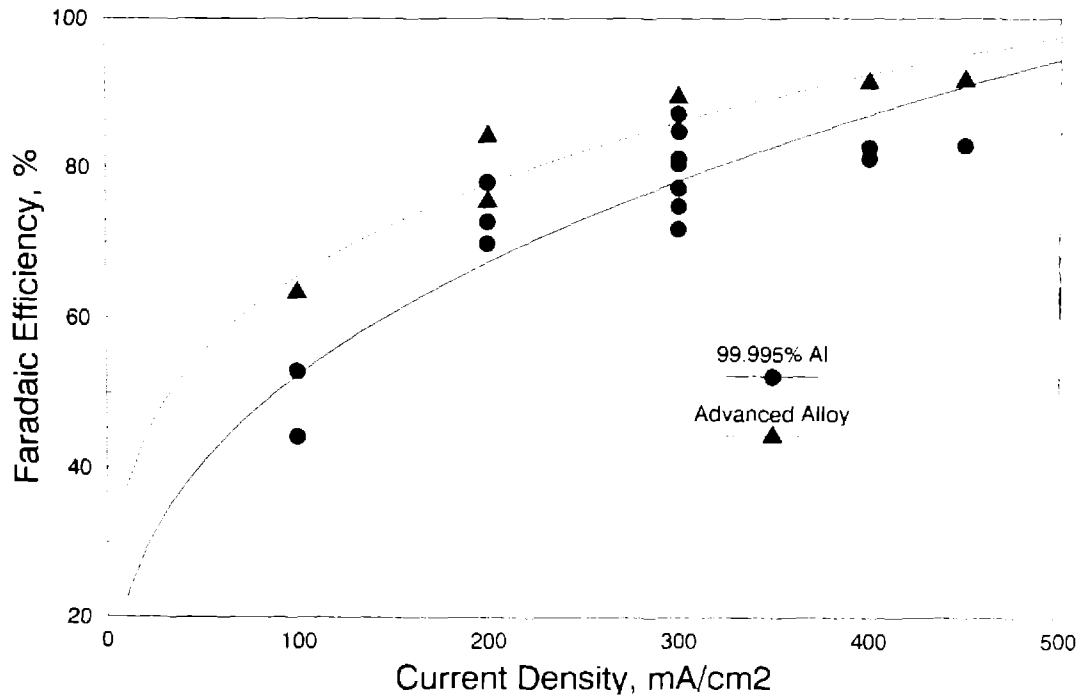


Figure 5-13. Faradaic Efficiency Comparison of Advanced Alloy and 99.995% Aluminum Anode

Appendix: Presentations and Publications

Presentations

- Arnold, C., Jr., and R. A. Assink, "Membrane and Durability Studies for the Zinc/Bromine Battery," Ninth Battery and Electrochemical Contractors' Conference, Alexandria, VA, November 1989.
- Arnold, C., Jr., and P. C. Butler, "Stability of Bipolar Electrodes and Flow Frames for Zn/Br₂ Cells," Zinc Battery R&D Review Meeting, Lawrence Berkeley Laboratory, February 1990.
- Arnold, C., Jr., and R. A. Assink, "The Development and Characterization of Ion Exchange Membranes for Selected Electrochemical Power Sources," International Congress of Membranes, Chicago, August 1990.
- Auxer, W., "Sodium Sulfur Battery Commercialization," Ninth Battery and Electrochemical Contractors' Conference, Alexandria, VA, November 1989.
- Auxer, W., and A. Koenig, "Sodium Sulfur and Sodium Metal Chloride Batteries for Electric Vehicles," Proc. Fifth Annual Battery Conference on Applications and Advances, January 1990, Paper 901T-4.
- Auxer, W., "An Overview of Beta Power Inc.," Beta Battery Workshop VIII, Chester, England, June 1990.
- Binden, P., "Thermal Modelling of Electric Vehicle Batteries," Beta Battery Workshop VIII, Chester, England, June 1990.
- Bolstad, J. J., and R. C. Miles, "Development Testing of Zinc/Bromine Batteries," 34th International Power Sources Symposium, Cherry Hill, NJ, June 1990.
- Braithwaite, J. W., and J. M. Freese, "Sodium/Sulfur Battery Studies at SNL," 1989 Electric and Hybrid Vehicle (EHV) Contractors' Meeting, Idaho Falls, ID, September 1989.
- Bush, D. M., "Nickel/Hydrogen Cell Evaluation at SNL," Ninth Battery and Electrochemical Contractors' Conference, Alexandria, VA, November 1989.
- Diegle, R. B., "Exploratory Battery Technology Development and Testing Project Overview," Ninth Battery and Electrochemical Contractors' Conference, Alexandria, VA, November 1989.
- Dodge, J. A., and P. A. Eidler, "Recent Advances in Zinc/Bromine Technology at Johnson Controls, Inc.," 1990 Annual Battery Conference on Applications and Advances, Long Beach, CA, January 1990.
- Eidler, P. A., "Zinc-Bromine Battery Development," Ninth Battery and Electrochemical Contractors' Conference, Alexandria, VA, November 1989.
- Freese, J. M., "Sodium/Sulfur Evaluation at SNL," Ninth Battery and Electrochemical Contractors' Conference, Alexandria, VA, November 1989.
- Gordon, R. S., S. N. Heavens, A. V. Virkar, and N. Webber, "On the Stability of Beta/Beta" Alumina in Sulfur/Sodium Polysulfide Melts," Beta Battery Workshop VIII, Chester, England, June 1990.
- Jones, I. W., and S. MacLachlan, "The Development of Sodium Sulfur Cells and Batteries," Secondary Battery Evolution - Recent Techniques, Paris, November 1989.
- Jones, I. W., "Overview of Sodium Sulphur Battery Development at CSPL," Beta Battery Workshop VIII, Chester, England, June 1990.
- Leo, A., "Zinc-Bromine Battery Development at Energy Research Corporation," Ninth Battery and Electrochemical Contractors' Conference, Alexandria, VA, November 1989.
- Leo, A., "Zinc-Bromine Cell and Stack Tests at Energy Research Corporation," Zinc Battery R&D Review Meeting, Lawrence Berkeley Laboratory, February 1990.
- Lott, S. E., "Experience with Zinc/Bromine Testing at SNL," Zinc Battery R&D Review Meeting, Lawrence Berkeley Laboratory, February 1990.

- MacLachlan, S., and C. O'Neil Bell, "The Development of a Metal: Ceramic Seal for Sodium Sulfur Cells," *Secondary Battery Evolution - Recent Techniques*, Paris, November 1989.
- MacLachlan, S., and I. Witherspoon, "Chloride Silent Power Limited (CSPL) Cell Performance Status," *Beta Battery Workshop VIII*, Chester, England, June 1990.
- Mangan, M. F., J. Molyneux, and P. G. Brocklehurst, "Sodium Sulfur EV Battery Development," *Ninth Battery and Electrochemical Contractors' Conference*, Alexandria, VA, November 1989.
- McNamee, M., and F. M. Stackpool, "Sodium Sulfur for Technology Development," *Ninth Battery and Electrochemical Contractors' Conference*, Alexandria, VA, November 1989.
- Molyneux, J., "Design and Performance of Na/S Batteries," *Beta Battery Workshop VIII*, Chester, England, June 1990.
- Petersen, R., "Experience with Zinc-Bromine Cell and Stack Tests at Johnson Controls, Inc.," *Zinc Battery R&D Review Meeting*, Lawrence Berkeley Laboratory, February 1990.
- Rudd, E. J., "Development of Aluminum-Air Batteries for Electric Vehicles," *Ninth Battery and Electrochemical Contractors' Conference*, Alexandria, VA, November 1989.
- Stackpool, F. M., "Advances in Sodium Sulfur Cell Safety," *176th Meeting of Electrochemical Society*, October 1989.
- Stackpool, F. M., "Safety Qualification of Sodium Sulphur Cells," *Beta Battery Workshop VIII*, Chester, England, June 1990.

Publications

- Assink, R. A., and C. Arnold, Jr., "Preparation of Oxidatively Stable Cationic Membranes by the Elimination of Tertiary Hydrogens," *Journal of Membrane Science*, July 1990.
- Bush, D. M., Terrestrial Nickel/Hydrogen Battery Evaluation, SAND90-0390, July 1990.
- Johnson, P. J., and A. A. Koenig, "Polarization Measurements in Sodium Sulfur Cells," *J. Electro Chem Soc*, v.137, April 1990, pp 1121-1125.
- Magnani, N. J., R. B. Diegle, J. W. Braithwaite, D. M. Bush, P. C. Butler, J. M. Freese, K. R. Grothaus, and K. D. Murphy, Exploratory Battery Technology Development and Testing Report for 1988, Sandia National Laboratories Report SAND89-3039, December 1989.

Distribution

Argonne National Laboratory (8)
9700 South Cass Avenue
Argonne, IL 60439
Attn: C. Christianson
W. DeLuca (3)
G. Henriksen
J. Marr
K. Myles
J. Smaga

California State Air Resources Board
Research Division
PO Box 2815
Sacramento, CA 95812
Attn: J. Holmes

Ceramatec, Inc.
2425 South 900 West
Salt Lake City, UT 84119
Attn: D. Richerson
A. Virkar

Beta Power, Inc. (3)
489 Devon Park Drive, Suite 315
Wayne, PA 19087
Attn: W. Auxer (3)

Beta Power, Inc.
163 West 1700 South
Salt Lake City, UT 84115
Attn: J. Rassmussen

Chloride Silent Power, Ltd. (4)
Davy Road
Astmoor
Runcorn, U.K. WA71PZ
Attn: W. Jones
M. McNamee (3)

Eagle Picher Industries
C & Portor Street
Joplin, MO 64802
Attn: James DeGruson

EG&G Idaho, Inc.
Idaho National Engineering Lab
PO Box 1625
Idaho Falls, ID 83415
Attn: G. Hunt
G. Cole

Electric Power Research Institute (6)
PO Box 10412
Palo Alto, CA 94303
Attn: R. Schainker
R. Weaver
P. Symons (3)
R. Swaroop

Electrochemical Engineering Consultants, Inc.
1295 Kelly Park Circle
Morgan Hill, CA 95037
Attn: P. Symons

Electrotek Concepts, Inc.
Electric Vehicle Operations
4605 Amnicola Hwy
PO Box 16548
Chattanooga, TN 37416
Attn: H. Barnett

Eltech Systems Corporation (6)
Research and Development Center
625 East Street
Fairport Harbor, OH 44077
Attn: E. Rudd (3)
R. Fenn
T. Gilligan
A. Homa

Energetics (3)
9210 Route 108
Columbia, MD 21044
Attn: J. Hurwitch (2)
H. Lowitt

Energy Research Corporation
Three Great Pasture Road
Danbury, CT 06810
Attn: A. Leo
J. Brown

Hughes Aircraft Co.
P.O. Box 2999
Torrance, CA 90509-2999
Attn: Robert Taenaka

Exxon Research Co.
P.O. Box 536
1900 E. Linden Ave.
Linden, NJ 07036
Attn: P. Grimes

Ford Motor Co.
Vehicle Systems Dept.
P.O. Box 2053
Dearborn, MI 48121-2053
Attn: Matt Dzieciuch

Johnson Controls, Inc.
PO Box 591
Milwaukee, WI 53201
Attn: P. Eidler
M. Eskra
J. Zagrodnik

Lawrence Berkeley Laboratory (5)
University of California
No 1 Cyclotron Road
Berkeley, CA 94720
Attn: E. Cairns
K. Kinoshita
F. McLammon (3)

Pacific Gas & Electric
3400 Crow Canyon Road
San Ramon, CA 94583
Attn: Jo Meglen

R. K. Sen & Associates
3808 Veazey St., NW
Washington, DC 20016
Attn: R. Sen

Science Applications International Corporation
10343 Roselle Street Suite G
San Diego, CA 92121
Attn: R. Davenport

Southern California Edison
2244 Walnut Grove Ave.
P.O. Box 800
Rosemeade, CA 91770
Attn: Robert Scheffler

Wright Patterson AFB
Air Force Wright Aeronautical Labs
WRDF/POOS
Wright Patterson AFB, OH 45433
Attn: W. Bishop
S. Vukson

U.S. Department of Energy (22)
Office of Energy Management
CE-142
FORSTL
Washington, DC 20585
Attn: R. Eaton
A. Landgrebe (20)
K. Klunder

U.S. Department of Energy
Office of Propulsion Systems
CE-321
FORSTL
Washington, DC 20585
Attn: K. Barber
E. Dowgiallo
K. Heitner
P. Patil
J. Brogan

U.S. Department of Energy (4)
Albuquerque Operations Office
Energy Technologies Division
Albuquerque, NM 87115
Attn: D. Krenz (2)
K. Smith
D. Christensen

U.S. Department of Energy
Sandia Area Office
PO Box 5800
Albuquerque, NM 87115
Attn: A. Sneddon, Jr.

20 O. Jones
140 M. J. Owen
143 R. Thorp
410 D. Arvizu
1811 C. Arnold, Jr.
1811 R. Clough
1812 R. Assink
1812 J. Zeigler
1845 E. Beauchamp
2000 J. Wirth, Acting
2500 R. Schwoebel
2520 N. Magnani
2522 R. Clark
2523 R. Diegle

2525 P. Butler (50)
3141 S. Landenberger (13)
3151 G. L. Esch, Acting
3710 L. Welchel
Attn: A. McConnell, 3714

6200 V. Dugan
6220 D. Schueler
6221 D. Schueler, Acting
6223 G. Jones
8523 R. Christman